nature neuroscience

Article

https://doi.org/10.1038/s41593-024-01819-9

Dissociable control of motivation and reinforcement by distinct ventral striatal dopamine receptors

Received: 23 June 2023

Accepted: 22 October 2024

Published online: 9 December 2024

Check for updates

Juan Enriquez-Traba[1,2,3], Miguel Arenivar[1], Hector E. Yarur-Castillo[1], Chloe Noh[1], Rodolfo J. Flores[1], Tenley Weil[4], Snehashis Roy[5], Ted B. Usdin[5], Christina T. LaGamma[1], Huikun Wang[1], Valerie S. Tsai[1], Damien Kerspern[6], Amy E. Moritz[7], David R. Sibley[7], Andrew Lutas[6], Rosario Moratalla[3], Zachary Freyberg[8,9] ✉ & Hugo A. Tejeda[1] ✉

Dopamine (DA) release in striatal circuits, including the nucleus accumbens medial shell (mNAcSh), tracks separable features of reward like motivation and reinforcement. However, the cellular and circuit mechanisms by which DA receptors transform DA release into distinct constructs of reward remain unclear. Here we show that DA D3 receptor (D3R) signaling in the mNAcSh drives motivated behavior in mice by regulating local microcircuits. Furthermore, D3Rs coexpress with DA D1 receptors, which regulate reinforcement, but not motivation. Paralleling dissociable roles in reward function, we report nonoverlapping physiological actions of D3R and DA D1 receptor signaling in mNAcSh neurons. Our results establish a fundamental framework wherein DA signaling within the same nucleus accumbens cell type is physiologically compartmentalized via actions on distinct DA receptors. This structural and functional organization provides neurons in a limbic circuit with the unique ability to orchestrate dissociable aspects of reward-related behaviors relevant to the etiology of neuropsychiatric disorders.

DA transmission is essential for reward processes, including motivation and reinforcement. Motivation is the internal process activating and directing behavior, while reinforcement increases the likelihood of a behavior through stimulus–response and action–outcome associations[1]. These separable constructs are coordinated to maximize reward outcomes[1], and are implicated in neuropsychiatric disorders like substance use and mood disorders[2,3]. The mNAcSh serves as a key hub for reward-related behaviors, receiving DAergic inputs from the ventral tegmental area (VTA)[4]. Various models propose that DA regulates reward via tonic and phasic activity patterns governed by VTA DA neuron spiking and local axonal control of DAergic terminals[5,6]. These dynamics likely underlie reinforcement, motivation and vigor[7,8]. However, how DA release translates into cellular changes through DA receptors to drive distinct aspects of reward function remains unclear.

mNAcSh medium spiny neurons (MSNs) express high levels of DA receptors, including D1 receptors (D1Rs) and D2 receptors (D2Rs), which segregate into largely nonoverlapping classes, D1-MSNs and

[1]Unit on Neuromodulation and Synaptic Integration, National Institute of Mental Health, Bethesda, MD, USA. [2]Department of Biochemistry, Universidad Autonoma de Madrid, Madrid, Spain. [3]Department of Functional and Systems Neurobiology, Instituto Cajal-CSIC, Madrid, Spain. [4]Section on Light and Circadian Rhythms, National Institute of Mental Health, Bethesda, MD, USA. [5]Systems Neuroscience Imaging Resource, National Institute of Mental Health, Bethesda, MD, USA. [6]Neuromodulation and Motivation Section, Diabetes, Endocrinology, & Obesity Branch, National Institute of Diabetes and Digestive and Kidney Diseases, Bethesda, MD, USA. [7]Molecular Neuropharmacology Section, National Institute of Neurological Disorders and Stroke, Bethesda, MD, USA. [8]Department of Psychiatry, University of Pittsburgh, Pittsburgh, PA, USA. [9]Department of Cell Biology, University of Pittsburgh, Pittsburgh, PA, USA. ✉e-mail: freyberg@pitt.edu; hugo.tejeda@nih.gov

D2-MSNs, respectively[9]. DA-mediated activation of these receptors produces contrasting effects on D1-MSNs and D2-MSNs[10–12]. The mNAcSh is also enriched with D3Rs, $G\alpha_{i/o}$-coupled G-protein-coupled receptors (GPCRs) of the D2-like receptor family[13,14]. Expression of D3Rs within ventral striatal circuits coincides with a motivational control by the mNAcSh[4]. D3R is a high-affinity DA receptor with a tenfold greater DA affinity than D2Rs[15], suggesting it may complement D2Rs in detection of tonic changes or DA dips. Although ventral striatal D3R expression is documented[13], its role in regulating reward-related behaviors remains poorly understood. Pharmacological antagonism of NAc D3R signaling inhibits drug-seeking behavior[16]. However, intra-NAc D3R antagonism may have off-target effects at D2Rs. Global overexpression or knockout of D3Rs increases vulnerability to cocaine or disrupted motivation, respectively[17,18]. However, this does not specifically target mNAcSh D3R function, and D3R signaling outside the NAc also regulates reward[19,20]. Thus, limited tools to selectively manipulate mNAcSh D3R function hindered understanding of their contribution to distinct reward features. Interestingly, NAc core/shell D1-MSNs coexpress D3R with D1R[20,21]. Because D3Rs and D1Rs have different affinities for DA and engage opposite signaling effectors ($G\alpha_{i/o}$ and $G\alpha_{s/olf}$ proteins, respectively), these differences may translate into differential detection of DA concentrations, impacting on D1-MSN physiology, and reward-seeking behavior. We, therefore, hypothesized that D1-MSNs in the mNAcSh use distinct DA receptors for orchestrating dissociable reward-related functions.

We addressed this hypothesis using anatomical tracing, slice electrophysiology and circuit-level manipulations of DA receptor function. We generated and characterized a new D3R conditional knockout (cKO) mouse to specifically target mNAcSh D3Rs. Leveraging this line, we show that mNAcSh D3R ablation impairs motivated running and operant motivation but not instrumental conditioning or negative reinforcement. In contrast, D1R knockout impairs instrumental conditioning and negative reinforcement, but not motivation. Moreover, we demonstrated dissociable roles for D3R and D1R in regulating MSN synaptic physiology. This provides a new framework by which DA signaling via D3R and D1R allows mNAcSh D1-MSNs to regulate dissociable constructs underlying reward-related behaviors.

Results

mNAcSh D3R genetic ablation results in motivational deficits

We first investigated whether mNAcSh D3R signaling regulates specific sub-features of reward-related behaviors. To this end, we generated *Drd3*$^{fl/fl}$ mice (Extended Data Fig. 1a) to selectively knockout D3R expression in the mNAcSh with intra-mNAcSh injections of adeno-associated virus AAV8-hSyn-GFP-Cre (NAc-D3RcKO; Fig. 1a). NAc-D3RcKO mice had decreased *Drd3* mRNA expression as assessed by fluorescence in situ hybridization (Fig. 1b). Furthermore, we observed decreased *Drd3*, but not *Drd1* or *Drd2*, mRNA expression as assessed by quantitative PCR (qPCR) measures from microdissected NAc (Fig. 1c), suggesting this manipulation is specific to D3R expression. We then assessed the impact of mNAcSh D3RcKO in regulating reward by first examining motivation for exercise using wheel running (Extended Data Fig. 1b), a rewarding stimulus for laboratory and feral rodents[22,23]. In this context, wild-type (WT) and *Drd3*$^{fl/fl}$ control mice injected with Cre-expressing and GFP-expressing virus, respectively, displayed robust wheel-running activity when exposed to a novel wheel during their inactive cycle (lights on; Fig. 1d), when locomotor activity is typically low. NAc-D3RcKO mice, conversely, had reduced wheel-running activity under the same conditions (Fig. 1d and Extended Data Fig. 1c). However, running triggered by active cycle (lights off) onset (Extended Data Fig. 1c) and locomotor activity in an open field did not differ between controls and NAc-D3RcKO mice (Extended Data Fig. 1f). Intact locomotor activity and running in response to diurnal shifts suggest that mNAcSh D3RcKO impacts the motivational value of running, not performance. Running triggered by novel wheel exposure during the subjective daytime in rodents contains a strong motivational component[24]. Further, running behavior is more sensitive to interference during acquisition of wheel running before habituation[25]. With extended exposure to voluntary running, running can be decoupled from motivational state and driven by other factors, including but not limited to habitual behavior, diurnal

Fig. 1 | cKO of D3Rs in the mNAcSh results in motivational deficits. **a**, Experimental scheme and representative image of the mNAcSh area targeted with AAV-GFP-Cre or AAV-eGFP. **b**, Representative in situ hybridization images showing *Cre* (green) and *Drd3* (white) mRNA expression in WT or NAc-D3RcKO mice. Insets depict higher-magnification images. **c**, Left: quantification of *Drd3* mRNA expression in *Cre*-positive neurons in the mNAcSh of WT ($n = 3$) and NAc-D3RcKO ($n = 3$) mice (unpaired *t*-test (two-tailed), $t_{(4)} = 7.421$; $^{**}P = 0.0018$). Right: quantitative real-time PCR analysis of *Drd1*, *Drd2* and *Drd3* mRNA expression in the NAc of WT (white, $n = 3$) and NAc-D3RcKO (blue, $n = 4$) mice injected with Cre-expressing virus (two-way repeated-measures analysis of variance (ANOVA): gene effect, $F_{(2,9)} = 4.291$, $P = 0.0491$; genotype effect, $F_{(1,6)} = 8.948$, $P = 0.0243$; gene × genotype, $F_{(2,6)} = 22.67$, $P = 0.0016$; Sidak's post hoc analysis, $^{**}P = 0.0012$). **d**, Left: time-course of wheel-running activity in WT-Cre (black, $n = 11$), *Drd3*$^{fl/fl}$-GFP (red, $n = 7$) and NAc-D3RcKO (blue, $n = 12$) mice during the first 12 h of running wheel exposure (two-way repeated-measures ANOVA: time effect, $F_{(7.449,201.1)} = 20.81$, $P < 0.0001$; treatment effect, $F_{(2,27)} = 12.97$, $P < 0.0001$; time × treatment, $F_{(286,3,861)} = 2.954$, $P < 0.0001$). Right: quantification of revolutions across the 12-h period (one-way ANOVA followed by two-sided Dunnett's test: $F_{(2,27)} = 12.97$. Group comparisons, WT-Cre versus *Drd3*$^{fl-fl}$-Cre, $^{****}P < 0.0001$, *Drd3*$^{fl-fl}$-GFP versus *Drd3*$^{fl-fl}$-Cre, $^{****}P < 0.0001$). **e**, Representative occupancy heat maps from WT (top) and NAc-D3RcKO (bottom) mice during running disks choice test. **f**, Left: quantification of time spent on the freely moving and fixed disk (WT-Cre, $n = 11$ mice; *Drd3*$^{fl/fl}$-GFP, $n = 6$ mice; NAc-D3RcKO, $n = 12$ mice; two-way repeated-measures ANOVA: disk effect, $F_{(1,52)} = 81.22$, $P < 0.0001$; treatment effect, $F_{(2,52)} = 14.65$, $P < 0.0001$; disk × treatment, $F_{(2,52)} = 28.59$, $P < 0.0001$). Middle: revolutions registered on the freely moving disk for WT, *Drd3*$^{fl/fl}$-GFP controls and NAc-D3RcKO mice (one-way ANOVA followed by two-sided Dunnett's test: $F_{(2,27)} = 12.97$. Group comparisons, WT-Cre versus *Drd3*$^{fl-fl}$-Cre, $^{****}P < 0.0001$, *Drd3*$^{fl-fl}$-GFP versus *Drd3*$^{fl-fl}$-Cre, $^{****}P < 0.0001$). Right: Spearman's correlation between time spent on the freely moving disk and revolutions. **g**, Timeline of operant conditioning experiment. **h**, Number of active (filled) and inactive (unfilled) lever presses of WT (black, $n = 15$ mice) and NAc-D3RcKO (blue, $n = 11$ mice) animals during FR1 acquisition sessions (two-way repeated-measures ANOVA: session effect, $F_{(3.679,86.09)} = 38.81$, $P < 0.0001$; genotype effect, $F_{(1,24)} = 0.5573$, $P = 0.4626$; session × genotype, $F_{(5,117)} = 1.334$, $P = 0.2546$). **i**, Number of active and inactive lever presses of WT (black, $n = 15$ mice) and NAc-D3RcKO (blue, $n = 11$ mice) animals during FR5 acquisition sessions (two-way repeated-measures ANOVA: session effect, $F_{(4.068,97.05)} = 2.321$, $P = 0.0611$; genotype effect, $F_{(1,24)} = 2.228$, $P = 0.1486$; session × genotype, $F_{(7,167)} = 2.360$, $P = 0.252$). * represents a session × genotype interaction. **j**, Left: scheme of the FR5 choice behavioral setup. Mice had free access to standard lab chow and could also lever press (FR5) to obtain higher-palatable chocolate food pellets. Right: amount of effort-based food (FR5; solid) or freely available lab chow (checkered) consumed (WT, $n = 11$ mice; NAc-D3RcKO, $n = 11$ mice) (two-way repeated-measures ANOVA: type of food effect, $F_{(1,24)} = 17.97$, $P = 0.0003$; genotype effect, $F_{(1,24)} = 0.2095$, $P = 0.6513$; type of food × genotype, $F_{(1,24)} = 6.883$, $P = 0.0149$). *** represents a significant difference between ad libitum chow and FR5 pellets in WT mice. * represents a significant difference between ad libitum chow between WT and mNAcSh-D3RcKO mice. **k**,**l**, Break points for WT and NAc-D3RcKO mice during PR3 (**k**) (two-way repeated-measures ANOVA: session effect, $F_{(1.436,32.30)} = 3.507$, $P = 0.0559$; genotype effect, $F_{(1,24)} = 5.679$, $P = 0.0254$; session × genotype, $F_{(2,45)} = 0.4779$, $P = 0.6232$) and PR7 (**l**) (two-way repeated-measures ANOVA: session effect, $F_{(1.833,43.99)} = 1.672$, $P = 0.2014$; genotype effect, $F_{(1,24)} = 12.61$, $P = 0.0016$; session × genotype, $F_{(3,72)} = 1.920$, $P = 0.1341$) sessions (WT, $n = 11$ mice; NAc-D3RcKO, $n = 11$ mice). * and ** in **k** and **l** represent a main effect of genotype. All data are presented as the mean ± s.e.m. Error bars indicate the s.e.m. Detailed figure statistics are included in Supplementary Table 1. Schematics were generated using BioRender.com. M, medial; V, ventral; a.u., arbitrary units; NS, not significant.

https://doi.org/10.1038/s41593-024-01819-9

shifts, internal states, arousal and/or non-photic circadian entrainment[25]. Accordingly, NAc inactivation does not impair habitual running but inhibits motivated running triggered by wheel deprivation[26]. Thus, initial motivation to engage in wheel running, but not locomotor activity or running performance, is decreased in NAc-D3RcKO mice.

To investigate whether mNAcSh D3RcKO impaired motivation to run, we designed a choice task wherein mice choose between a fixed or a freely moving disk, a distinct running apparatus, during the active cycle (Fig. 1e). WT-Cre and *Drd3*$^{fl/fl}$-GFP control mice spent more time on the freely moving disk than the fixed disk (Fig. 1e,f). Conversely, NAc-D3RcKO mice did not prefer the freely moving disk and displayed minimal running (Fig. 1e,f). Running disks require persistence for optimal running to develop since early attempts are marked by mice consistently falling off the disk. In control mice, but not NAc-D3RcKO mice, entries into and preference for the freely moving disk increased across the session (Extended Data Fig. 1d,e), consistent with increased persistence. These data provide support for NAc-D3RcKO in decreasing motivated running behavior, independent of diurnal cycle. We subsequently determined whether mNAcSh D3RcKO impacts approach to other rewarding stimuli. NAc-D3RcKO mice displayed a non-significant decrease in sucrose preference relative to controls (Extended Data Fig. 1g), and normal social approach (Extended Data Fig. 1h), suggesting that pursuit of low-effort rewards is unaffected. Anxiety-like behavior in the open field and light–dark box (Extended Data Fig. 1f,i), as well

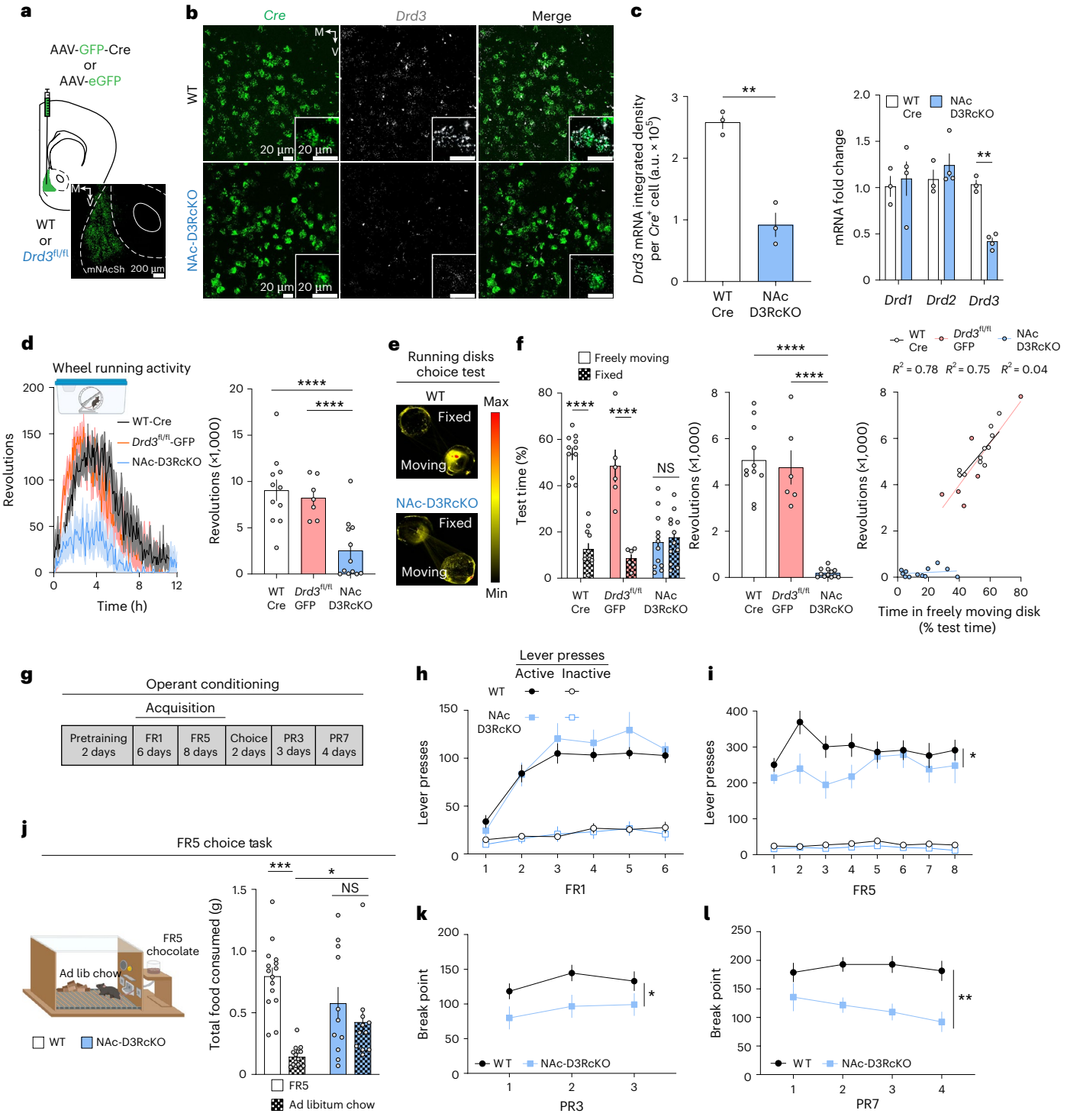

as novel object recognition (Extended Data Fig. 1j), was not different between controls and NAc-D3RcKO mice, demonstrating that exploratory behavior or interaction with novel stimuli are not impacted by mNAcSh D3RcKO. These results collectively suggest that mNAcSh D3RcKO disrupts running behavior associated with a motivated state.

We subsequently determined the role of mNAcSh D3Rs in effort-based instrumental motivation using operant procedures in which animals press a lever to acquire a chocolate reward (Fig. 1g). mNAcSh *Drd3* cKO did not modify body weight (Extended Data Fig. 2a). Animals first underwent an initial acquisition phase consisting of fixed-ratio (FR) 1 and 5 schedules to determine whether loss of mNAcSh D3R signaling impacted reinforcement of food-seeking behavior. NAc-D3RcKO and WT groups displayed similar active lever pressing and accuracy during FR1 sessions (Fig. 1h and Extended Data Fig. 2b,c), indicating that mNAcSh D3R signaling is not essential for reward reinforcement. Interestingly, NAc-D3RcKO mice transiently displayed less responses when the effort required to obtain reward increased to an FR5 schedule (Fig. 1i), suggesting a deficit in adapting to higher effort. We further assessed whether mNAcSh D3RcKO compromises motivation in an effort-based choice task where WT controls preferred to work for chocolate reward under an FR5 schedule over consuming freely available standard chow[27] (Fig. 1j). In contrast, NAc-D3RcKO mice consumed more standard chow than controls and did not show a chocolate reward preference (Fig. 1j). Importantly, overall food intake was similar across groups (Extended Data Fig. 2d), suggesting that decreased effort-based motivation is not a consequence of altered energy homeostatic drive. The same effect was observed when given a choice between operant-obtained chocolate reward and freely available chocolate reward (Extended Data Fig. 2e,f). Thus, control mice prefer to exert effort versus obtaining freely available reward and loss of mNAcSh D3Rs biases choice toward reward-seeking behaviors requiring less effort. This is consistent with reports demonstrating that decreasing NAc DA signaling increases intake of low-effort food rewards and decrease effort-based or activity-based reward seeking, without impacting overall food intake[28]. Subsequently, mice were subjected to progressive ratio (PR) schedules to further dissect the role of mNAcSh D3RcKO in regulating motivation. NAc-D3RcKO mice had decreased break points relative to WT controls in both PR3 (Fig. 1k) and PR7 (Fig. 1l) schedules, and decreased PR session lengths (Extended Data Fig. 2g,h). Collectively, these data demonstrate that motivated running and effort to obtain appetitive reward is disrupted with mNAcSh D3RcKO.

mNAcSh D3Rs are primarily expressed in D1-MSNs

The NAc is primarily composed of dichotomous cell types defined by DA receptor subtype (D1R-expressing and D2R-expressing MSNs), in addition to markers such as prodynorphin and proenkephalin[9]. To examine the NAc cell type expressing D3Rs, we performed fluorescence in situ hybridization experiments for *Drd1*, *Drd2* and *Drd3* mRNA. *Drd3* mRNA, along with *Drd1* and *Drd2*, was widely expressed in the NAc (Fig. 2a). Most mNAcSh *Drd3*-positive cells coexpressed *Drd1* (79.07%), with 20.51% coexpressing *Drd2* (Fig. 2b,c). Further, 86.69% and 13.26% of mNAcSh *Drd1*-positive and *Drd2*-positive neurons coexpressed *Drd3*, respectively (Fig. 2d), consistent with *Drd3* expression representing a substantial subpopulation of D1-MSNs. These percentages were lower in the NAc core, where 68.8% of *Drd3*-positive cells coexpressed *Drd1* (Extended Data Fig. 3a). Moreover, *Drd3* mRNA expression in D1-MSNs was 15% higher than in D2-MSNs (Fig. 2e). *Drd3* mRNA intensity was similar between *Drd1*-positive and *Drd2*-positive neurons in the NAc core and mNAcSh (Extended Data Fig. 3a). Moreover, *Drd3*-Cre mice crossed with tdTomato reporter had robust tdTomato labeling in the mNAcSh, islands of Calleja and medial core, but not dorsal striatum or NAc lateral shell (Extended Data Fig. 3b). Evidence of preferential expression of *Drd3* in mNAcSh D1-MSNs was also obtained when we recorded ChR2-mediated photocurrents in slices obtained from *Drd1*-tdtomato/*Drd3*-Cre mice injected with AAV-DIO-ChR2-eYFP (Fig. 2f). Consistent with in situ hybridization results, 77% of ChR2-positive neurons were tdTomato positive (Fig. 2f). *Drd3* is, therefore, expressed in mNAcSh D1-MSNs and less robustly in D2-MSNs, suggesting that DA generates divergent functions via distinct receptor subtypes in D1-MSNs.

NAc MSNs select appropriate goal-directed behaviors through connectivity with downstream brain regions. NAc D1-MSNs project to the ventral pallidum (VP), lateral hypothalamus (LH) and VTA, while NAc D2-MSNs projections are largely restricted to the VP[29,30]. We mapped *Drd3*-positive MSN projections using viral-assisted

Fig. 2 | mNAcSh D3Rs are primarily expressed in D1-MSNs and D3-MSNs display D1-MSN projection pattern. a, Representative low-magnification confocal image of RNA in situ hybridization for *Drd1* (green), *Drd2* (red) and *Drd3* (white) transcripts in the NAc. Orange inset shows the region targeted for zoomed images in **b**. **b**, Split high-magnification images of *Drd1*/*Drd3*, *Drd2*/*Drd3* and *Drd3* RNA expression in the mNAcSh. Right image is an overlay of all channels. Filled arrowheads show co-labeled cells, and empty arrowheads show single-labeled cells. **c**, Percentage of *Drd3*$^+$ cells coexpressing *Drd1* or *Drd2* RNA in the mNAcSh of WT mice ($n = 3$ mice; unpaired *t*-test (two-tailed), $t_{(4)} = 127.3$; $^{****}P < 0.0001$). **d**, Percentage of *Drd1*$^+$ or *Drd2*$^+$ cells coexpressing *Drd3* mRNA in the mNAcSh ($n = 3$ mice; unpaired *t*-test (two-tailed), $t_{(4)} = 33.52$; $^{****}P < 0.0001$). **e**, Mean relative expression levels of *Drd3* mRNA (mean integrated density/area) relative to D1-MSNs in *Drd3* mRNA-positive D2-MSNs ($n = 3$ mice; unpaired *t*-test (two-tailed), $t_{(4)} = 3.598$; $^{*}P = 0.0228$). **f**, Schematic for quantification of *Drd3*$^+$ cells using electrophysiological recordings. Representative trace showing light-evoked ChR2-mediated inward current in a ChR2-EYFP$^+$ NAc MSN evoked by 1-s stimulation with 470-nm blue light. Pie chart shows quantification of tdTomato-positive (D1-MSNs) versus tdTomato-negative (putative D2-MSNs) in recorded ChR2-positive cells. **g**, Left: Cre-dependent AAV-Syn-FLEX-tdTomato-T2A-Synaptophysin-GFP was injected in the mNAcSh of *Drd3*-Cre mice to visualize fibers (red) and synaptic terminals (green) in the outputs from D3-MSNs. Right: Representative images showing a high density of NAc D3-MSN synaptic terminals in the VP, LH and VTA. Dashed and solid white lines in fluorescent images depict borders between brain nuclei. **h**, Schematics of the electrophysiology experiment to assess functional connectivity from NAc D3-MSNs. A Cre-dependent AAV vector expressing ChR2-eYFP was injected in the mNAcSh of *Drd3*-Cre mice. Acute slices containing the VP, LH or VTA were prepared from brains of *Drd3*-Cre mice 2–3 weeks after viral injection. Right: representative traces showing oIPSCs in VP, LH and VTA cells. Red trace denotes bath application of picrotoxin (PTX). **i**, Same as in **h** but for mNAcSh to LH projections. **j**, Same as in **h** but for mNAcSh to VTA projections. **k**, Mean oIPSC amplitudes evoked by light stimulation of NAc D3-MSN terminals versus connectivity of D3-MSNs to VP, LH and VTA neurons. oIPSCs were detected in the majority of neurons recorded (VP, $n = 11$ of 12 neurons/7 mice; LH, $n = 12$ of 14 neurons/8 mice; VTA, $n = 11$ of 14 neurons/9 mice; one-way ANOVA followed by two-sided Tukey's test: $F_{(2,29)} = 1.993$. Group comparisons, VP versus LH, $P = 0.0025$, VP versus VTA, $P = 0.013$, LH versus VTA, $P = 0.937$). **l**, Left: schematic of the retrograde tracing approach to compare NAc *Drd3*-expressing projection MSNs. Red retrobeads were injected into the VP, LH or VTA of WT mice. NAc sections were probed for *Drd3* mRNA using in situ hybridization. Right: representative confocal images showing retrobead labeling from VP-projecting, LH-projecting or VTA-projecting NAc MSNs. High-magnification images showing red-labeled retrobeads in the NAc colocalized with *Drd3* mRNA indicated by filled arrowheads. **m**, Quantification of the percentage of retrobead-positive cells projecting to VP ($n = 5$ mice), LH ($n = 3$ mice) or VTA ($n = 3$ mice) that express *Drd3* in the NAc (one-way ANOVA followed by two-sided Tukey's test: $F_{(2,8)} = 17.69$. Group comparisons, VP versus LH, $^{**}P = 0.0078$, VP versus VTA, $^{**}P = 0.0015$, LH versus VTA, $P = 0.4929$). **n**, Mean expression levels of *Drd3* mRNA (mean integrated density/area) in neurons projecting to VP ($n = 5$ mice), LH ($n = 3$ mice) or VTA ($n = 3$ mice; one-way ANOVA followed by two-sided Tukey's test: $F_{(2,8)} = 14.83$. Group comparisons, VP versus LH, $^{**}P = 0.0025$, VP versus VTA, $^{*}P = 0.013$, LH versus VTA, $P = 0.5325$). All data are presented as mean ± s.e.m. Error bars indicate the s.e.m. Schematics were generated using BioRender.com. SNc, substantia nigra pars compacta; SNr, substantia nigra reticulata; BL, baseline.

https://doi.org/10.1038/s41593-024-01819-9

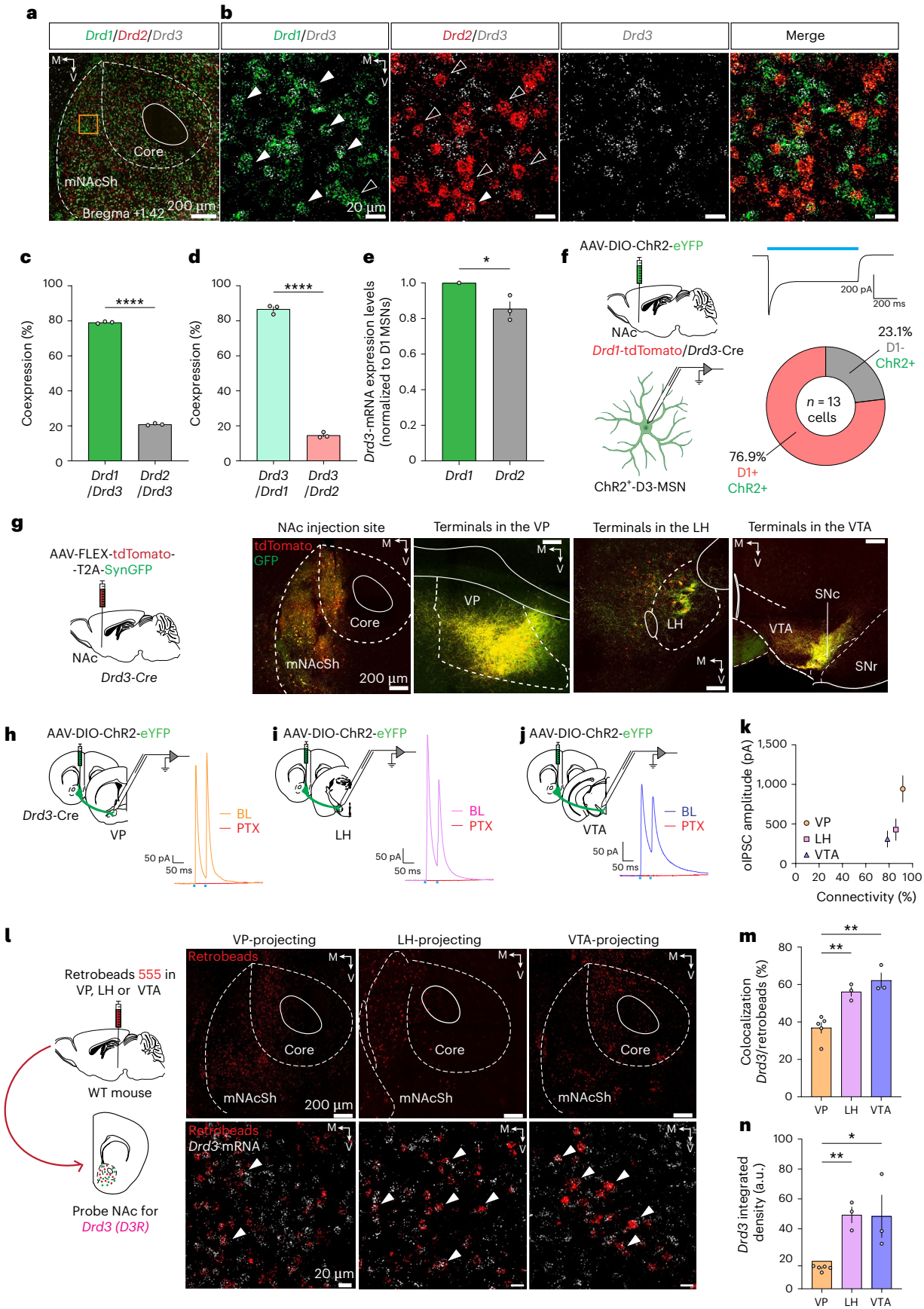

anterograde tracing. Intra-mNAcSh injection of AAV-FLEX-tdTomato-T2A-synaptophysin-eGFP in *Drd3*-Cre mice (Fig. 2g) labeled putative presynaptic terminals with synaptophysin-eGFP, distinct from bundles of tdTomato-positive fibers lacking eGFP (Supplementary Video 1). Consistent with D3R expression in D1-MSNs, GFP fluorescence revealed dense innervation within the mNAcSh, VP, LH and VTA (Fig. 2g). Quantification of tdTomato fluorescence showed that fibers of passage were most prominent in more anterior regions (that is, VP), in contrast to putative terminals in the LH or VTA (Extended Data Fig. 3c). Thus, *Drd3*-expressing MSNs project downstream to the VP, LH and VTA and form discrete synaptic contacts. We next used ChR2-assisted mapping to assess the functional connectivity between mNAcSh *Drd3*-expressing MSNs and output regions. Slice electrophysiology recordings from *Drd3*-Cre mice injected with Cre-dependent ChR2 showed picrotoxin (PTX)-sensitive, optogenetically evoked inhibitory postsynaptic currents (oIPSCs) in VP, LH and VTA neurons (Fig. 2h–k), indicating synaptic transmission mediated by $GABA_A$ receptors (Fig. 2h–j). These findings demonstrate mNAcSh D3-MSNs may regulate limbic circuits by sending inhibitory outputs to the VP, LH and VTA.

Distinct NAc D1-MSNs project to the VP, LH, and VTA[30–32]. Importantly, D1-MSN outputs constitute largely nonoverlapping NAc MSN populations with limited collateralization that exhibit differential plasticity in response to behavioral experiences[33,34]. However, collateralization of MSN outputs may be underestimated given various technical limitations, including inefficient retrograde labeling (for example, limited viral tropism) and incomplete coverage of output regions with tracers. To determine the proportion of *Drd3*-expressing MSNs projecting to each output, we performed retrograde tracing experiments in combination with in situ hybridization (Fig. 2l and Extended Data Fig. 3d). We found anatomical segregation between distinct NAc MSN-projecting neurons, as reported[30–32]. VP-projecting MSNs were present in both the NAc core and mNAcSh (Fig. 2l), LH-projecting MSNs were mainly in the mNAcSh (Fig. 2l) and VTA-projecting MSNs were in both the NAc core and mNAcSh (Fig. 2l). The proportion of *Drd3*-expressing MSNs projecting to the LH and VTA was higher than VP projectors (Fig. 2m). Further, *Drd3* mRNA expression was lower in VP-projecting MSNs, consistent with reduced expression in D2-MSNs (Fig. 2n). This illustration of how *Drd3*-expressing MSNs connect within the NAc and to the VP, LH and VTA led us to determine whether the role of mNAcSh D3Rs in regulating motivation varies by MSN projection.

Projection-independent mNAcSh D3R control of motivation

mNAcSh MSN projections to VP, LH and VTA control reward-related behaviors[32–34]. We thus hypothesized that D3R signaling in different MSN projections could differentially modulate motivated behavior. We tested this hypothesis by performing an intersectional cKO of mNAcSh *Drd3* expression in MSNs targeting the VP, LH or VTA. *Drd3*$^{fl/fl}$ mice or WT control mice were injected with CAV-Flp-GFP in VP, LH or VTA to express Flp recombinase in distinct mNAcSh MSN projection neurons (Fig. 3a,b). We then injected AAV-fDIO-Cre and AAV-FLEX-tdTomato (injection site confirmation) in the NAc to express Cre recombinase in VP-, LH- or VTA-projecting NAc neurons infected with retrograde expressing Flp, consequentially knocking out D3Rs in a pathway-specific manner (Extended Data Fig. 4a–c). Mice were tested for motivation in running and operant tasks. Selective deletion of D3Rs from MSNs projecting to the VP, LH or VTA decreased motivation to run in wheel running (Fig. 3c–e) and disk choice (Fig. 3f–h) tasks. D3RcKO in VP-projecting, LH-projecting or VTA-projecting MSNs diminished wheel-running activity upon first exposure during the light, inactive cycle (Fig. 3c–e), but not in response to diurnal shift to the dark, active cycle (Extended Data Fig. 5a). The only exception were mice lacking D3R expression from VTA-projecting mNAcSh MSNs, which displayed decreased dark cycle-initiated running (Extended Data Fig. 5a). We addressed if our CAV approach was toxic to highly vulnerable DA neurons of the VTA by injecting CAV-FlpO-GFP in the VTA of *Drd3*$^{fl/fl}$ and performing tyrosine hydroxylase (TH) immunohistochemistry in both injected and uninjected sides (Extended Data Fig. 4d). CAV-Flp-GFP did not change the number of TH-positive cells and TH levels (Extended Data Fig. 4e,f). D3R is essential for promoting motivated running behavior irrespective of projection target and/or is required in limited MSNs that collateralize multiple outputs.

We then assessed the effect of pathway-specific D3RcKO from VP-projecting, LH-projecting or VTA-projecting mNAcSh MSNs in operant procedures. *Drd3*$^{fl/fl}$ mice did not show changes in body weights (Extended Data Fig. 5b) or acquisition of responding on an FR1 schedule (Fig. 3i and Extended Data Fig. 5c,d) relative to WT controls in all pathways. Interestingly, mice with selective cKO of *Drd3* from VTA-projecting mNAcSh neurons had increased lever pressing under FR5 schedules (Extended Data Fig. 5e). This may reflect (1) enhanced reward seeking, (2) decreased reward value and compensatory increases in reward seeking and/or (3) differential hunger/satiety. During choice tests between freely available chow versus

Fig. 3 | NAc D3R is essential for motivated behavior independent of projection neuron. a, Diagram of viral injections for pathway-specific deletion of NAc *Drd3* from distinct MSN projections. Flp-dependent Cre and Cre-dependent tdTomato were injected bilaterally in the NAc of WT or *Drd3*$^{fl/fl}$, and CAV-Flp-GFP was injected in the VP, LH or VTA to selectively knockdown *Drd3* expression in VP-projecting, LH-projecting or VTA-projecting NAc MSNs. **b**, Left: scheme showing fDIO-dependent Cre expression and recombination resulting in excision of exon 1 of the *Drd3* gene between flanking loxP sites. Right: representative images of GFP and tdTomato expression in mNAcSh MSNs. Note that AAV-fDIO-Cre did not cause recombination in Ai14-tdTomato reporter mice injected in the mNAcSh (Extended Data Fig. 4b). Dashed and solid white lines in fluorescent images depict borders between brain nuclei. **c**–**e**, Time-course of revolutions of wheel-running activity during the first 12 h of running wheel exposure in WT or *Drd3*$^{fl/fl}$ mice with pathway-specific deletion in the VP (**c**; unpaired *t*-test (two-tailed), $t_{(10)} = 3.261$; $^{**}P = 0.0086$), LH (**d**; unpaired *t*-test (two-tailed), $t_{(9)} = 2.388$; $^{*}P = 0.0407$) and VTA (**e**; unpaired *t*-test (two-tailed), $t_{(12)} = 2.819$; $^{*}P = 0.0155$). **f**–**h**, Quantification of both time spent and wheel revolutions on the freely moving and fixed disk for mice with the following injections: WT-VP ($n = 5$ mice) and *Drd3*$^{fl/fl}$-VP ($n = 7$ mice) (**f**; time spent two-way repeated-measures ANOVA: disk effect, $F_{(1,22)} = 14.35$, $P = 0.01$; genotype effect, $F_{(1,22)} = 5.528$, $P = 0.0281$; disk × genotype, $F_{(1,22)} = 6.613$, $P = 0.0174$; revolutions unpaired *t*-test (two-tailed), $t_{(11)} = 4.909$; $^{***}P = 0.0005$), WT-LH ($n = 5$ mice) and *Drd3*$^{fl/fl}$-LH ($n = 6$ mice) (**g**; time spent two-way repeated-measures ANOVA: disk effect, $F_{(1,14)} = 48.84$, $P < 0.0001$; genotype effect, $F_{(1,14)} = 11.43$, $P = 0.0045$; disk × genotype, $F_{(1,14)} = 17.13$, $P = 0.001$; revolutions unpaired *t*-test (two-tailed), $t_{(9)} = 6.117$; $^{***}P = 0.0002$) and WT-VTA ($n = 5$ mice) and *Drd3*$^{fl/fl}$-VTA ($n = 9$ mice) (**h**; time spent two-way repeated-measures ANOVA: disk effect, $F_{(1,24)} = 10.93$, $P = 0.003$; genotype effect, $F_{(1,24)} = 3.092$, $P = 0.0914$; disk × genotype, $F_{(1,24)} = 7.790$, $P = 0.0101$; revolutions unpaired *t*-test (two-tailed), $t_{(12)} = 3.825$; $^{**}P = 0.0024$). ** in **f** represents a difference between time spent on the freely-moving and fixed disk in WT mice. **** in **g** represents a difference between time spent on the freely-moving and fixed disk in WT mice. **i**, Number of active and inactive lever presses of WT (black, $n = 12$ mice), *Drd3*$^{fl/fl}$-VP (orange, $n = 7$ mice), *Drd3*$^{fl/fl}$-LH (pink, $n = 6$ mice) and *Drd3*$^{fl/fl}$-VTA (purple, $n = 7$ mice) animals during FR1 sessions (two-way repeated-measures ANOVA: session effect, $F_{(3.340,82.84)} = 57.05$, $P < 0.0001$; genotype effect, $F_{(3,26)} = 0.3733$, $P = 0.7729$; session × genotype, $F_{(15,124)} = 1.452$, $P = 0.1341$). **j**, Amount of freely available food consumed in the FR5 choice task (WT, $n = 10$ mice; *Drd3*$^{fl/fl}$-VP, $n = 7$ mice; *Drd3*$^{fl/fl}$-LH, $n = 6$ mice; *Drd3*$^{fl/fl}$-VTA, $n = 7$ mice; one-way ANOVA followed by two-sided Dunnett's test: $F_{(3,28)} = 5.602$. Group comparisons, WT versus *Drd3*$^{fl/fl}$-VP, $P = 0.0572$, WT versus *Drd3*$^{fl/fl}$-LH, $^{*}P = 0.0219$, WT versus *Drd3*$^{fl/fl}$-VTA, $^{**}P = 0.0031$). **k**, Break points for WT and *Drd3*$^{fl/fl}$ mice during PR7 sessions (WT, $n = 13$ mice; *Drd3*$^{fl/fl}$-VP, $n = 7$ mice; *Drd3*$^{fl/fl}$-LH, $n = 7$ mice; *Drd3*$^{fl/fl}$-VTA, $n = 8$ mice; one-way ANOVA followed by two-sided Dunnett's test: $F_{(3,31)} = 5.322$. Group comparisons, WT versus *Drd3*$^{fl/fl}$-VP, $^{*}P = 0.0131$, WT versus *Drd3*$^{fl/fl}$-LH, $^{**}P = 0.0043$, WT versus *Drd3*$^{fl/fl}$-VTA, $P = 0.2061$). All data are presented as mean ± s.e.m. Error bars indicate the s.e.m.

https://doi.org/10.1038/s41593-024-01819-9

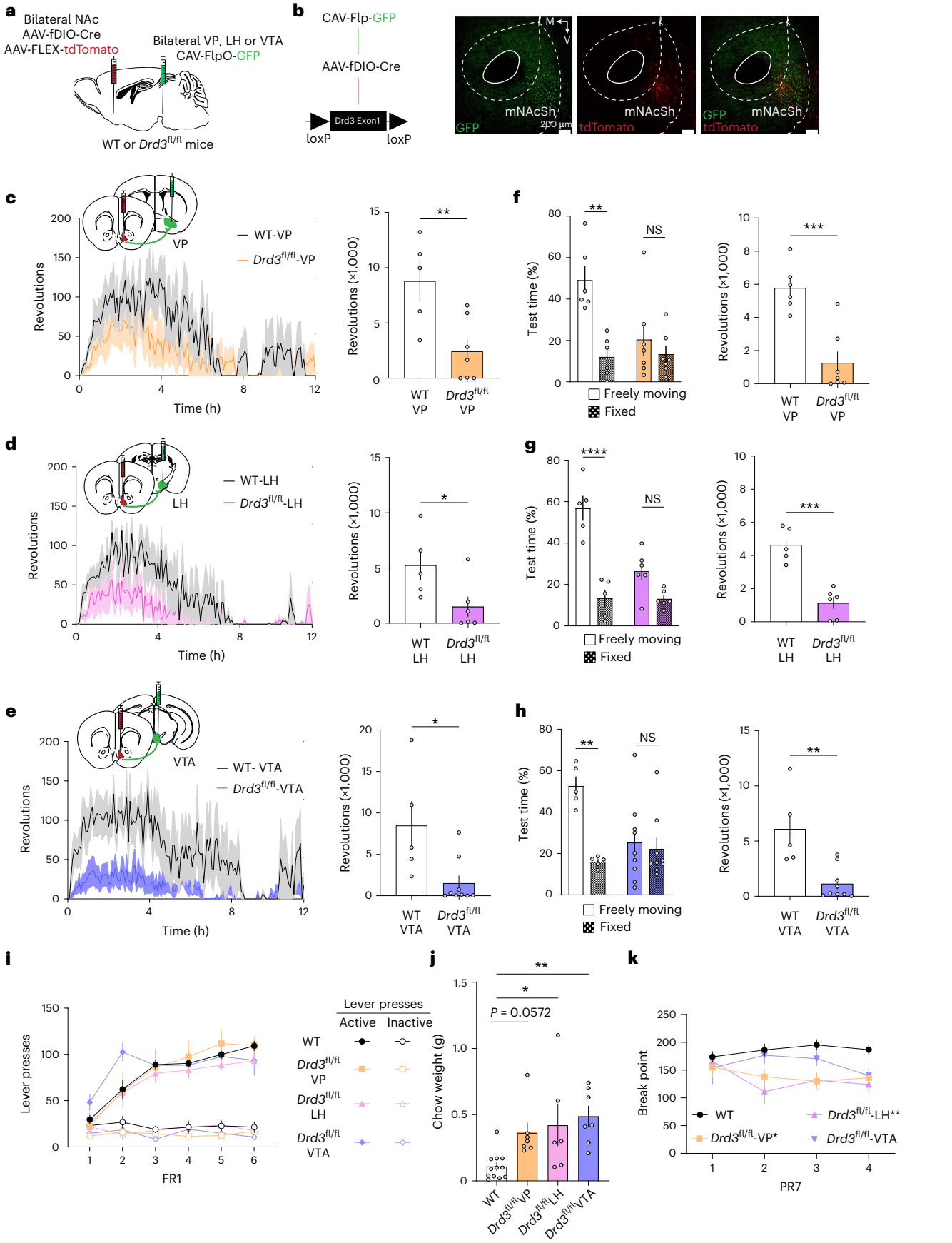

operant-derived chocolate, selective D3RcKO from VP-projecting, LH-projecting or VTA-projecting MSNs increased freely available chow intake (Fig. 3j and Extended Data Fig. 5f). This effect was also present during choice testing involving operant-derived and freely available chocolate (Extended Data Fig. 5g,h), indicating that *Drd3* cKO from either pathway biased consummatory behavior toward low-effort rewards. mNAcSh D3RcKO from VP-projecting and LH-projecting MSNs resulted in deficits in motivation as shown by decreased breaking points in PR7 (Fig. 3k), but not PR3 (Extended Data Fig. 5i), with no significant effect in mice lacking D3Rs in VTA-projecting MSNs. This demonstrates that pathway-specific cKO of D3Rs in LH-projecting and VP-projecting neurons suppresses running and operant-based motivated behavior, but not instrumental reinforcement. In contrast, D3RcKO from NAc to VTA neurons impacted running behavior and had mixed effects in operant settings.

D3R regulates local mNAcSh collaterals and VP outputs

$G_{i/o}$-coupled GPCRs, like D3Rs, regulate circuit function by inhibiting neurotransmitter release from axon terminals[35]. Local collaterals arising from NAc MSNs constitute a large portion of inhibitory synapses onto MSNs, which are regulated by $G_{i/o}$-coupled GPCRs and are implicated in controlling striatal circuit recruitment during reward-related behaviors[36,37]. We determined the functional effects of D3R signaling on inhibitory synaptic transmission from MSN collaterals to neighboring MSNs. *Drd1*-tdTomato/*Drd3*-Cre mice were injected with a virus expressing ChR2-eYFP in Cre-expressing neurons (Cre-ON; AAV-DIO-ChR2-eYFP) or Cre-negative neurons (Cre-OFF; AAV-DO-ChR2-eYFP), to selectively evoke GABA release from *Drd3*-positive MSNs or *Drd3*-negative mNAcSh cells, respectively (Fig. 4a,b). Baseline oIPSC amplitudes evoked from *Drd3*-negative mNAcSh cells were larger than from *Drd3*-positive neurons (Extended Data Fig. 6a). In ChR2-negative mNAcSh MSNs recorded from mice expressing ChR2-eYFP in D3R-positive MSNs (Cre-ON), D3R activation with the D3R-selective agonist PD-128907 (1 µM) decreased oIPSC amplitude (Fig. 4c). Conversely, oIPSCs evoked from D3R-negative mNAcSh cells (Cre-OFF) were insensitive to PD-128907 (Fig. 4c). These results suggest a presynaptic site of action for depression of D3-MSN collateral transmission by D3Rs. In line with a role for presynaptic D3R in the regulation of mNAcSh collaterals, the paired-pulse ratio (PPR) increased (Fig. 4d), and the inverse square of the coefficient of variation ($1/CV^2$) decreased (Fig. 4e) with PD-128907 in the Cre-ON group relative to baseline. Changes in PPR and $1/CV^2$ in the Cre-ON group also differed from the Cre-OFF group (Fig. 4d,e). These findings validate the selectivity of PD-128907 for the D3R and selective viral-mediated transgene expression in *Drd3*-expressing mNAcSh MSNs in *Drd3*-Cre mice. The novel, highly selective D3R agonist ML417 (ref. 38) also inhibited mNAcSh MSN collaterals (Extended Data Fig. 6b–d). The frequency of spontaneous inhibitory postsynaptic currents (sIPSCs), but not amplitude, was decreased with PD-128907 application (Extended Data Fig. 6f,g), consistent with widespread D3R expression in D1-MSNs and subsets of D2-MSNs. We next determined whether presynaptic D3R signaling differentially inhibited MSN collaterals onto D1-MSNs and D2-MSNs (Fig. 4b). Application of PD-128907 similarly inhibited oIPSCs evoked by optogenetic stimulation of D3-MSN collaterals onto D1-MSNs and D2-MSNs (Extended Data Fig. 6h,i). Moreover, we injected *Drd3*-Cre mice in the mNAcSh with a Cre-dependent AAV expressing the cAMP sensor, cADDis, to monitor cAMP activity in acute NAc slices (Extended Data Fig. 6j). Using ex vivo imaging, we isolated D3R effects on cAMP activity using the D1R antagonist SCH-39166 (Extended Data Fig. 6k). cAMP activity was inhibited with application of DA in the presence of SCH-39166 (Extended Data Fig. 6l), with the caveat that responses may also be mediated by DA acting in D2Rs expressed in D3R/D2R MSNs. Collectively, these results demonstrate that presynaptic D3R inhibits GABAergic outputs from MSN collaterals onto D1-MSNs and D2-MSNs.

We next identified whether presynaptic D3Rs regulate GABAergic synaptic transmission to VP, LH and VTA neurons. D3R activation with PD-128907 decreased GABA release onto VP neurons that was optogenetically evoked from *Drd3*-positive MSNs (Fig. 4f,g), in addition to increasing the PPR and decreasing the $1/CV^2$ relative to baseline (Fig. 4h,i). Conversely, GABA release from D3R-negative mNAcSh neurons (Cre-OFF ChR2) onto VP neurons was not inhibited by PD-128907 (Fig. 4g). These findings demonstrate that D3Rs inhibit GABA release from MSNs onto VP neurons via a presynaptic site of action. Interestingly, D3R activation failed to decrease oIPSC amplitude in both LH and VTA neurons (Fig. 4j–q), suggesting that MSN connections onto LH and VTA neurons lack functional D3R. Taken together, these results show that presynaptic D3R on mNAcSh MSNs selectively inhibits local collaterals and GABAergic transmission to the VP, but not in the outputs to the LH and VTA.

Motivated behavior requires local mNAcSh D3R signaling

Our electrophysiology results demonstrate that mNAcSh collaterals and VP, but not LH and VTA, outputs, are inhibited by D3Rs. Despite this, mNAcSh D3Rs cKO VP-projecting, LH-projecting or VTA-projecting neurons each produced motivational deficits. We hypothesized that D3R signaling is acting within mNAcSh circuits to influence motivated behavior. Intra-mNAcSh microinfusion of the D3R antagonist SB-277011A[39] (1.8 ng per infusion site) decreased preference for, and running on, the disk choice task (Fig. 5a–c), consistent with intra-mNAcSh D3R signaling being essential for motivated running.

Fig. 4 | D3Rs regulate GABAergic transmission from NAc collaterals and to the VP via a presynaptic site of action. a, Diagram of virus injection of AAV-EF1a-DIO-ChR2-eYFP (Cre-ON) and AAV-EF1a-DO-ChR2-eYFP (Cre-OFF) in the NAc of *Drd1*-tdTomato/*Drd3*-Cre mice. ChR2-eYFP-expressing cell bodies of D3R-positive and D3R-negative terminals in the mNAcSh and total NAc area. Note the lack of expression in the Islands of Calleja (ICj) in mice expressing Cre-OFF ChR2 in the ventral striatum. **b**, oIPSCs originating from D3R-positive and D3R-negative collaterals were recorded from mNAcSh D1-MSNs or D2-MSNs. **c**,**g**,**k**,**o**, Time-course of oIPSCs in mNAcSh MSNs (**c**; two-way repeated-measures ANOVA: time effect, $F_{(3.099,89.38)} = 39.75$, $P < 0.0001$; treatment effect, $F_{(1,29)} = 28.21$, $P < 0.0001$; time × treatment, $F_{(19,548)} = 13.08$, $P < 0.0001$), VP cells (**g**; two-way repeated-measures ANOVA: time effect, $F_{(1.912,34.41)} = 11.18$, $P = 0.0002$; treatment effect, $F_{(1,18)} = 7.030$, $P = 0.0162$; time × treatment, $F_{(19,342)} = 4.923$, $P < 0.0001$), LH cells (**k**, $n = 9$ cells/8 mice) and VTA cells (**o**, $n = 10$ cells/8 mice) before, during and after bath application of the D3R-selective agonist PD-128907 (1 µM). For mNAcSh MSNs and VP neurons, Cre-ON groups for mNAcSh (blue, $n = 16$ cells/9 mice) or VP neurons (orange, $n = 10$ cells/7 mice), while the Cre-OFF group is shown in black ($n = 15$ cells/7 mice for NAc; $n = 10$ cells from 6 mice for VP). Insets show representative oIPSCs traces recorded in mNAcSh MSNs before and after bath application of PD-128907. **d**,**h**,**l**,**p**, PPR (% baseline) versus oIPSC (% baseline) for mNAcSh MSNs (**d**; PPR unpaired *t*-test (two-tailed), $t_{(29)} = 2.732$; $^{*}P = 0.0106$; oIPSC amplitude unpaired *t*-test (two-tailed), $t_{(29)} = 5.181$; $^{****}P < 0.0001$), VP cells (**h**; PPR unpaired *t*-test (two-tailed), $t_{(18)} = 2.457$; $^{*}P = 0.0244$; oIPSC amplitude unpaired *t*-test (two-tailed), $t_{(18)} = 2.503$; $^{*}P = 0.0222$), LH cells (**l**) and VTA cells (**p**). **e**,**i**,**m**, Coefficient of variation ($1/CV^2$, % baseline) versus oIPSC (% baseline) for mNAcSh MSNs (**e**; $1/CV^2$ unpaired *t*-test (two-tailed), $t_{(29)} = 3.632$; $^{**}P = 0.0011$; oIPSC amplitude unpaired *t*-test (two-tailed), $t_{(29)} = 5.181$; $^{****}P < 0.0001$), VP cells (**i**; $1/CV^2$ unpaired *t*-test (two-tailed), $t_{(18)} = 2.457$; $^{*}P = 0.0455$; oIPSC amplitude unpaired *t*-test (two-tailed), $t_{(18)} = 2.148$; $^{*}P = 0.0222$) and LH cells (**m**). **f**,**j**,**n**, Images of ChR2-positive fibers in the VP (**f**), LH (**j**) and VTA (**n**). Dashed and solid white lines in fluorescent images in **a**, **f**, **j** and **n** depict borders between brain nuclei. **q**, Summary graph of the inhibition of oIPSCs by PD-128907 from mNAcSh ($n = 16$ cells from 9 mice), VP ($n = 10$ cells/7 mice), LH ($n = 9$ cells/8 mice) or VTA ($n = 10$ cells/8 mice) neurons in Cre-ON condition (one-way ANOVA followed by two-sided Tukey's test: $F_{(3,41)} = 6.750$. Group comparisons, NAc versus VP, $P > 0.9999$, NAc versus LH, $^{**}P = 0.0051$, NAc versus VTA, $^{*}P = 0.02$, VP versus LH, $^{*}P = 0.013$, VP versus VTA, $^{*}P = 0.0436$, LH versus VTA, $P = 0.9451$). All data are presented as the mean ± s.e.m. Error bars indicate the s.e.m. BL, baseline.

https://doi.org/10.1038/s41593-024-01819-9

However, mNAcSh D3R antagonism blocks D3R signaling in MSNs plus putative afferent inputs expressing D3Rs at their terminals[40,41]. To specifically assess whether D3R acting on MSNs locally within mNAcSh microcircuitry drives motivation, we implemented new functional disconnection procedures involving pharmacological D3R antagonism and mNAcSh D3RcKO (Fig. 5d). Control *Drd3*$^{fl/fl}$ mice received direct microinfusion of SB-277011A and ipsilateral AAV-hSyn-GFP-Cre into the mNAcSh (Fig. 5d). In controls, the unmanipulated hemisphere contains intact D3R signaling, supporting motivated behavior (Fig. 5e–g). Our experimental group (contralateral *Drd3*$^{fl/fl}$ mice) underwent functional disconnections wherein mNAcSh microinjections of SB-277011A and AAV-hSyn-GFP-Cre were made in contralateral hemispheres. Here, only D3R signaling in MSNs within the mNAcSh undergoes bilateral disruption (Fig. 5e). If motivated running behavior does not rely on local MSN D3R signaling, then independently manipulating D3R activity in each hemisphere should not disrupt mNAcSh D3R-mediated motivation. Conversely, if motivation is mediated by intra-mNAcSh D3R signaling in MSNs, then contralateral disconnection should disrupt motivation. Indeed, contralateral *Drd3*$^{fl/fl}$ mice displayed decreased running behavior and preference toward the freely moving disk relative to ipsilateral counterparts (Fig. 5f,g). As additional controls, we also quantified running disk performance in *Drd3*$^{fl/fl}$ mice unilaterally

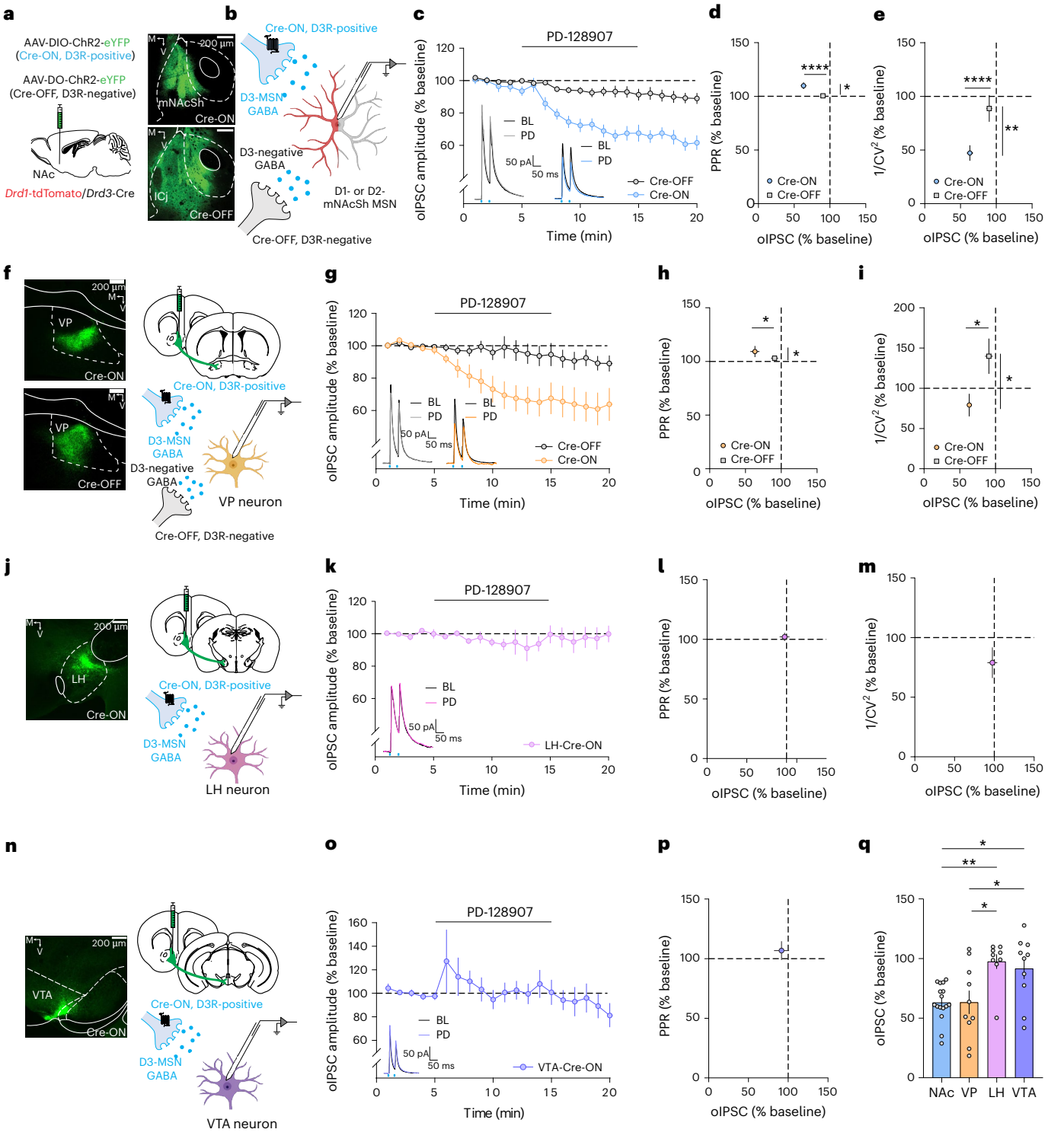

https://doi.org/10.1038/s41593-024-01819-9

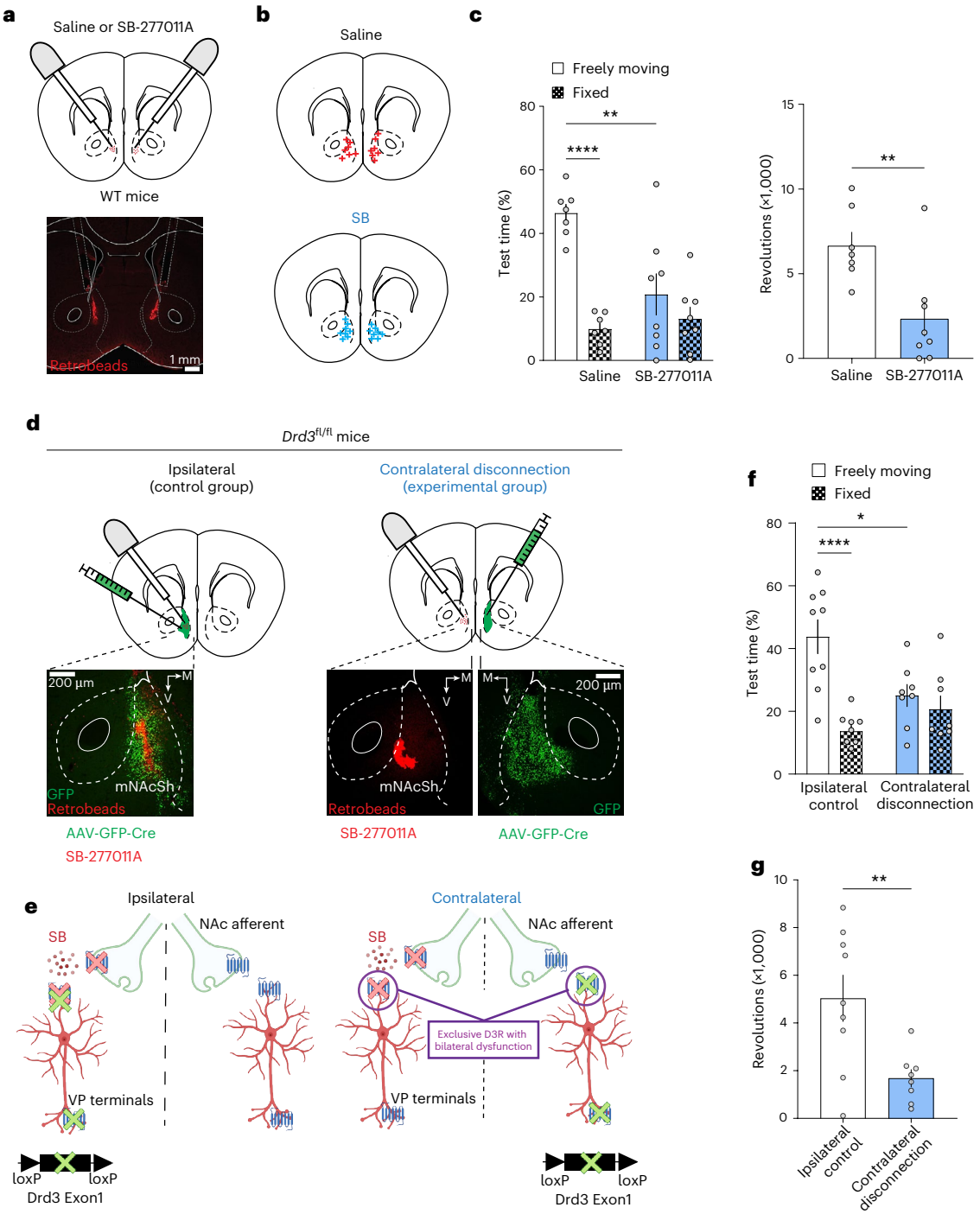

injected with Cre-expressing virus or WT mice that had unilateral infusions of SB-277011A, which failed to modify preference for the freely moving disk (Extended Data Fig. 7a,b). Together, these results suggest that D3Rs acting on MSNs locally within mNAcSh microcircuitry are necessary for motivated behavior.

Specific effects of D3R signaling, such as inhibition of local collaterals and outputs to the VP, may underlie regulation of motivation. We compared the effects of non-selectively activating $G_{i/o}$-coupled GPCRs broadly throughout the cell using chemogenetics, which contrast with $G_{i/o}$-coupled D3Rs, which likely have specialized localization within MSNs. In contrast to D3R control of motivated running, chemogenetic inhibition with clozapine *N*-oxide (CNO) reduced preference for the freely moving disk and decreased running behavior in hM4Di-expressing mice relative to mCherry controls (Extended Data Fig. 7c,d). Chemogenetic inhibition of D3-MSNs did not affect locomotor activity or anxiety-like behavior in the open field (Extended Data Fig. 7e). These results suggest that specialized cellular consequences of D3R signaling in mNAcSh MSNs rather than broad inhibition controls motivation to run.

mNAcSh D1Rs mediate action–outcome contingencies

As *Drd3* is largely coexpressed with *Drd1* (Fig. 2a–d), we determined whether D3R and D1R differ in controlling reward. As low-affinity receptors, NAc D1Rs modulate reward-related behaviors presumably by detecting phasic DA and modifying synaptic transmission onto MSNs[42,43]. To assess this, *Drd1*$^{fl/fl}$ mice were injected with intra-mNAcSh

Fig. 5 | Motivated behavior requires local D3R signaling within the mNAcSh. **a**, Diagram and representative image of bilateral microinjection of the D3R antagonist SB-277011A (1.8 ng per hemisphere) into the mNAcSh of WT mice. Red retrobeads were infused after the experiment to confirm accuracy of cannula placement. **b**, Cannula tip placements for saline and SB-277011A groups. **c**, Percentage of time spent on the freely moving and fixed disk for saline (white, $n = 7$ mice) and D3R antagonist (blue, $n = 8$ mice) groups during the running disk choice task (two-way repeated-measures ANOVA: disk effect, $F_{(1,26)} = 25.56$, $P < 0.0001$; treatment effect, $F_{(1,26)} = 6.573$, $P = 0.0165$; disk × treatment, $F_{(1,26)} = 10.83$, $P = 0.0029$). Number of revolutions recorded in the freely moving disk (unpaired t-test (two-tailed), $t_{(13)} = 3.206$; $^{**}P = 0.0069$). **** represents a difference between time spent on the freely-moving and fixed disk in saline controls. **d**, Diagrams and representative images of selective inactivation of local mNAcSh D3R function using functional disconnection experiments. Mice were injected unilaterally with AAV8-Syn-GFP-Cre into the mNAcSh of *Drd3*$^{fl/fl}$ mice. Ipsilateral (control) and contralateral disconnection (experimental) groups were infused with SB-277011A into the ipsilateral and contralateral mNAcSh, respectively. Dashed and solid white lines in fluorescent images depict borders between brain nuclei. **e**, Diagram describing rationale for disconnection procedures. In the ipsilateral group, one hemisphere was targeted with SB-277011A and AAV-GFP-Cre to suppress D3R signaling within the mNAcSh and at terminals in the VP, while the other hemisphere had intact D3R signaling. For the contralateral group, the only common D3R dysfunction in both hemispheres was local D3R signaling within the mNAcSh (purple circles), which was targeted by antagonist infusion and contralateral injection of AAV-GFP-Cre. **f**, Percentage of time spent on the freely moving (solid) and fixed (checkered) disks for ipsilateral control (white, $n = 9$ mice) and contralateral disconnection (blue, $n = 8$ mice) groups (two-way repeated-measures ANOVA: disk effect, $F_{(1,30)} = 18.60$, $P = 0.0002$; treatment effect, $F_{(1,30)} = 2.149$, $P = 0.1531$; disk × treatment, $F_{(1,30)} = 10.30$, $P = 0.0032$). **** represents a difference between time spent on the freely-moving and fixed disk in ipsilateral controls. * represents a significant difference between time spent on freely-moving disk between ipsilateral controls and contralateral disconnection mice. **g**, Number of revolutions registered in the freely moving disk (ipsilateral, $n = 9$ mice; contralateral, $n = 8$ mice; unpaired t-test (two-tailed), $t_{(15)} = 3.072$; $^{**}P = 0.0077$). All data are presented as the mean ± s.e.m. Error bars indicate the s.e.m. Schematics were generated using BioRender.com.

AAV-Cre (NAc-D1RcKO) and run concomitantly with NAc-D3RcKO experiments from Fig. 1 (Fig. 6a). mNAcSh *Drd1* cKO decreased FR1 acquisition (Fig. 6b), which transiently persisted under FR5 schedules (Fig. 6c). Together, these results indicate that mNAcSh D1RcKO impairs action–outcome contingencies associated with reinforcement, although motivation impairments cannot be fully excluded. To further dissect the impact of mNAcSh D1RcKO on motivated behavior, we tested animals on the effort-based choice task. Unlike NAc-D3RcKO mice, NAc-D1RcKO mice preferred to work for a higher-palatable reward (Fig. 6d). Furthermore, break points during PR schedules did not differ between WT and NAc-D1RcKO mice (Fig. 6e), indicating that motivation to seek palatable rewards remained unaffected. Similarly, mNAcSh *Drd1* cKO did not strongly impact motivated running in the running wheel and disk choice tasks (Fig. 6f,g and Extended Data Fig. 8a). Furthermore, mNAcSh *Drd1* cKO did not alter sucrose preference (Extended Data Fig. 8b), sociability (Extended Data Fig. 8c) and light–dark box (Extended Data Fig. 8d) or novel object recognition (Extended Data Fig. 8e) tests, indicating that mNAcSh D1R function is not essential for hedonic processing, anxiety-like or novelty-seeking behaviors, respectively. Together, this suggests that D1Rs, but not D3Rs, play a role in instrumental reinforcement possibly delaying the development of action–outcome associations.

Fig. 6 | mNAcSh D1Rs mediate reinforcement but not motivation. **a**, Scheme and representative image depicting the mNAcSh area targeted with AAV-GFP-Cre (green) for experiments shown in **b**–**i**. Dashed and solid white lines in fluorescent images depict borders between brain nuclei. **b**, Number of active (filled) and inactive (unfilled) lever presses of WT (black, $n = 15$ mice), NAc-D3RcKO (blue, $n = 11$ mice) and NAc-D1RcKO (green, $n = 15$ mice) animals during sessions with FR1 (two-way repeated-measures ANOVA: session effect, $F_{(5,225)} = 28.09$, $P < 0.0001$; genotype effect, $F_{(2,225)} = 22.75$, $P < 0.0001$; session × genotype, $F_{(10,225)} = 2.009$, $P = 0.0335$). **c**, Active and inactive lever presses during FR5 schedule of reinforcement (two-way repeated-measures ANOVA: session effect, $F_{(4.192,158.1)} = 3.664$, $P = 0.0061$; genotype effect, $F_{(2,38)} = 1.288$, $P = 0.2876$; session × genotype, $F_{(14,264)} = 2.455$, $P = 0.0029$). ** in **b** represents a main effect of genotype. **d**, Amount of food consumed during the effort-related choice task represented as FR5 effort-based (solid) or freely available (checkered) lab chow (WT, $n = 15$ mice; NAc-D3RcKO, $n = 11$ mice; NAc-D1RcKO, $n = 15$ mice; two-way repeated-measures ANOVA: type of food effect, $F_{(1,38)} = 54.48$, $P < 0.0001$; genotype effect, $F_{(2,38)} = 0.3460$, $P = 0.7098$; type of food × genotype, $F_{(2,38)} = 5.604$, $P = 0.0074$). * represents a significant difference between mNAcSh-D3RcKO and mNAcSh-D1RcKO in ad libitum chow intake. **e**, Break points for WT, NAc-D3RcKO and NAc-D1RcKO mice during PR7 sessions (WT, $n = 15$ mice; NAc-D3RcKO, $n = 11$ mice; NAc-D1RcKO, $n = 15$ mice; two-way repeated-measures ANOVA: session effect, $F_{(2.083,77.06)} = 1.343$, $P = 0.2673$; genotype effect, $F_{(2,38)} = 7.908$, $P = 0.0013$; session × genotype, $F_{(6,111)} = 1.458$, $P = 0.1992$). **f**, Left: time-course of wheel-running activity during the initial 12-h period of wheel exposure (in the animal's inactive cycle) in WT-Cre ($n = 11$ mice), NAc-D3RcKO ($n = 12$ mice) and NAc-D1RcKO ($n = 8$ mice) mice (two-way repeated-measures ANOVA: time effect, $F(7.527, 210.7) = 16.63$, $P < 0.0001$; genotype effect, $F_{(2,28)} = 10.86$, $P = 0.0003$; time × genotype, $F_{(286,4,004)} = 2.216$, $P < 0.0001$). Right: quantification of revolutions during the 12-h period (one-way ANOVA followed by two-sided Dunnett's test: $F_{(2,28)} = 12.20$. Group comparisons, NAc-D1RcKO versus WT, $P = 0.1044$, NAc-D1RcKO versus NAc-D3RcKO, $^{*}P = 0.0324$). **g**, Quantification of time (left) and revolutions (right) for WT ($n = 11$ mice), NAc-D3RcKO ($n = 12$ mice) and NAc-D1RcKO ($n = 8$ mice) groups during the running disk choice task. Percentage of test time spent on the freely moving and fixed disk (two-way repeated-measures ANOVA: disk effect, $F_{(1,28)} = 98.11$, $P < 0.0001$; genotype effect, $F_{(2,28)} = 20.86$, $P < 0.0001$; disk × genotype, $F_{(2,28)} = 33.49$, $P < 0.0001$). Number of revolutions recorded in the freely moving disk for each group (one-way ANOVA followed by two-sided Dunnett's test: $F_{(2,28)} = 56.43$. Group comparisons, NAc-D1RcKO versus WT, $P = 0.0614$, NAc-D1RcKO versus NAc-D3RcKO, $^{****}P < 0.0001$). **h**, Scheme of the platform-mediated avoidance task. Mice were placed in an operant box and were presented with 20 pairings of conditioned stimulus (CS) and a footshock as the unconditioned stimulus (US). Animals could step onto the platform to actively avoid a footshock. ITI, intertrial interval. **i**, Quantification of trial outcome (avoidance or shock) as a percentage of total trials for day 1 (left; two-way repeated-measures ANOVA: outcome effect, $F_{(1,35)} = 31.35$, $P < 0.0001$; genotype effect, $F_{(2,35)} = 1.089$, $P = 0.3478$; outcome × genotype, $F_{(2,35)} = 6.589$, $P = 0.0037$) and percentage of time spent on the platform for day 1 (right; one-way ANOVA followed by two-sided Dunnett's test: $F_{(2,35)} = 14.14$. Group comparisons, NAc-D1RcKO versus WT, $^{****}P < 0.0001$, NAc-D1RcKO versus NAc-D3RcKO, $^{***}P = 0.0004$) in WT-Cre ($n = 12$ mice), NAc-D3RcKO ($n = 9$ mice) and NAc-D1RcKO mice ($n = 17$ mice). ** represents a significant difference between WT and mNAcSh-D1RcKO mice. * represents a significant difference between mNAcSh-D3RcKO and mNAcSh-D1RcKO mice. **j**, Pavlovian conditioning procedures. Experiments involved learning to discriminate reward-predictive cues (CS+) and a neutral cue (CS−), as well as subsequent extinction procedures. **k**, Time-course of nose pokes for the last day of training on CS+ (left; two-way repeated-measures ANOVA: time effect, $F_{(3.834,115.0)} = 115.6$, $P < 0.0001$; genotype effect, $F_{(2,30)} = 1.025$, $P = 0.371$; time × genotype, $F_{(40,620)} = 1.175$, $P = 0.2174$) and CS− (right; two-way repeated-measures ANOVA: time effect, $F(2.974, 92.18) = 2.280$, $P = 0.0851$; genotype effect, $F_{(2,31)} = 1.222$, $P = 0.3083$; time × genotype, $F_{(40,620)} = 0.6634$, $P = 0.9458$) sessions for WT-Cre ($n = 11$ mice), NAc-D3RcKO ($n = 14$ mice) and NAc-D1RcKO ($n = 8$ mice) mice. **l**, Quantification of the area under the curve (AUC) after CS in WT ($n = 11$ mice), NAc-D3RcKO ($n = 14$ mice) and NAc-D1RcKO ($n = 8$ mice) groups for sessions 1, 3 and 6 of reward learning for CS+ (two-way repeated-measures ANOVA: session effect, $F_{(2,56)} = 28.90$, $P < 0.0001$; genotype effect, $F_{(2,29)} = 0.6674$, $P = 0.5208$; session × genotype, $F_{(4,56)} = 0.5773$, $P = 0.0.6803$) and CS− sessions (left) and extinction sessions on days 7 and 8 (right). Note that operant and running data from WT and NAc-D3RcKO groups were acquired concomitantly with NAc-D1RcKO mice and were replicated from Fig. 1. Thus, data from WT and NAc-D3RcKO groups are displayed differently (mean and error bars). All data are presented as the mean ± s.e.m. Error bars indicate the s.e.m. Schematics were generated using BioRender.com.

https://doi.org/10.1038/s41593-024-01819-9

The role of mNAcSh D1Rs may extend to reinforcement of threat avoidance (negative reinforcement), given that aversive cues elicit increased phasic DA transmission within the mNAcSh[43]. We determined whether reinforcement of footshock avoidance requires mNAcSh D1Rs using a modified platform-mediated avoidance paradigm[44]. Here, auditory cue (CS, tone) co-terminated with a footshock (Fig. 6h), and mice could avoid the footshock by mounting a platform located in a chamber corner. NAc-D1RcKO, but not NAc-D3RcKO, mice had avoidance deficits, received more shocks, and spent less time on the platform than WT mice (Fig. 6i). Deficits in avoidance behavior in NAc-D1RcKO mice were also observed upon reexposure to the platform-mediated avoidance task 24 h later (Extended Data Fig. 8f), supporting a sustained deficit in threat avoidance. As in operant training, deficits in motivation in NAc-D1RcKO mice cannot be fully excluded in this setting. Thus, mNAcSh D1R, but not D3R, activity is essential for negative reinforcement, suggesting that D1Rs regulate action–outcome contingencies during both positive and negative reinforcement.

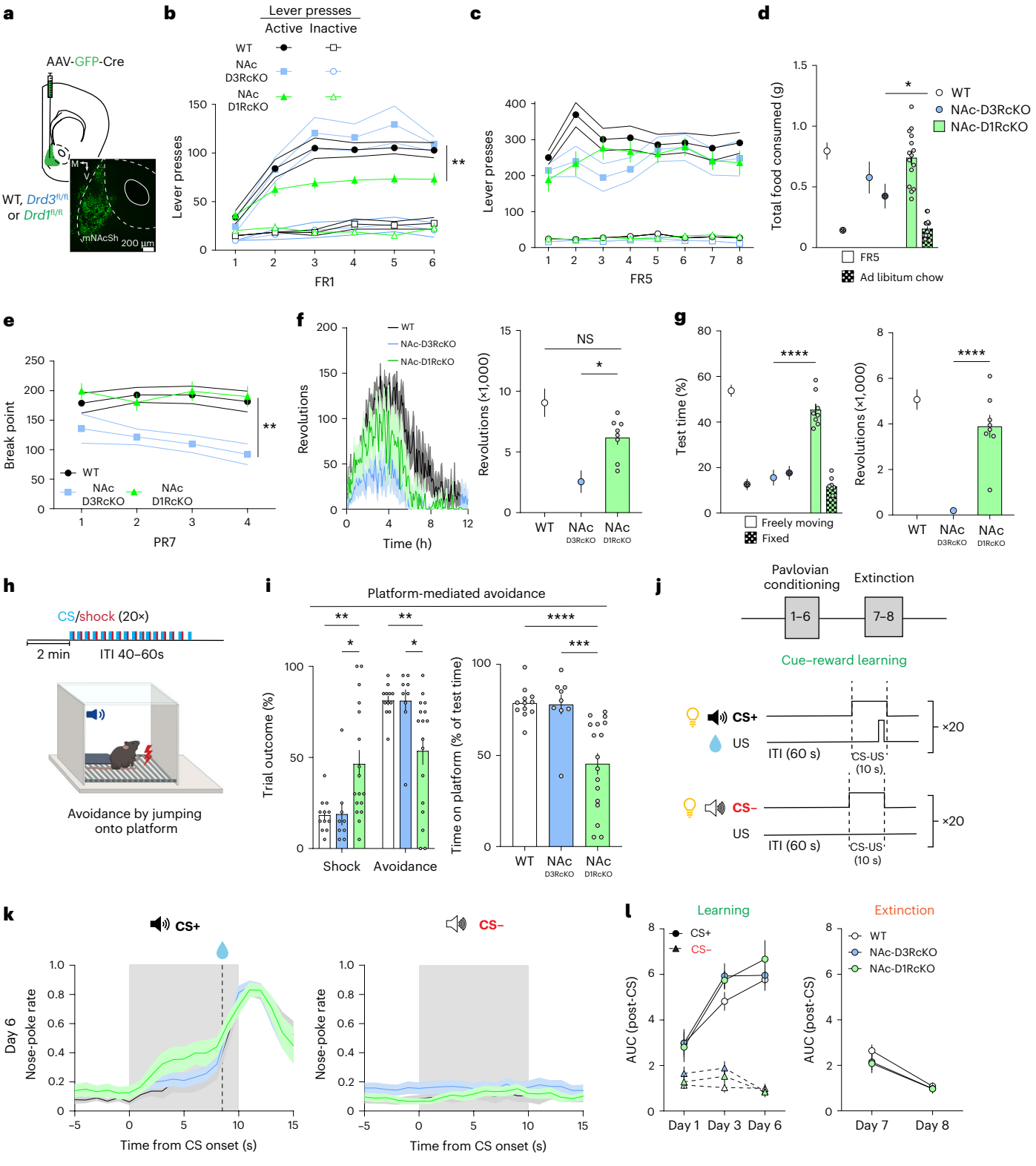

To gain deeper insights into mNAcSh D1R and D3R roles in stimulus–response associations, we performed Pavlovian reward conditioning. Mice were trained to associate a sucrose reward with an auditory tone presentation (CS+; Fig. 6j). A neutral tone (CS−) that did not precede a reward was also presented (Fig. 6j). After repeated tone–sucrose pairings across days, WT, NAc-D3RcKO and NAc-D1RcKO groups increased anticipatory nose pokes into the food receptacle during CS+ presentation (Fig. 6k), with minimal nose pokes during the intertrial interval (ITI) and CS− (Fig. 6k). Interestingly, no differences in anticipatory licking were observed between WT, NAc D3R-cKO and NAc D1R-cKO mice (Fig. 6l). All groups stopped nose poking during extinction sessions, when the US was omitted (Fig. 6l). These results demonstrate that mNAcSh D1RcKO does not impair all facets of reinforcement, but rather reinforcement based on outcomes derived from instrumental actions. Collectively, these results demonstrate that D3Rs and D1Rs play dissociable roles in regulating motivation and instrumental reinforcement, respectively.

Separable regulation of D1-MSN physiology by D3R and D1R

We hypothesized that the dissociable roles of D3Rs and D1Rs in motivation and reinforcement may derive from divergent physiological effects in mNAcSh D1-MSNs. D1R regulation of NMDA receptor (NMDAR)-dependent plasticity is key to reward learning[11,45]. Using glutamate uncaging to evoke isolated postsynaptic NMDAR currents (Fig. 7a), we found that D1R activation with the D1-like receptor agonist SKF-81297 potentiated AP5-sensitive NMDAR currents in mNAcSh D1-MSNs (Fig. 7b–d), an effect that was blocked with bath application of the D1R-selective antagonist SCH-39166 (Fig. 7b–d). Interestingly, D3R activation failed to modify NMDAR currents (Fig. 7b–d). Furthermore, SKF-81297 did not potentiate NMDAR currents in D1-MSNs with *Drd1* cKO, demonstrating specificity of our pharmacological and genetic manipulations (Fig. 7e–h). Thus, D1Rs, but not D3Rs, potentiate mNAcSh NMDAR currents, providing a potential substrate for reinforcement. In contrast, D1R activation using SKF-81297 did not modify GABA release from mNAcSh collaterals by D3R MSNs (Fig. 7i–l), consistent with separable control of inputs and outputs of mNAcSh MSNs by D1Rs and D3Rs, respectively. Altogether, dissociable control of motivated and reinforced behaviors by D1Rs and D3Rs likely stems from dissociable physiological effects in D1-MSNs.

Lastly, to determine if D1R–NMDAR interactions are necessary for instrumental reinforcement, we performed disconnection experiments of mNAcSh D1R and NMDAR function during acquisition of FR1 lever pressing. *Drd1*$^{fl/fl}$ mice were injected with AAV-Cre-GFP and infused with AP5 (700 ng) in the ipsilateral hemisphere (control group) or injected with AAV-Cre and infused with AP5 in the contralateral hemisphere (experimental group; Fig. 7m). AP5 microinjection on day two of FR1 acquisition session decreased FR1 lever pressing in D1R–NMDA contralateral disconnection mice (Fig. 7n), consistent with deficits in instrumental reinforcement. Importantly, decreased lever pressing was not influenced by the number of lever presses during the day 1 baseline session (Extended Data Fig. 8g). Decreased FR1 lever pressing was not sustained as levels of lever pressing were similar the day after AP5 microinjection. Collectively, our results reveal a key role of mNAcSh D1Rs in positive and negative action reinforcement potentially via potentiation of postsynaptic NMDAR-mediated plasticity in mNAcSh D1-MSNs.

Discussion

We identified distinct roles for mNAcSh D3Rs and D1Rs in regulating different features of D1-MSN physiology underlying complementary aspects of reward-related behaviors. Activation of presynaptic D3Rs, but not D1Rs, in mNAcSh MSNs inhibits GABAergic transmission within

Fig. 7 | D3R and D1Rs regulate separable synaptic features of mNAcSh D1-MSNs. a, Schematic showing location of patch-clamp recordings and glutamate uncaging. MNI-glutamate (50 µM) was uncaged using 365 nm of ultraviolet (UV) light (150-ms pulses), and biophysically isolated NMDAR currents were recorded at +40 mV from mNAcSh D1-MSNs using 6,7-dinitroquinoxaline-2,3-dione (DNQX; 10 µM), PTX (50 µM) and tetrodotoxin (TTX; 1 µM). **b**, Representative traces of evoked NMDAR currents in mNAcSh D1-MSNs before and after bath application of the D1R agonist SKF-81297 (green), application of SKF-81297 in the presence of the D1R antagonist SCH-39166 (gray) and application of the D3R agonist PD-128907 (blue). Red trace indicates that evoked NMDAR currents were eliminated with AP5 (50 µM) application. Purple bars indicate UV light pulses. **c**, Time-course of normalized NMDAR-current amplitude in mNAcSh D1-MSNs before and during bath application of SKF-81297 (10 µM, green, $n = 10$ cells/6 mice), preincubation with SCH-39166 (1 µM) and application of SKF-81297 (black, $n = 5$ cells/4 mice) or application of PD-128907 (1 µM, blue, $n = 10$ cells/6 mice; two-way repeated-measures ANOVA: time effect, $F_{(1.610,35.42)} = 11.61$, $P = 0.0003$; treatment effect, $F_{(2,22)} = 6.713$, $P = 0.0053$; time × treatment, $F_{(28,308)} = 5.628$, $P < 0.0001$). **d**, Amplitude of evoked NMDAR currents after treatment with SKF-81297 ($n = 10$ cells/6 mice), preincubation with SCH-39166 ($n = 5$ cells/4 mice) and treatment with SKF and application of PD-128907 ($n = 10$ cells/6 mice) (% baseline) (one-way ANOVA followed by two-sided Dunnett's test: $F_{(2,22)} = 7.070$. Group comparisons, SKF-81297 versus SCH-39166, $^{**}P = 0.0094$, SKF-81297 versus PD-128907, $^{**}P = 0.0084$). **e**, Schematic of experimental details to demonstrate D1R–NMDAR interactions and validation of *Drd1* cKO in the NAc of *Drd1*$^{fl/fl}$ mice. AAV8-Syn-GFP-Cre was injected bilaterally in the mNAcSh of WT or *Drd1*$^{fl/fl}$ mice to genetically ablate *Drd1*, and the retrograde tracer Alexa Fluor 594-conjugated cholera toxin subunit B (CTB-594) was injected into the LH or VTA to selectively label NAc D1-MSNs. **f**, Representative images of CTB injection sites in LH and VTA, and co-labeling of GFP and CTB in the mNAcSh. Recordings were made from co-labeled GFP$^+$/CTB$^+$ mNAcSh MSNs. Dashed and solid white lines in fluorescent images depict borders between brain nuclei. **g**, Time-course of normalized NMDAR-current amplitude in mNAcSh D1-MSNs before and during and after bath application of SKF-81297 in WT ($n = 8$ cells/4 mice) or *Drd1*$^{fl/fl}$ ($n = 8$ cells/5 mice) groups (two-way repeated-measures ANOVA: time effect, $F_{(3.710,51.68)} = 8.461$, $P < 0.0001$; treatment effect, $F_{(1,14)} = 37.23$, $P < 0.0001$; time × treatment, $F_{(14,195)} = 10.78$, $P < 0.0001$). Insets show representative NMDAR traces recorded in mNAcSh D1-MSNs for each genotype. **h**, I_{NMDAR} (% baseline) change after treatment with SKF-81297 for WT ($n = 8$ cells from 4 mice) and *Drd1* ($n = 8$ cells from 5 mice) groups (unpaired *t*-test (two-tailed), $t_{(14)} = 5.383$; $^{****}P < 0.0001$). **i**, Schematics of experiment to determine regulation of mNAcSh collaterals by D1Rs and D3Rs. *Drd1*-tdTomato/*Drd3*-Cre mice were injected with AAV5-Ef1a-DIO-ChR2-eYFP (Cre-ON) in the mNAcSh and GABA release was evoked from D3R-positive terminals (1-ms pulses). Biophysically isolated oIPSCs were recorded from mNAcSh D1-MSNs. **j**, Time-course analysis of oIPSCs in mNAcSh MSNs from D3R collaterals before, during and after bath application of SKF-12897 ($n = 12$ cells from 6 mice) or PD-128907 ($n = 16$ cells from 9 mice; two-way repeated-measures ANOVA: time effect, $F_{(6.474,167.3)} = 26.75$, $P < 0.0001$; treatment effect, $F_{(1,26)} = 16.74$, $P = 0.0004$; time × treatment, $F_{(19,491)} = 7.256$, $P < 0.0001$). Insets show representative traces recorded in mNAcSh MSNs before and after bath application of PD-128907 (blue) or SKF-81297 (green). Note that data using PD-12897 were replicated from Fig. 4 and were, therefore, displayed with different error bars. **k**, PPR (% baseline) versus oIPSC (% baseline; SKF-12897, $n = 12$ cells from 6 mice; PD-128907, $n = 16$ cells from 9 mice; PPR unpaired *t*-test (two-tailed), $t_{(26)} = 2.146$; $^{*}P = 0.0414$; oIPSC amplitude unpaired *t*-test (two-tailed), $t_{(26)} = 4.803$; $^{****}P < 0.0001$). **l**, Coefficient of variation ($1/CV^2$, % baseline) versus oIPSC (% baseline; SKF-12897, $n = 12$ cells from 6 mice; PD-128907, $n = 16$ cells from 9 mice; $1/CV^2$ unpaired *t*-test (two-tailed), $t_{(26)} = 2.271$; $^{*}P = 0.0317$; oIPSC amplitude unpaired *t*-test (two-tailed), $t(26) = 4.803$; $^{****}P < 0.0001$). **m**, Diagram of disconnection procedures of D1R and NMDAR function in the mNAcSh. Mice were injected unilaterally with AAV-Syn-GFP-Cre into the mNAcSh of *Drd1*$^{fl/fl}$ mice. Ipsilateral control and contralateral disconnection groups were infused with AP5 into the ipsilateral and contralateral mNAcSh, respectively. **n**, Change in active lever presses under an FR1 schedule of reinforcement relative to day 1 in ipsilateral (black, $n = 8$ mice) and contralateral (blue, $n = 7$ mice) groups. AP5 was microinjected on day 2 of FR1 sessions (day 2 unpaired *t*-test (two-tailed), $t_{(13)} = 6.001$; $^{***}P = 0.0003$). All data are presented as the mean ± s.e.m. Error bars indicate the s.e.m. Schematics were generated using BioRender.com.

https://doi.org/10.1038/s41593-024-01819-9

local microcircuits to promote effort-based motivation to run and operant responding. Conversely, mNAcSh D1R, but not D3R, cKO impairs instrumental conditioning via interactions with NMDARs. These findings indicate that the effects of DA on mNAcSh MSNs are more complex than canonical models of striatal function where D1Rs and D2Rs are largely segregated. We propose a model wherein DA signaling at distinct receptors (D3R and D1R) within a single cell type differentially mediates motivation and reinforcement.

Integration of genetic and pharmacological manipulations enabled us to isolate the roles of mNAcSh D3R signaling in reward function, overcoming limitations of previous pharmacological and constitutive knockout approaches. mNAcSh D3RcKO disrupts motivation as assessed by decreased break points in operant responding under PR schedules and biased choice for low-effort rewards versus high-effort rewards, consistent with a loss in motivation. Hunger-driven food-seeking behavior was unaffected in NAc-D3RcKO mice, suggesting

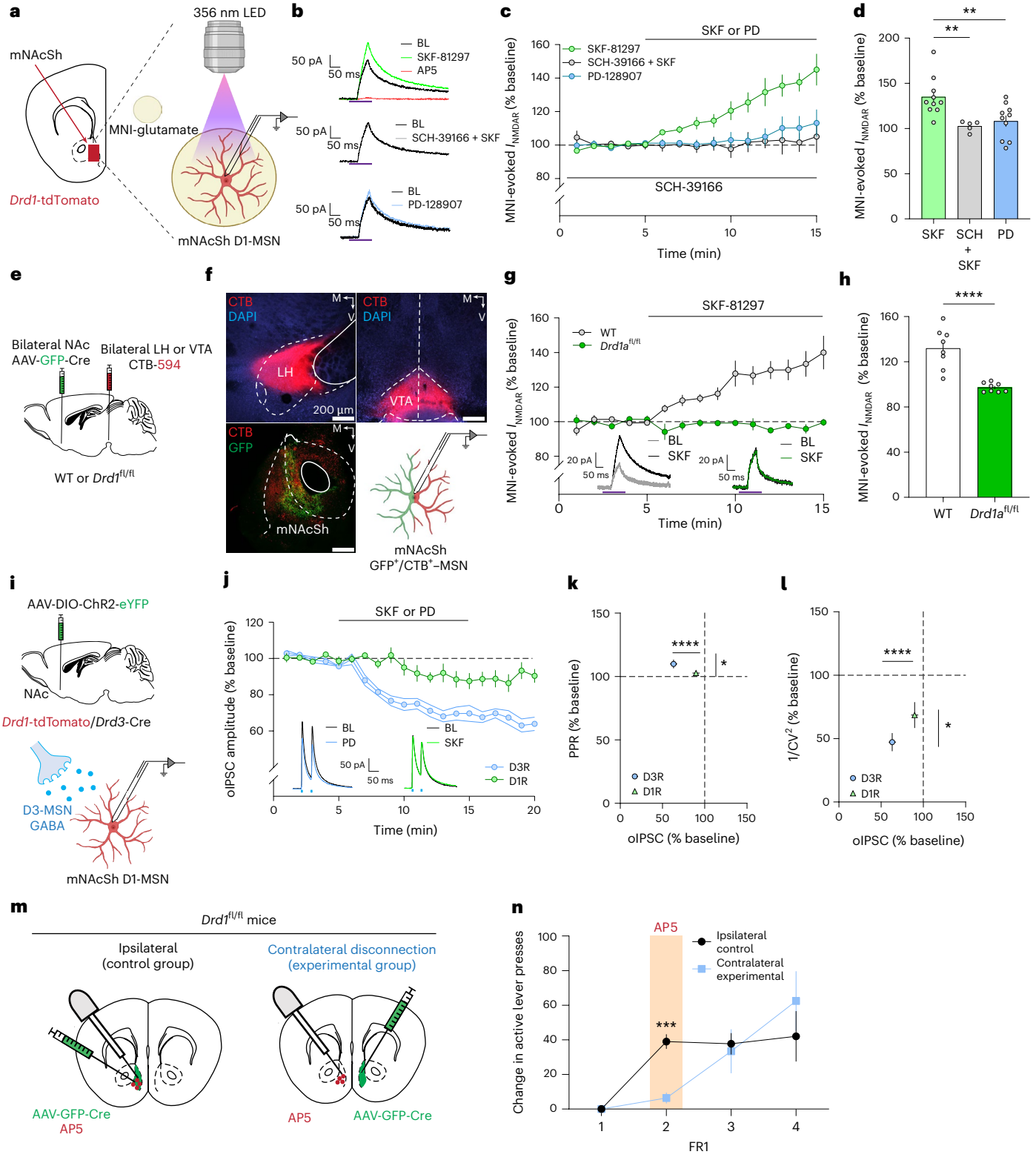

mNAcSh D3Rs regulate effort-based motivation but not homeostatic drive. We also utilized running to demonstrate that mNAcSh D3Rs regulate the motivational component of a non-food-based rewarding stimulus. mNAcSh D3R signaling was necessary for promoting running on a novel wheel during mice's inactive cycle and in a choice task during the active cycle, but not general locomotor activity or wheel running under the control of diurnal cycle shifts. Accordingly, mNAcSh DA signaling underlies motivation to exercise[46]. These results support the hypothesis that D3Rs regulate the activational components of motivation, including effort, persistence and/or vigor[1,7,47]. This is of relevance because physical activity and effort, or lack thereof, are linked to fluctuations in motivation in neuropsychiatric diseases[48].

Our study indicates that DA acting on presynaptic D3Rs inhibits GABAergic transmission from local MSN collaterals, potentially disinhibiting MSNs and activating downstream targets to enhance motivation. This advances our understanding of the behavioral relevance of mNAcSh collateral connections in regulating behavior[36,49]. D3R expression follows a ventromedial (highest) to dorsolateral (lowest) gradient across the ventral striatum[50] (Extended Data Fig. 3b). However, it is unclear whether this explains differences in modulation of motivation across the ventromedial to dorsolateral striatal gradient[4,7,51]. NAc D1-MSNs collaterals also co-release dynorphin and substance P neuropeptides, which display a ventromedial to dorsolateral striatal gradient[4]. Dynorphin and substance P mediate appetitive or avoidance behaviors when acting in the dorsal or ventral mNAcSh[52,53]. D3R constitutive knockout mice display enhanced prodynorphin gene expression[54]. Thus, D3R signaling may regulate reward through regulation of GABA and neuropeptides, which have distinct striatal gradients and spatiotemporal profiles. Additionally, D3Rs may regulate different aspects of D1-MSN physiology, such as intrinsic excitability[16], within the mNAcSh. Whether these physiological actions of D3R signaling are also important for regulating reward function is presently unclear.

Despite classical definitions of striatal MSNs by single DA receptor subtypes[9], we found that most mNAcSh D1-MSNs coexpress *Drd3*, suggesting D3Rs complement D1R function. In contrast, only a subset of D2-MSNs express *Drd3* and at lower levels than D1-MSNs. Coexpression of *Drd3* and *Drd1* in mNAcSh D1-MSNs might enable these cells to transform DA signaling into distinct cellular outcomes and behaviors. Electron microscopy shows colocalization of D1Rs and NMDARs colocalize in the somatodendritic compartment of mNAcSh MSNs[55], consistent with the present and previous electrophysiological findings showing that D1Rs, but not D3Rs, potentiate NMDA receptor currents[11,45]. Further, presynaptic D3R, but not D1R, signaling inhibits GABA release from MSN collaterals. This dissociation suggests that functional D1R and D3R may be localized to distinct subcellular compartments not explored in the present study. Even if D1Rs and D3Rs both regulate common MSN physiological substrates, D3Rs and D1Rs are coupled to inhibitory G_i and stimulatory G_s proteins, respectively[15], likely exerting differential effects on MSN physiology. D3Rs have 100-fold greater affinity for DA than D1Rs[9,15]. Preferential engagement of D3R at low concentrations and activation of D1Rs at higher concentrations has potential implications for the role of distinct spatiotemporal profiles (for example, tonic and ramping versus phasic DA release) in regulating distinct cellular functions and potentially distinct features of reward. Further studies could clarify how tonic and phasic DA release interact with D3R and D1R signaling to regulate motivation and reinforcement.

We found that D1Rs acting on postsynaptic NMDAR-mediated currents are critical for reinforcement of reward-seeking behavior. DA acting via D1Rs permit D1-MSNs to integrate representations carried by coincidentally active excitatory afferent inputs via NMDA-dependent plasticity and changes in excitability[11], strengthening representations conveyed by upstream excitatory neuronal ensembles converging on individual D1-MSNs to support execution of reinforced operant behavior and active avoidance. Despite dissociable effects of D1R and D3R signaling on reinforcement and motivation, it is unclear if D1Rs modulate other aspects of motivation. This could contribute to deficits during early phases of operant training and the marginal, non-significant effects seen on wheel-running and disk-running tasks in mNAcSh D1RcKO mice. Furthermore, a subset of D2-MSNs coexpresses D3Rs, and D3Rs may modulate synaptic transmission from collaterals or terminals in VP arising from D2R/D3R-positive NAc cells. D3R signaling may complement D2R action, whose suppression on D2 MSN collaterals are implicated in drug reward, locomotion and obesity[56,57]. D3R expression in mNAcSh MSNs provides additional effectors for DA transmission to influence circuit function and reward-related behavior.

In conclusion, our work refines our circuit-level understanding on how DA signaling in the mNAcSh is translated into dissociable aspects of motivated running, instrumental behavior and active avoidance via coexpressed D3Rs and D1Rs in MSNs. This provides a new description of separable control of reward and physiological features by DA within the same cell type. Psychiatric and neurological disorders are characterized by dysfunctional or amplified motivation and/or reinforcement. The present study provides insights into how dysfunction in DA release and/or signaling in brain disorders may impact specific reward domains via mNAcSh D1Rs and D3Rs, providing potential reward feature-specific therapeutic targets.

Online content

Any methods, additional references, Nature Portfolio reporting summaries, source data, extended data, supplementary information, acknowledgements, peer review information; details of author contributions and competing interests; and statements of data and code availability are available at https://doi.org/10.1038/s41593-024-01819-9.

References

1. Wise, R. A. Dopamine, learning and motivation. *Nat. Rev. Neurosci.* **5**, 483–494 (2004).
2. Volkow, N. D., Wise, R. A. & Baler, R. The dopamine motive system: implications for drug and food addiction. *Nat. Rev. Neurosci.* **18**, 741–752 (2017).
3. Russo, S. J. & Nestler, E. J. The brain reward circuitry in mood disorders. *Nat. Rev. Neurosci.* **14**, 609–625 (2013).
4. Castro, D. C. & Bruchas, M. R. A motivational and neuropeptidergic hub: anatomical and functional diversity within the nucleus accumbens shell. *Neuron* **102**, 529–552 (2019).
5. Berke, J. D. What does dopamine mean? *Nat. Neurosci.* **21**, 787–793 (2018).
6. Mohebi, A., Wei, W., Pelattini, L., Kim, K. & Berke, J. D. Dopamine transients follow a striatal gradient of reward time horizons. *Nat. Neurosci.* **27**, 737–746 (2024).
7. Jong, J. W. D., Fraser, K. M. & Lammel, S. Mesoaccumbal dopamine heterogeneity: what do dopamine firing and release have to do with it? *Annu. Rev. Neurosci.* **45**, 109–129 (2022).
8. Liu, C., Goel, P. & Kaeser, P. S. Spatial and temporal scales of dopamine transmission. *Nat. Rev. Neurosci.* **22**, 345–358 (2021).
9. Gerfen, C. R. & Surmeier, D. J. Modulation of striatal projection systems by dopamine. *Annu. Rev. Neurosci.* **34**, 441–466 (2011).
10. Lee, S. J. et al. Cell-type-specific asynchronous modulation of PKA by dopamine in learning. *Nature* **590**, 451–456 (2021).
11. Shen, W., Flajolet, M., Greengard, P. & Surmeier, D. J. Dichotomous dopaminergic control of striatal synaptic plasticity. *Science* **321**, 848–851 (2008).
12. Iino, Y. et al. Dopamine D2 receptors in discrimination learning and spine enlargement. *Nature* **579**, 555–560 (2020).
13. Schwartz, J. C. et al. The dopamine D3 receptor in nucleus accumbens: selective cellular localisation, function and regulation. *Eur. Neuropsychopharmacol.* **4**, 190–191 (1994).

14. Sokoloff, P., Giros, B., Martres, M.-P., Bouthenet, M. -L. & Schwartz, J.-C. Molecular cloning and characterization of a novel dopamine receptor (D3) as a target for neuroleptics. *Nature* **347**, 146–151 (1990).
15. Beaulieu, J.-M. & Gainetdinov, R. R. The physiology, signaling, and pharmacology of dopamine receptors. *Pharmacol. Rev.* **63**, 182–217 (2011).
16. Manvich, D. F. et al. Selective D2 and D3 receptor antagonists oppositely modulate cocaine responses in mice via distinct postsynaptic mechanisms in nucleus accumbens. *Neuropsychopharmacology* **44**, 1445–1455 (2018).
17. Song, R. et al. Increased vulnerability to cocaine in mice lacking dopamine D3 receptors. *Proc. Natl Acad. Sci. USA* **109**, 17675–17680 (2012).
18. Simpson, E. H. et al. Selective overexpression of dopamine D3 receptors in the striatum disrupts motivation but not cognition. *Biol. Psychiatry* **76**, 823–831 (2014).
19. Shin, S. et al. *Drd3* signaling in the lateral septum mediates early life stress-induced social dysfunction. *Neuron* **97**, 195–208 (2018).
20. Pribiag, H. et al. Ventral pallidum *DRD3* potentiates a pallido-habenular circuit driving accumbal dopamine release and cocaine seeking. *Neuron* **109**, 2165–2182 (2021).
21. Ridray, S. et al. Coexpression of dopamine D1 and D3 receptors in islands of Calleja and shell of nucleus accumbens of the rat: opposite and synergistic functional interactions. *Eur. J. Neurosci.* **10**, 1676–1686 (1998).
22. Meijer, J. H. & Robbers, Y. Wheel running in the wild. *Proc. Biol. Sci.* **281**, 20140210 (2014).
23. Greenwood, B. N. et al. Long-term voluntary wheel running is rewarding and produces plasticity in the mesolimbic reward pathway. *Behav. Brain Res.* **217**, 354–362 (2011).
24. Greenwood, B. N. & Fleshner, M. Voluntary wheel running: a useful rodent model for investigating the mechanisms of stress robustness and neural circuits of exercise motivation. *Curr. Opin. Behav. Sci.* **28**, 78–84 (2019).
25. Garland, T. Jr et al. The biological control of voluntary exercise, spontaneous physical activity and daily energy expenditure in relation to obesity: human and rodent perspectives. *J. Exp. Biol.* **214**, 206–229 (2011).
26. Basso, J. C. & Morrell, J. I. The medial prefrontal cortex and nucleus accumbens mediate the motivation for voluntary wheel running in the rat. *Behav. Neurosci.* **129**, 457–472 (2015).
27. Salamone, J. D. et al. Haloperidol and nucleus accumbens dopamine depletion suppress lever pressing for food but increase free food consumption in a novel food choice procedure. *Psychopharmacology* **104**, 515–521 (1991).
28. Baldo, B. A. & Kelley, A. E. Discrete neurochemical coding of distinguishable motivational processes: insights from nucleus accumbens control of feeding. *Psychopharmacology* **191**, 439–459 (2007).
29. Kupchik, Y. M. et al. Coding the direct/indirect pathways by D1 and D2 receptors is not valid for accumbens projections. *Nat. Neurosci.* **18**, 1230–1232 (2015).
30. Tejeda, H. A. et al. Pathway- and cell-specific kappa-opioid receptor modulation of excitation-inhibition balance differentially gates D1 and D2 accumbens neuron activity. *Neuron* **93**, 147–163 (2017).
31. Baimel, C., McGarry, L. M. & Carter, A. G. The projection targets of medium spiny neurons govern cocaine-evoked synaptic plasticity in the nucleus accumbens. *Cell Rep.* **28**, 2256–2263 (2019).
32. Creed, M., Ntamati, N. R., Chandra, R., Lobo, M. K. & Lüscher, C. Convergence of reinforcing and anhedonic cocaine effects in the ventral pallidum. *Neuron* **92**, 214–226 (2016).
33. Gibson, G. D. et al. Distinct accumbens shell output pathways promote versus prevent relapse to alcohol seeking. *Neuron* **98**, 512–520 (2018).
34. Larson, E. B., Wissman, A. M., Loriaux, A. L., Kourrich, S. & Self, D. W. Optogenetic stimulation of accumbens shell or shell projections to lateral hypothalamus produce differential effects on the motivation for cocaine. *J. Neurosci.* **35**, 3537–3543 (2015).
35. Lovinger, D. M. et al. Local modulation by presynaptic receptors controls neuronal communication and behaviour. *Nat. Rev. Neurosci.* **23**, 191–203 (2022).
36. Burke, D. A., Rotstein, H. G. & Alvarez, V. A. Striatal local circuitry: a new framework for lateral inhibition. *Neuron* **96**, 267–284 (2017).
37. Dobbs, L. K. et al. Dopamine regulation of lateral inhibition between striatal neurons gates the stimulant actions of cocaine. *Neuron* **90**, 1100–1113 (2016).
38. Moritz, A. E. et al. Discovery, optimization, and characterization of ML417: a novel and highly selective D3 dopamine receptor agonist. *J. Med. Chem.* **63**, 5526–5567 (2020).
39. Khaled, M. A. T. M., Pushparaj, A., Di Ciano, P., Diaz, J. & Le Foll, B. Dopamine D3 receptors in the basolateral amygdala and the lateral habenula modulate cue-induced reinstatement of nicotine seeking. *Neuropsychopharmacology* **39**, 3049–3058 (2014).
40. Gao, C. et al. Molecular and spatial profiling of the paraventricular nucleus of the thalamus. *eLife* **12**, e81818 (2023).
41. Clarkson, R. L., Liptak, A. T., Gee, S. M., Sohal, V. S. & Bender, K. J. D3 Receptors regulate excitability in a unique class of prefrontal pyramidal cells. *J. Neurosci.* **37**, 5846–5860 (2017).
42. Calipari, E. S. et al. In vivo imaging identifies temporal signature of D1 and D2 medium spiny neurons in cocaine reward. *Proc. Natl Acad. Sci. USA* **113**, 2726–2731 (2016).
43. Badrinarayan, A. et al. Aversive stimuli differentially modulate real-time dopamine transmission dynamics within the nucleus accumbens core and shell. *J. Neurosci.* **32**, 15779–15790 (2012).
44. Bravo-Rivera, C., Roman-Ortiz, C., Brignoni-Perez, E., Sotres-Bayon, F. & Quirk, G. J. Neural structures mediating expression and extinction of platform-mediated avoidance. *J. Neurosci.* **34**, 9736–9742 (2014).
45. Cahill, E. et al. D1R/GluN1 complexes in the striatum integrate dopamine and glutamate signalling to control synaptic plasticity and cocaine-induced responses. *Mol. Psychiatry* **19**, 1295–1304 (2014).
46. Dohnalová, L. et al. A microbiome-dependent gut–brain pathway regulates motivation for exercise. *Nature* **612**, 739–747 (2022).
47. Salamone, J. D., Yohn, S. E., López-Cruz, L., San Miguel, N. & Correa, M. Activational and effort-related aspects of motivation: neural mechanisms and implications for psychopathology. *Brain* **139**, 1325–1347 (2016).
48. Ashdown-Franks, G. et al. Exercise as medicine for mental and substance use disorders: a meta-review of the benefits for neuropsychiatric and cognitive outcomes. *Sports Med.* **50**, 151–170 (2020).
49. Wilson, C. J. GABAergic inhibition in the neostriatum. *Prog. Brain Res.* **160**, 91–110 (2007).
50. Lammers, C. H., Diaz, J., Schwartz, J. C. & Sokoloff, P. Dopamine D3 receptor gene expression in the shell of nucleus accumbens is increased by chronic antidepressant treatment. *Mol. Psychiatry* **5**, 229 (2000).
51. Saunders, B. T., Richard, J. M., Margolis, E. B. & Janak, P. H. Dopamine neurons create Pavlovian conditioned stimuli with circuit-defined motivational properties. *Nat. Neurosci.* **21**, 1072–1083 (2018).
52. Al-Hasani, R. et al. Distinct subpopulations of nucleus accumbens dynorphin neurons drive aversion and reward. *Neuron* **87**, 1063–1077 (2015).

53. Belilos, A. et al. Nucleus accumbens local circuit for cue-dependent aversive learning. *Cell Rep.* **42**, 113488 (2023).
54. Zhang, L. et al. Cocaine-induced intracellular signaling and gene expression are oppositely regulated by the dopamine D1 and D3 receptors. *J. Neurosci.* **24**, 3344–3354 (2004).
55. Hara, Y. & Pickel, V. M. Overlapping intracellular and differential synaptic 1445 distributions of dopamine D1 and glutamate *N*-methyl-D-aspartate receptors in rat 1446 nucleus accumbens. *J. Comp. Neurol.* **492**, 442–455 (2005).
56. Lemos, J. C. et al. Enhanced GABA transmission drives bradykinesia following loss of dopamine D2 receptor signaling. *Neuron* **90**, 824–838 (2016).
57. Friend, D. M. et al. Basal ganglia dysfunction contributes to physical inactivity in obesity. *Cell Metab.* **25**, 312–321 (2017).

Publisher's note Springer Nature remains neutral with regard to jurisdictional claims in published maps and institutional affiliations.

This is a U.S. Government work and not under copyright protection in the US; foreign copyright protection may apply 2024

Methods

Subjects

All procedures were approved by the National Institute of Mental Health (NIMH) Animal Care and Use Committee. For every experiment, adult female and male mice (aged 8–20 weeks at the start of experiments) were used throughout the study. No significant differences were found between both sexes, therefore, data were pooled to complete final group sizes. DA D3 receptor-IRES-Cre (*Drd3*-Cre) (Tg(Drd3-cre)KI196Gsat/Mmucd, GENSAT, KI196, a gift from C. Gerfen) and *Drd3*-Cre crossed with Ai14-tdTomato reporter mice (*Drd3*-Cre/Ai14; JAX, 007914) were made congenic with a C57BL/6J background and were used for anatomical characterization and electrophysiological experiments. *Drd3*$^{fl/fl}$ mice (kindly provided by Z. Freyberg) were also bred on a C57/BL6J background and were used for behavioral experiments. *Drd1*$^{fl/fl}$ mice were acquired from The Jackson Laboratory (JAX, 025700). Drd1-tdTomato mice were acquired from Jackson Laboratories (JAX, 016204) and Drd1-tdTomato/Drd3-Cre mice were bred in NIMH facilities. C57/BL6J mice (JAX, 000664) is the strain used when referring to WT controls. *Drd3*-Cre mice were heterozygous for Cre recombinase.

For the generation of *Drd3*$^{fl/fl}$ mice, loxP elements were inserted flanking the transcriptional start site in exon 1 of *Drd3* (Extended Data Fig. 1a). Specifically, a targeting vector was designed via recombineering as described previously[58,59]. We first retrieved approximately 12.2 kb of *Drd3* genomic sequence encompassing 8.3 kb of the 5′-upstream region preceding exon 1 through 3.5 kb of the intron 1 sequence from the BAC, RP24-135K7. This genomic sequence was inserted into a pDTA vector containing the PGK-DTA negative selectable marker by gap repair. We then inserted the 5′ loxP site approximately 4 kb upstream of the *Drd3* transcriptional start site in exon 1 followed by insertion of Frt-PGFneo-Frt-LoxP approximately 500 bp 3′ downstream of exon 1. The final vector contains 5′ and 3′ arms of 4.2 kb and 3.2 kb, respectively. The vector was then linearized by NotI digestion, purified and electroporated into mouse embryonic stem (ES) cells derived from an F1 (129Sv/C57BL/6J) blastocyst. Electroporated cells were cultured in the presence of G418 48 h after electroporation to select for cells with successful genomic integration of our construct. G418-resistant colonies were subsequently picked and screened by long-range PCR using primers corresponding to sequences outside the arms and specific to the 5′ and 3′ loxP sites to identify targeted ES clones. Targeted ES clones were then expanded and further analyzed by long-range PCR for confirmation before using them for ES–morula aggregation to generate chimeric animals. The resulting chimeric mice were then bred with ROSA26-FlpoER mice to remove the PGKneo cassette to generate the final *Drd3*$^{fl/fl}$ mice. These *Drd3*$^{fl/fl}$ mice were then made congenic with the C57BL/6J genetic background via backcrossing for ten generations (N10). For PCR genotyping, the following primers were used: *Drd3* Lox gtF 5′-TGAGACTAAGCAGCGTCCAC-3′, *Drd3* Lox gtR 5′-CTCTGAGTTAGATCTCCCCAGC-3′ for WT 372 bp/floxed 468 bp and *Drd3* Frt gtF 5′-GCTGGCTCTCCATAGATTCTGC-3′, *Drd3* Frt gtR 5′-CTTGAACAGATGTAGGCACCCTG-3′ for WT 254 bp/floxed 347 bp.

Mice were group housed (2–5 mice per cage) in temperature-controlled (21–24 °C) and humidity-controlled (40–65%) facilities and maintained on a reverse 12-h light/12-h dark cycle with lights off at 08:00. All mice were maintained in filter-topped cages and provided food and water ad libitum, except for animals undergoing testing in operant procedures. Single housing was necessary for experiments requiring food restriction (operant conditioning) or acclimation to behavioral tasks (wheel-running experiments) and is explicitly denoted in those cases. All purchased mice were kept in the local animal facility for at least 1 week following delivery before initiating experimental procedures. Mice were monitored for health status daily and before experimentation for the entirety of the study. All efforts were made to minimize pain and distress and the number of mice used.

Viral constructs

Recombinant AAVs and type 2 canine adenoviruses (CAV2) were implemented to allow expression of transgenes of interest. AAVs were purchased from Addgene, the NIDA Genetic Engineering and Viral Vector Core, Boston Children's Viral Vector Core and UNC Viral Vector Core. CAV2 was acquired from the Institut de Génétique Moléculaire de Montpellier. All constructs were aliquoted and stored at −80 °C. Titers ranged from 10^{12} to 10^{13} genomic copies per ml. Specific details on each viral construct can be found in Supplementary Table 2.

Stereotaxic surgeries and optical fiber/guide cannula implantation

All surgeries were conducted under aseptic conditions, and body temperature was maintained at approximately 36 °C with a heating pad. Mice, at 8–16 weeks of age, were anesthetized with a mixture of ketamine (100 mg per kg body weight; intraperitoneal injection) and xylazine (10 mg per kg body weight; intraperitoneal injection) as confirmed by complete absence of flinching response to pinch. The animal's head was shaved, and ophthalmic ointment (GenTeal) was applied to the eyes to prevent drying. Mice were subsequently placed in a stereotaxic apparatus (David Kopf Instruments Model 1900) and the surgical site was exposed using a sterile scalpel after cleaning with povidone–iodine and 70% ethanol. The mouse's head was leveled by ensuring the difference in dorsoventral distance between bregma and lambda was within 50 µm. A small craniotomy window was then made above the injection site with a stereotax-mounted drill. The following injection coordinates were used: [anteroposterior (AP) and mediolateral (ML) relative to bregma; dorsoventral (DV) relative to dura mater at target coordinate]: mNAcSh (AP: +1.40 mm; ML: ±1.65 mm; DV −4.50 mm, 12° angle toward midline), VP (AP: +0.40 mm; ML: ±1.35 mm; DV −5.35 mm), LH (AP: −1.35 mm; ML: ±1.10 mm; DV −5.25 mm), VTA (AP: −3.30 mm; ML: ±1.85 mm; DV −4.60 mm, 14° angle). Infusions (300 nl) were made at a rate of 100 nl min^{-1} utilizing 29-gauge microinjection needles connected to FEP tubing secured to a 2 µl Hamilton syringe and a microinjection pump (UMP3, World Precision Instruments). The infusion system was filled with distilled water and separated from the infused virus or drug by a small air bubble. The injector tip was first lowered 100 µm deeper than the target DV coordinate and then raised to the planned coordinate before infusion to facilitate viral diffusion at the site of injection, instead of along the needle track. After infusion, the injector was kept for 8 min at the injection site to allow for diffusion and was then slowly withdrawn.

For cKO of *Drd1* or *Drd3* in the mNAcSh, homozygous *Drd1*$^{fl/fl}$ or *Drd3*$^{fl/fl}$ mice received bilateral injections of AAV8-hSyn-GFP-Cre (4.50×10^{12} genome copies (GCs) per ml) or AAV1-EF1α-eGFP; WT mice were used as controls.

For anatomical tracing experiments, *Drd3*-Cre mice were injected with AAV2/9-phSyn1(S)-FLEX-tdTomato-T2A-synaptophysin-EGFP or AAV1-Syn-FLEX-Chrimson-tdTomato (4.10×10^{12} GCs per ml) into the mNAcSh to characterize downstream projections and terminals of mNAcSh D3R-containing neurons.

For pathway-specific deletion of mNAcSh *Drd3*, CAV-Flp-GFP (1.05×10^{13} GCs per ml) was delivered to the VP, LH or VTA and a mixture of AAV5-EF1α-fDIO-Cre (5.00×10^{12} GCs per ml) and AAV1-CAG-FLEX-tdTomato (5.90×10^{12} GCs per ml) was delivered to the mNAcSh at a ratio of 9 to 1, respectively.

For validation of lack of toxicity induced by CAV infection, CAV-Flp-GFP (1.05×10^{13} GCs per ml) was injected into the VTA.

For electrophysiological studies examining *Drd3*-expressing MSN connectivity and D3R modulation of synaptic transmission, *Drd1*-tdTomato/*Drd3*-Cre mice received bilateral injections of AAV5-EF1α-DIO-ChR2(H134R)-eYFP (4×10^{12} GCs per ml) or AAV1-EF1α-DO-hChR2(H134R)-eYFP (5.88×10^{12} GCs per ml) targeting the mNAcSh.

For drug microinjection experiments, mice were bilaterally implanted with stainless-steel guide cannulas (26-gauge, 3.5 mm in length, P1 Technologies) 1 mm above the mNAcSh (AP: +1.40 mm; ML: ±1.65 mm; DV −3.50 mm from dura, 12° angle toward midline). Guide cannulas were then secured to the skull using MetaBond cement, and dummy cannulas were used to maintain cannula patency and removed only during the injection period.

For disconnection procedures, *Drd3*$^{fl/fl}$ or *Drd1*$^{fl/fl}$ mice were injected with AAV8-Syn-GFP-Cre and implanted with a guide cannula above the mNAcSh in the same hemisphere (ipsilateral group) or injected with virus and implanted with the guide cannula in the contralateral hemisphere (contralateral group).

For validation of the *Drd1*$^{fl/fl}$ line, *Drd1*$^{fl/fl}$ mice received bilateral injections of CTB-594 in PBS (1.0 mg ml^{-1}, Thermo Fisher) in either LH or VTA brain regions.

For chemogenetic inhibition experiments, *Drd3*-Cre mice received bilateral injections of AAV1-EF1α-DIO-hM4D(Gi)-mCherry in the mNAcSh to inhibit *Drd3*-expressing mNAcSh MSNs. AAV5-hSyn-DIO-mCherry (1.2×10^{13} GCs per ml) was used for control groups.

For slice experiments using the cADDis sensor to record the cAMP responses in NAc MSNs, *Drd3*-Cre mice were bilaterally injected with 300 nl of AAV1-hSyn-DIO-cADDis (diluted 2× in PBS) in the mNAcSh using glass pipettes (30–50 µm diameter at the tip).

Following all surgical procedures, incisions were closed using VetBond (3M) or surgical staples. Mice were allowed to recover from anesthesia in heating pads until they showed regular breathing and locomotion, at which point they were transferred back to the vivarium. Animals received subcutaneous injections of ketoprofen (5 mg per kg body weight) for three consecutive days for postoperative analgesia and anti-inflammatory purposes. Experiments involving the use of AAVs were initiated 3–4 weeks after injection, 3 weeks for CAV2-Flp-GFP and 7 days for retrobead and CTB injection procedures.

Anatomical characterization of *Drd3*-expressing MSNs

RNAscope fluorescence in situ hybridization. Multiplex fluorescence in situ hybridization (RNAscope, Advanced Cell Diagnostics) was used to detect the expression of *Drd1*, *Drd2*, *Drd3* and *Cre* mRNAs in the NAc of adult WT and *Drd3*$^{fl/fl}$ mice. For all RNAscope procedures, tools, slides and equipment were cleaned with 70% ethanol and RNase inhibitors (RNAZap, Invitrogen) before use. Mice were euthanized by cervical dislocation, brains were rapidly dissected and flash frozen for 20 s in 50 ml of 2-methylbutane chilled on dry ice. Subsequently, brains were stored at −80 °C until sectioning. Next, 16-µm slices containing the NAc were obtained using a cryostat (CM3050 S; Leica Biosystems) at −20 °C and thaw-mounted onto Superfrost microscope slides (Fischer Scientific) in a series of four slides. Slides containing sections were stored at −80 °C until in situ hybridization processing. *Drd1*, *Drd2*, *Drd3* or *Cre* mRNA signal was detected using the RNAscope fluorescent kit following the ACDBio manual[60]. Briefly, slides containing the NAc were removed from −80 °C, fixed with prechilled 4% paraformaldehyde (PFA) for 20 min at 4 °C, and subsequently washed twice for 1 min with PBS, before gradual dehydration with 50% ethanol (1 × 5 min), 70% ethanol (1 × 5 min) and 100% ethanol (2 × 5 min). Next, slides were air-dried at room temperature for 10 min and a hydrophobic barrier was drawn around the slides using a hydrophobic pen (Vector Laboratories). Sections were then incubated with Protease Pretreat-IV solution for 20 min at room temperature. Slides were washed with double-distilled water (2 × 1 min), before being incubated with the appropriate probes for 2 h at 40 °C in the HybEZ oven (Advanced Cell Diagnostics) and undergoing hybridization. Probes used were purchased from Advanced Cell Diagnostics as follows: Mm-*Drd1*-C1 (nucleotide target region 444–1358; accession no. NM_010076.3), Mm-*Drd2*-C2 (nucleotide target region 69–1175; accession no. NM_010077.2), Mm-*Drd3*-C3 (nucleotide target region 23–1253; accession no. NM_007877.1), *Cre* recombinase (nucleotide target region 2–972; accession no. not applicable). Probes were warmed up to 40 °C in a water bath until use.

Slides were washed in wash buffer twice for 2 min, before being incubated with three drops of amplification 1 buffer, amplification 2 buffer, amplification 3 buffer and amplification 4-Alt A/C buffer at 40 °C in the HybEZ oven for 30, 15, 30 and 15 min, respectively. Slides were washed in wash buffer twice for 2 min. DAPI solution was applied to sections at room temperature for 20 s to label nuclei. Finally, slides were coverslipped using Vectashield Hard Set mounting medium (Vector Laboratories). Slides were stored at 4 °C until imaging. *z*-stacked images including the NAc core and mNAcSh were acquired using an A1R confocal microscope (Nikon) with a ×20 objective. This produced a tiled image containing the entirety of the NAc that was used for quantification. The following combinations of laser excitation and emission filters were used for various fluorophores: DAPI (405 nm excitation; 450/30 nm emission), eGFP (491 nm laser excitation; 528/38 nm emission), tdTomato (561 nm laser excitation; 586/15 nm emission) and Cy5 (647 nm laser excitation; 665/35 nm emission). All samples were imaged with the same settings to allow comparison between samples. Background subtraction and thresholds were set uniformly for all images.

In situ quantification. Image analysis and cell quantification were performed using ImageJ software (Fiji, version 2017) and CellProfiler software (version 3.1.9.; Broad Institute)[61,62]. To analyze the images, each image was opened in ImageJ and converted to a maximum intensity projection. Images were overlapped onto the Allen Mouse Brain atlas to set boundaries for the NAc core or mNAcSh area to be analyzed. Two to three serial sections (between approximately AP +1.42 and +1.21) were analyzed for each mouse. For quantification, images were imported to an automated CellProfiler pipeline that was kept identical across samples from the same experiment. Here, only cells with a clear DAPI-positive nucleus were counted, which were then registered and used as markers for individual cells. Regions of interest (ROIs) for analysis were defined as the 3 µm area surrounding the DAPI signal. A blinded experimenter set thresholds for each channel, which determines the minimum intensity of fluorescence for a probe to be counted. These thresholds were validated by visual spot-check throughout the image to ensure cells and probes were being appropriately counted. CellProfiler software provided CSV files with the total counts of cells and levels of overlap, which are reported in the data. For quantification of *Drd3* mRNA reduction in NAc-D3RcKO, the integrated pixel intensity of the *Drd3* signal in each GFP-positive neuron was calculated around the NAc region infected and compared against WT controls. For coexpression of *Drd1*, *Drd2* and *Drd3*, cells considered as positive consisted of an area within the radius of a DAPI nuclear staining that measured at least ten positive pixels for receptor probes. For the percentage of retrobead-positive cells expressing *Drd3* mRNA, retrobead-positive cells contained at least six for retrobead labeling.

Anterograde tracing of Drd3-expressing mNAcSh MSNs. To examine the projection pattern of *Drd3*-expressing mNAcSh neurons, 300 nl of AAV1-hSyn1-FLEX-Chrimson-tdTomato or AAV2/9-phSyn1(S)-FLEX-tdTomato-T2A-synaptophysin-EGFP were bilaterally injected into the mNAcSh of *Drd3*-Cre mice as described above. Mice were perfused 3 weeks following viral injection and 50-µm-thick coronal brain slices were prepared. Images were taken at approximately 300-µm intervals from brain regions expressing tdTomato and/or GFP using a Nikon A1R confocal microscope with a ×20 objective. ROIs were labeled relative to bregma based on Paxinos and Franklin's the Mouse Brain in Stereotaxic Coordinates[63]. Total integrated fluorescence intensity tdTomato and GFP from each downstream target were quantified using ImageJ with identical pinhole, gain and laser settings. For each brain region, four images were acquired at the same focal point from each animal. No additional post-processing was performed for any of the images analyzed here.

Retrobead retrograde tracing of Drd3-expressing NAc MSNs. C57BL/6J WT mice were injected bilaterally with 200 nl of Red and Green Retrobeads IX (Lumafluor) into the VP, LH or VTA/SNc as described above. Per the manufacturer's protocol, red retrobeads were injected at a 1:4 dilution and green retrobeads were left undiluted. Seven days after injection, brains were collected and processed for RNAscope procedures as described above.

Quantitative real-time PCR

WT and *Drd3*$^{fl/fl}$ mice expressing Cre recombinase in the mNAcSh were euthanized by cervical dislocation. Brains were rapidly dissected, and 1-mm coronal brain slices containing the ventral striatum were obtained by slicing the brain placed in an iron matrix (Kent Scientific). The NAc was microdissected bilaterally and immediately transferred to microcentrifuge tubes on dry ice; samples were stored at −80 °C for RNA isolation and processing. Total RNA was extracted from dissected NAc samples using the NZY RNA Total Isolation kit (ref. MB13402, Nzytech), and purified mRNA samples were reverse transcribed using the SuperScript IV First-strand cDNA synthesis kit (Thermo Fisher Scientific). Target sequences were amplified from the cDNA using the TaqMan Gene Expression Assay Kit (Thermo Fisher Scientific) and the SYBER Green system (Power SYBR Green PCR Master Mix, Applied Biosystems). All TaqMan probes were purchased from Applied Biosystems and were as follows: *Drd1* (Mm02620146_s1), *Drd2* (Mm00438545_m1), *Drd3* (Mm00432887_m1) and GAPDH (Mm99999915_g1). qPCR was performed using TaqMan Fast Polymerase (Applied Biosystems) in an ABI PRISM 7900HT SDS Real-Time PCR system (Applied Biosystems). Cycling conditions were as follows: initial hold at 95 °C for 20 s; 40 cycles of step 1 (95 °C for 1 s); and step 2 (60 °C for 20 s). Samples were run in triplicates, and negative controls were run in parallel. The relative mRNA expression level for each sample was calculated using the ΔΔCt method, where Ct was the cycle threshold for each reaction and GAPDH was used as internal control (DCt = Ct (gene of interest) − Ct (GAPDH)[64]. Gene expression fold change was calculated by normalizing the value of each sample to the mean of the control samples.

Histology

Upon completion of all experiments, mice were deeply anesthetized with euthanasia solution (VedCo), and then transcardially perfused with 40 ml of cold PBS (1×, pH 7.4), followed by 40 ml of cold 4% wt/vol PFA in PBS. Brains were extracted and post-fixed in 4% PFA at 4 °C overnight and then cryoprotected in 20% sucrose-PBS for 24 h, followed by 30% sucrose-PBS for 24 h, at which point they were stored in PBS or prepared for sectioning on a cryostat. To this end, brains were embedded on the mounting disk with Tissue-Tek Optimum Cutting Temperature Compound (Sakura Finetek) for freezing over dry ice. Brains were subsequently placed in the cryostat at −20 °C, and consequently sectioned into 50-µm or 100-µm slices. Slices were mounted on slide glasses with DAPI Fluoromount-G mounting medium (0100-20, Southern Biotech) for visualization on a Nikon A1R confocal microscope (×10 objective, NA 0.45, lasers: 405 nm, 488 nm and 561 nm). Injection sites and optical fiber placements were routinely confirmed in all animals by preparing coronal sections containing the ROI. After histological verification, animals with insufficient transgene expression, off-target transgene expression outside the region of interest by visual inspection and/or inaccurate implant placement were excluded from data analyses. A representative scheme of the viral spread for NAc-D3RcKO mice included in this study is included in Extended Data Fig. 1k.

Immunostaining

To address the potential toxicity of CAV injection and its impact on VTA DA cell degeneration, we performed immunostaining of TH after unilateral injection of CAV-FlpO-GFP in the VTA (300 nl) of *Drd3*$^{fl/fl}$ mice. Three weeks after injection, animals were perfused, brains were sliced in a vibratome (Leica VT1200) and sections containing the VTA (50 µm) were collected. Sections were then processed immunohistochemically for visualization of GFP and TH expression. Briefly, sections were rinsed with PBS and incubated for 1 h in PBS supplemented with 4% bovine serum albumin and 0.3% Triton X-100. This was followed by a 48-h incubation at 4 °C with rabbit anti-TH monoclonal antibody (1:1,000 dilution; PelFreez Biologicals, P40101-150) and chicken anti-GFP antibody (1:1,000 dilution; Abcam, ab13970). After being rinsed three times for 10 min each in PBS, sections were processed with secondary antibody Donkey anti-rabbit Alexa Fluor 594 (1:500 dilution; Jackson ImmunoResearch, 711-585-152) and goat-anti-chicken Alexa Fluor 488 (1:500 dilution; Abcam, ab150173) for 2 h at room temperature. Free-floating sections were mounted on coated slides. Slides were exposed in the dark at 4 °C for 1 week before development. TH^+ and TH^+/GFP^+ cells were detected and segmented from images using the Cellpose3 pretrained super-generalist 'cyto3' segmentation model (https://www.cellpose.org/) followed by manual removal of failed detections as necessary. Integrated density of TH signal was measured using ImageJ with cell outlines exported from Cellpose. The control group comprises VTA sections from mice that had no GFP expression and contralateral VTA sections that had minimal GFP expression.

Ex vivo electrophysiology

Slice electrophysiology recordings were performed as previously described[30]. Briefly, 3 to 8 weeks after surgery, mice were deeply anesthetized with euthanasia (200 mg per kg body weight intraperitoneally; VedCo) and subsequently decapitated after confirmation of absent toe and tail pain reflexes. Brains were rapidly removed and chilled for 2 min in ice-cold NMDG-based slicing solution containing 92 mM NMDG, 20 mM HEPES, 25 mM glucose, 30 mM $NaHCO_3$, 2.5 mM KCl, 1.2 mM NaH_2PO_4, 5 mM sodium ascorbate, 3 mM sodium pyruvate, 2 mM thiourea, 10 mM $MgSO_4$ and 0.5 mM $CaCl_2$ (pH 7.35, 303–306 mOsm) and saturated with 95% O_2/5% CO_2. Brains were rapidly blocked, dried on filter paper and glued to a platform containing ice-cold NMDG slicing solution within a vibratome (VT1200, Leica). Coronal sections (300 µm) containing the mNAcSh, VP, LH and VTA were cut at a speed of 0.07 mm s^{-1} while the brain was submerged in ice-cold NMDG-based slicing solution. Following slicing, sections were kept in a custom-built chamber containing NMDG slicing solution for 7 min at 34 °C. Slices were subsequently transferred to a chamber filled with modified holding artificial cerebrospinal fluid (aCSF) saturated with 95% O_2/5% CO_2 containing 92 mM NaCl, 20 mM HEPES, 25 mM glucose, 30 mM $NaHCO_3$, 2.5 mM KCl, 1.2 mM $NaPO_4$, 5 mM sodium ascorbate, 3 mM sodium pyruvate, 2 mM thiourea, 10 mM $MgSO_4$ and 0.5 mM $CaCl_2$ (pH 7.35, 303–306 mOsm) at room temperature for at least 1 h. Slices remained in this solution for recovery until transferred to the recording chamber. For recordings, the recording chamber was kept at 31 °C and perfused with a pump (World Precision Instruments) at a flow rate of 1.5–2.0 ml per minute with aCSF containing 126 mM NaCl, 2.5 mM KCl, 1.4 mM NaH_2PO_4, 1.2 mM $MgCl_2$, 2.4 mM $CaCl_2$, 25 mM $NaHCO_3$ and 11 mM glucose (303–305 mOsm) at 31 °C. Cells were visualized with a ×40 water-immersion objective on an Olympus BX5iWI inverted microscope equipped with infrared-differential interference contrast (IR-DIC) optics and epifluorescence (Olympus Corp). Patch pipettes (2–4 MΩ) were pulled from borosilicate glass (G150TF-4, Warner Instruments) and filled with a freshly filtered (0.22-µm syringe filter) cesium-based internal solution containing 117 mM cesium methanesulfonate, 20 mM HEPES, 0.4 mM EGTA, 2.8 mM NaCl, 5 mM TEA-Cl, 4 mM Mg-ATP, 0.4 mM Na-GTP and 5 mM QX-314 (pH 7.35; 280–285 mOsm). Whole-cell access was obtained from individual neurons after acquisition of a giga-ohm seal recording. All recordings were made utilizing a Multiclamp 7400B amplifier (Molecular Devices) and data were digitized at 10 kHz and filtered at 1–2 kHz using a 1440A Digidata Digitizer and Clampex software (Molecular Devices). Series and input resistances (10–20 MΩ) were monitored online using a −5 mV, 70-ms voltage pulse through the recording electrode. Cells with >20% change in

access resistance were discarded from further analysis. Liquid junction potentials were ≈ −7 mV and were left uncorrected. Data were analyzed offline using Clampfit 10.6 (Molecular Devices).

To isolate $GABA_A$ responses evoked by optogenetic stimulation of *Drd3*-expressing MSNs, the AMPA receptor antagonist DNQX (10 µM) and NMDAR antagonist D-AP5 (50 µM) were included in the aCSF, and neurons were voltage-clamped at 0 mV. oIPSCs were elicited every 10 s by photostimulating ChR2 using two 1-ms pulses of 473-nm LED light (pE-300^{ultra}, CoolLED) separated by a 50-ms interstimulus interval. ChR2-negative cells were identified by the lack of ChR2 currents evoked by blue-light stimulation. ChR2 currents were characterized by sustained, steady-state currents in response to 1-s blue-light stimulation with an onset immediately at the start of the laser pulse. Synaptic GABAergic currents in ChR2-negative cells were outward currents that were not sustained for the duration of a 100–1,000-ms blue-light pulse and had a delayed onset beyond the 1 ms optical pulse. Cells that did not show a peak that exceeded baseline noise in this window were counted as nonresponders. Connectivity was calculated as the percentage of cells receiving oIPSCs from mNAcSh *Drd3*-expressing MSNs. IPSCs were recorded until their amplitudes were stable for at least 5 min, at which point PD-128907 (1 µM), ML417 (1 µM) or SKF-81297 (10 µM) were added to the bath for 10 min. After bath application, drugs were washed out for 5 additional minutes. Time-course graphs of the effects of drug application were generated by averaging raw oIPSC measurements in 1-min bins and expressing each point as a percentage of the average of the 5-min baseline. The averaged baseline and 5 min after drug application were used for quantification of modulation of synaptic transmission. PPRs were calculated as the amplitude of the second peak divided by the amplitude of the first peak. It should be noted that ChR2 expression has been documented to alter presynaptic release probability[65] and, as such, absolute PPR and $1/CV^2$ values likely do not reflect that absolute physiological state of presynaptic release and may even influence presynaptic D3R modulation. To differentiate between D1-MSNs and D2-MSNs, slices were obtained from *Drd1*-tdTomato mice and recordings were made from tdTomato-positive (D1-MSNs) or tdTomato-negative (putative D2-MSNs) cells. Because the electrophysiological results from the two MSN populations were similar, data were grouped. Recordings in the VP, LH and VTA were made irrespective of the identity of the cell. sIPSCs were collected in the presence of DNQX (10 µM) and D-AP5 (50 µM) and the last 5 min of baseline and the last 5 min of drug application were used for quantification. Events were filtered online at 1 kHz and counted manually utilizing MiniAnalysis 6.0.3. software (Synaptosoft). At least 100 events per cell were acquired in 6-s blocks and detected using a threshold of 7 pA.

For the modulation of NMDAR currents, recordings were made at a +40 mV holding potential with DNQX (10 µM), the $GABA_A$ receptor antagonist PTX (50 µM) and TTX (1 µM) in the bath to isolate glutamate uncaging-evoked NMDAR currents and eliminate circuit effects evoked by glutamate uncaging. Glutamate uncaging was achieved by applying a single 150-ms pulse of UV light (356 nm) through the microscope objective every 20 s to a bath containing MNI-glutamate (50 µM, Tocris, Bioscience). NMDA components were measured as currents 20 ms after the peak. LED intensity was chosen to evoke responses at approximately half of maximal amplitude. Evoked NMDAR currents were recorded until their amplitudes were stable for at least 5 min, at which point PD-128907 (1 µM) or SKF-81297 (10 µM) was added to the bath for 10 min. SCH-39166 (1 µM) was already present in the bath to pharmacologically antagonize D1R signaling. Time-course graphs were generated by averaging raw NMDAR measurements in 1-min bins and expressing each point as a percentage of the average of the 5-min baseline. The averaged baseline and last 5 min of drug application were used for quantification. Bath application of AP5 at the end of the experiment abolished glutamate uncaging-evoked currents, confirming that evoked currents were mediated by NMDARs. For validation of *Drd1* KO, AAV8-Syn-GFP-Cre was injected into the mNAcSh of *Drd1*$^{fl/fl}$ mice to genetically ablate *Drd1*, and CTB-594 was delivered in the LH or VTA to visualize putative NAc D1R-expressing MSNs. Whole-cell recordings of NMDAR currents were performed on GFP-positive and CTB-594-positive neurons as detailed above.

After recordings, images of the recording pipette were acquired for post hoc estimation of recording location using the same camera as above and using a ×4 Nikon objective. For all pharmacological experiments, one neuron per slice was recorded. In some cases, the slice was transferred to 4% PFA overnight for post hoc imaging on a confocal microscope. The Clampfit suite v10.6 (Molecular Devices) was used for data display, acquisition and storage.

Two-photon slice imaging

We sought to address the relationship between D3R function with intracellular cAMP signaling by performing acute brain slice imaging of a cAMP sensor (cADDis) in mNAcSh. Following 3 weeks of viral expression, acute slices were prepared as described above, and two-photon fluorescence imaging was performed on an upright multiphoton microscope (FVMPE-RS, Olympus) using an ×20 1.0-NA objective (Olympus) and GaAsP photomultiplier tube detectors. Fluorescence excitation for imaging was achieved using an infrared femtosecond pulse laser tuned to 920 nm (Spectra Physics X3). Image acquisition was performed using Olympus Fluoview software. The image acquisition frame rate was ~1 Hz for cADDis fluorescence imaging using galvo-galvo scanning mirrors. Volumetric imaging was used (20 planes, 5 µm between planes) to sample more cells and correct for any *z*-drift during imaging. During imaging, slices were continuously superfused (flow rate, 2–5 ml min^{-1}) with oxygenated (95% O_2 and 5% CO_2) aCSF at room temperature. Application of DA was performed in the presence of 1 µM of D1R antagonist (SCH-39166) to test for specific effects of D3R function on downstream cAMP signaling. To prevent oxidation of DA, 50 µM sodium metabisulfite was included in all aCSF solutions during DA application experiments.

Analysis of two-photon slice imaging

Acquired movies were first corrected for minor *XYZ* drift using Fast-4Dreg (ImageJ v1.54f) and excluded if drift remained following this registration. For selection of ROIs corresponding to putative presynaptic terminals, ROIs were manually circled based on visualization (ImageJ). ROIs were further selected based on the criteria of having a normalized change in fluorescence greater than 5% at the maximal concentration of DA used, and these ROIs were used for plotting time courses and analysis of response magnitude to various DA concentrations. The normalized change in fluorescence was calculated by subtracting a baseline fluorescence ($F_0(t)$) from $F(t)$, then dividing by $F_0(t)$: $\Delta F/F(t) = (F(t) - F_0(t))/F_0(t)$, where $F_0(t)$ was the mean of the final 2 min of the 5-min baseline period and F(t) is the entire fluorescence recording.

Behavior

Behavioral experiments were conducted during the dark cycle (between 10:00 and 18:00) unless otherwise specified. Mice were allowed to recover from surgery for at least 3 weeks before behavioral testing was conducted. Animals were matched according to age, sex and date of birth and single housed at least 1 day before the start of testing. To minimize the effect of stress on behavioral outcome, mice were acclimated to the soundproofed testing room under red light for at least 30 min before the start of each assay.

Animals undergoing running behavioral testing were subjected to the following assays in this order: wheel running, running disks choice test, open-field test, sucrose preference test, social interaction, light–dark box and novel object recognition test (Extended Data Fig. 1b). Separate cohorts of mice were used for operant conditioning experiments. For pathway-specific D3RcKO, mice underwent testing in running wheel, running disk choice-behavior and operant procedures.

Wheel running. Voluntary running was performed in mice with free access to a running wheel in their cage. At least 24 h before the start of the experiment, mice were singly housed in clean, standard cages to habituate them with social isolation in activity recording chambers. At the start of the light cycle (that is, 20:00), mice were transferred into cages that contained a running wheel connected to an infrared sensor that recorded beam breaks on the wheel to calculate distance traveled (ACT-551-FIL-MS-SS, Coulbourn Instruments). Animals were provided with ad libitum access to food and water, and running activity was monitored for 60 consecutive hours. Data were collected every 5 min from each mouse using ClockLab (Actimetrics).

Running disks test. We designed an effort-related choice-behavior task to disentangle motivational running behavior. Mice had to choose between two disks, one that was fixed, where animals could not run, and another one that was freely moving, where animals experienced reward by running. Disks were angled at approximately 30° relative to the floor. Each session consisted of baseline and test phases. During baseline, the animal was placed in the empty open-field arena and allowed to explore the environment for 10 min. After baseline, the fixed and freely moving disks were inserted into the arena, and disk-running activity and general locomotion were recorded for 3 h. There was no interruption between baseline and test phases. Visual (circles or stripes) and odor (double-distilled water or 5% acetic acid) cues were attached adjacent to each disk to further facilitate the recognition of each area of the arena. Tracking data were analyzed offline using TopScan software (CleverSys). The position of the mouse was defined as the zone in which both front paws and center were located.

Open-field test. Mice were placed singly in an open-field arena (43.8 cm × 43.8 cm × 39.4 cm) to assess general locomotor activity and anxiety-like behavior. For the former, the total distance traveled was measured for 30 min. For the latter, the arena was divided into 'center' (23 × 23 cm) and 'edges' zones and the percentage of time spent in the center of the arena was measured. For both analyses, TopScan (CleversSys) video tracking software was used to score the movement and location of the animals.

Sucrose preference test. Hedonic reward seeking was measured using the sucrose preference test. Single-housed mice were first habituated by being placed in a standard cage (45 × 27 × 15 cm) that contained two bottles of tap water. Water intake was measured by weighing the bottles 4 h after the start of the habituation period. The following day, one of the bottles was replaced with a 1% sucrose solution (wt/vol), and animals were again given a free choice between the two bottles. The total amount of tap water and sucrose consumed was recorded by again weighing the bottles after 4 h. Sucrose preference was calculated as the amount of sucrose solution consumed relative to the total amount of liquid consumed and multiplied by 100 [(sucrose solution intake/total intake) × 100]. To control for side preferences, the location of the sucrose and water bottles was counterbalanced between cages. Sucrose preference testing occurred approximately 2 h after the start of the animal's active cycle.

Light–dark box. The light–dark box test was performed to assess anxiety-like behavior. Mice were placed in an open-field arena (43.8 cm × 43.8 cm × 39.4 cm) divided into two compartments connected by a small circular aperture (4 cm wide × 5cm high). One side was exposed to light in the room and the other was enclosed and dark. During testing, mice were placed in the lit side of the box, facing the wall farthest from the entrance to the dark side. Animals were allowed to explore the two compartments for 5 min. Videos were recorded with a camera positioned above the chamber. The latency to enter the dark compartment and the time spent in each side were quantified offline with TopScan. Room lighting was measured with the aid of a lux meter during testing (~100 Lux).

Novel object recognition test. The novel object recognition task assessed novelty-seeking behavior, capitalizing on rodents' natural inclination to spend more time with a novel object than a familiar one[66]. Object recognition testing was carried out in a Plexiglas open-field box (43.8 cm × 43.8 cm × 39.4 cm) and consisted of two sessions—habituation and recognition. During the habituation session, animals were allowed to freely explore the environment, which contained two identical Lego constructs in opposite corners of the box, for 10 min. Items were placed on a metal base to ensure they could not be moved or knocked over by the animals. Subsequently, mice were taken back to their home cages for an ITI of 1 h and were reintroduced in the apparatus for the recognition test lasting 10 min. In this 10-min session, one of the two objects used in the habituation phase was replaced with a novel object that was differently colored and shaped compared to the original, familiar object. The identity and position of the novel and familiar objects were counterbalanced across groups. Objects were thoroughly cleaned with water between phases to remove odor traces. Total time spent exploring each of the objects during both phases was quantified offline using TopScan. The discrimination ratio was calculated as the time spent interacting with the novel object area divided by the time spent in a novel object area plus the time spent in the familiar object area.

Social interaction assay. For social interaction experiments, mice were temporarily moved to a target-free holding arena (56 × 24 × 24 cm) that contained two empty mesh pencil cups (5 × 6.5 × 8 cm) in opposite corners of the arena. Animals were first allowed to freely explore the chamber for 2.5 min before a novel juvenile mouse (3–6 weeks) of the same sex and strain (to avoid mutual aggression) was placed into one of the holders. The test mouse was allowed to freely interact for 7.5 min, and video was recorded with a camera suspended above the arena. The 'interaction zone' encompassed a circular area projecting 6.5 cm around the pencil cup. The 'corner zones' encompassed a 9 cm × 9 cm area projecting from both corner joints opposing the wire-mesh enclosure. Social interaction was automatically scored with AnyMaze software (Stoelting) and defined as the ratio of time spent in the interaction zone with a juvenile mouse (that is, in active contact with the intruder's snout, flank or anogenital area, grooming, 6.5 cm from the enclosure of the pencil cup) over time spent with the target absent.

Operant conditioning. Before initiating operant procedures, mice were weighed to the nearest 0.1 g to determine a baseline for free-feeding body weight. Mice were singly housed and maintained under food restriction to achieve 85–90% of their free-feeding body weights for 3 days before and throughout the experiments, which motivated them to perform the operant tasks. Mice were weighed daily and fed 1 h after their daily behavioral sessions with 2 g of standard laboratory chow. Animals had free access to water throughout. Operant procedures were conducted 7 days per week over a 4-week period.

Chocolate pellet self-administration was used to examine reward-related behaviors and took place in sound-attenuated mouse operant chambers (ENV307A-CT, Med Associates; PC 5 software). Chambers were equipped with two retractable levers and a reward pellet dispenser. One lever was designated as 'active' and was paired with the delivery of chocolate pellets (20 mg, Bio-Serv), while the other lever was designated 'inactive' where lever pressing had no consequence on reward delivery. The assignment of active and inactive levers was counterbalanced across animals and chambers were kept dark (house light off) during all sessions. There was a 5-s time-out after every pellet delivery during which lever pressing did not trigger any delivery. A house light was positioned above the levers and a fan was present to maintain ventilation throughout testing. Before the start of the

conditioning experiments, animals first underwent two pretraining sessions in which chocolate pellets were delivered at a random interval schedule (mean of 45 s, range 4–132 s), where pressing in either lever had no consequence on reward delivery. Days 1–6 of operant training were conducted on an FR1 schedule, and days 7–12 were conducted on an FR5 schedule, where mice had to press the active lever one and five times, respectively, to earn a reward. Mice underwent testing in one session each day. All FR sessions lasted 45 min.

Operant choice task. Our operant choice task was modified from previous reports[47]. After 6 days of testing on an FR5 schedule, mice underwent testing on the operant choice task. First, mice experienced a session where they were presented with a food receptacle containing freely available regular laboratory chow or chocolate pellets in the corner of the operant chamber opposite of the wall containing the active lever and operant reward receptacle. This was done to pre-expose the animals to freely available food in the operant chambers. During this session, active and inactive levers were retracted. Mice were subsequently tested in a choice task, where they could either press the lever on an FR5 schedule to obtain a highly palatable food (20 mg chocolate food pellets) or consume the freely available food located on the opposite side of the operant chamber in a food receptacle. Choice sessions with regular laboratory chow or chocolate pellets were conducted on different days. After a choice session, a retrain session where only chocolate pellets delivered on the FR5 schedule were available was presented to the mice. The number of lever presses, quantity of freely available food (standard chow or chocolate pellet) consumed, total amount of food consumed (pellets plus chow) and the amount of chocolate pellets obtained by lever pressing were recorded.

PR operant tasks. After FR schedule sessions, a PR schedule of reinforcement was used to assess the motivation to work for chocolate pellets. To familiarize animals with a schedule requiring more effort, a PR3 schedule was used for 3 days. Under this schedule, response increments linearly increase by three lever presses (3, 6, 9, 12, 15) for delivery of each subsequent food pellet. Animals subsequently underwent 4 days of training on a PR7 schedule to assess motivation under a schedule with higher demands. In each PR session, the break point (the final number of responses an animal completes where a reward is delivered) and session length were recorded. All PR sessions ended after 3 h or until 5 min elapsed without the animal responding in the active lever.

Platform-mediated avoidance task. This modified tone-shock conditioning experiment tested for reinforcement of avoidance behavior. Experiments were conducted in sound-attenuated fear conditioning chambers (30 cm length × 25 cm width × 25 cm height, Med Associates) that were illuminated with red light. The floor of the chamber was composed of a metal grid that delivered an electric foot shock. All tests began with a 2-min baseline habituation. Following the baseline period, 20 pairings of a conditioned stimulus (CS, 30 s, 80 dB, 4 kHz noise) co-terminating with an unconditioned footshock stimulus (US, 0.4 mA, 2 s) were presented. The ITI was 40–60 s. Animals could avoid the shock by jumping onto a square Plexiglas platform (8 × 8 × 0.33 cm) located on a corner of the chamber that was fixed to the shock floors. Each experiment lasted for 2 days with one 30-min session conducted each day. Day 2 consisted of identical stimuli presentations as day one. Between experiments, shock grids and floor trays were cleaned with soap and water, and chamber walls were cleaned with wet paper towels. Data were acquired and analyzed using AnyMaze software. This task was modified from previous reports[44] to adapt it to mice.

Pavlovian cue–reward learning task. WT, *Drd3*$^{fl/fl}$ and *Drd1*$^{fl/fl}$ were bilaterally injected with AAV8-hSyn-GFP-Cre in the mNAcSh using glass pipettes (diameter 30–50 µm). Three weeks after injection, animals were food restricted to 85–90% of their free-feeding body weight for 3 days before testing. Mice were then trained in sound-attenuated boxes (ENV-307W, Med Associates) equipped with a tone generator, cue lights and a receptacle for 10% sucrose delivery that could detect head entries and individual licks. A 70-dB 4-kHz tone was given as a CS+ for 10 s, and US (that is, 20 µl of 10% sucrose water) was available 8 s after each CS+ onset. A 3.5-kHz tone was given as a CS−. Each session consisted of 40 trials wherein 20 trials corresponded to CS+ US pairings and 20 trials to CS− presentation. A 60 s ITI was followed by a 10 s tone/light cue presentation that terminated with delivery of 20 µl of a 10% sucrose solution. Licks that were made after cue onset but before reward delivery were counted as 'anticipatory' licks, while licks made after reward delivery were counted as 'consummatory' licks. Learning was assessed by comparing nose-poke rate during CS+ presentation with rate during ITI or CS−. Mice received six sessions of 60 min each, separated by 24 h. The next day after the last cue–reward learning session, mice began cue–reward extinction. Identical CS+ were given ten times per session, now without US delivery. Mice underwent a total of two extinction sessions. Chambers and lick ports were sanitized with Accel and 70% ethanol between animals to remove any odor. Cue onset, reward delivery, lick and port-entry timestamps were recorded with MED-PC (Med Associates) software and analyzed using Python and Excel (version 16.16.26, Microsoft).

D3R pharmacological inactivation

Microinjection of the D3R antagonist SB-277011A (Tocris) was used to pharmacologically inhibit D3R signaling in the mNAcSh. Animals were allowed to recover for 4 weeks after surgery before habituation to the microinjection procedure. For 2 days before the start of the experiments, mice were habituated to handling and cannula manipulation. On the experimental day, 350 nl of 10 µM SB-277011A (1.79 ng, dissolved in 1% dimethyl sulfoxide (DMSO) or vehicle (1% DMSO)) was bilaterally infused into the mNAcSh. This was accomplished using 33-gauge injector cannulas connected to a syringe pump (UMP3, World Precision Instruments) with PE20 tubing that protruded 1 mm beyond the tip of the 26-gauge guide cannula. All microinjections were delivered over the course of 1 min. After infusion, injectors were left in place for 2 min to allow for complete drug diffusion. For D3R functional disconnection procedures, mice were habituated 2 days before the experiment by receiving an infusion of vehicle (1% DMSO). Five minutes after the end of the intra-mNAcSh injection, animals were placed in the open-field arenas and running disk choice testing was conducted. Cannula placements were verified by histology after injection of 300 nl (per hemisphere) of red fluorescent retrobeads (Lumafluor).

D1R–NMDAR functional disconnection

For 2 days before the start of D1R–NMDAR operant procedures, mice were habituated to handling and cannula manipulation. On the experiment day, 350 nl per hemisphere of the competitive NMDAR antagonist AP5 (700 ng per infusion, dissolved in 0.9% saline) was infused according to the same procedure as D3R pharmacological inactivation. Cannula placements and spread of infused AP5 were verified by histology after injection of 300 nl per hemisphere of red fluorescent retrobeads (Lumafluor).

Chemogenetic inhibition of *Drd3*-expressing mNAcSh MSNs

Drd3-Cre mice undergoing inhibitory DREADD testing were allowed to recover for 4 weeks following viral injection before the start of experiments. On the day before testing, mice received an intraperitoneal injection of saline to habituate them with the injection procedure. On the day of the experiment, the DREADD agonist CNO (Enzo Life Sciences) was administered intraperitoneally 30 min before the running disks test. CNO solutions were intraperitoneally injected at 0.1 ml solution per 10 g of mouse for a final concentration of 1 mg per kg body weight (in sterile saline).

Drugs

(+)-PD-128907 hydrochloride (PD-128907, Tocris), ML417 (Sibley Lab, NINDS) and SKF-81297 (Tocris) were dissolved in distilled water. SCH-39166 (Tocris) was dissolved in DMSO. For electrophysiology experiments, 1 mM PD-128907 and 1 mM SCH-39166 were diluted to a final concentration of 1 µM in aCSF and 10 mM SKF-81297 was diluted to a final concentration of 10 µM in aCSF. AP5 (Abcam) was diluted in sterile 0.9% saline. SB-277011A (Tocris Biosciences) was dissolved in 1% DMSO and administered at 10 µM. AP5 (Abcam) was diluted in sterile 0.9% saline.

Quantification and statistical analysis

Data analysis was performed using GraphPad Prism 9.3.0. (GraphPad Software). Data distribution was assumed to be normal, but this was not formally tested. Paired *t*-tests were used for within-group comparison of two treatments and an unpaired test was used for comparison between two groups. Differences across more than two groups were analyzed with a one-way ANOVA with Tukey's or Dunnet's multiple-comparison post hoc test, a two-way ANOVA for data with Tukey's or Sidak's multiple-comparison post hoc test for two independent variables or a two-way repeated-measures ANOVA for data with two independent variables and multiple measurements from the same subject. ANOVAs were followed by post hoc tests with multiple-comparisons correction. In the case of datasets with missing values, we analyzed the data instead by fitting a (one-way) mixed model as implemented in GraphPad Prism 9.3.0. The Kolmogorov–Smirnov test was used for cumulative probability plots. *P* values for linear regressions were calculated by using Pearson's correlation. For each experiment, the values and definitions of sample size (*n*) are explicitly explained in the corresponding figure legend, as well as in Supplementary Table 1. Statistical significance was defined as $^{*}P < 0.05$, $^{**}P < 0.01$, $^{***}P < 0.001$, $^{****}P < 0.0001$. R^2 represents a Pearson's correlation coefficient. Results are shown as the mean ± s.e.m. unless stated otherwise. Error bars represent the s.e.m. See Supplementary Table 1 for detailed statistics. No statistical method was used to predetermine sample size. Sample sizes were based on pilot experiments, previous experience with similar types of experiments and/or sample sizes typical of the technique used in literature from the field. Data were only excluded from the analyses for technical reasons, including misplaced viral injection, guide cannula, insufficient expression and a change in access resistance or cell health during electrophysiological recordings. Allocation to groups or treatment was randomized, where possible. Experimenters were not blinded in some cases during data acquisition as some information was not blinded (for example, type of virus injected). However, analyses were performed blinded to the scorer and/or did not require manual scoring.

Reporting summary

Further information on research design is available in the Nature Portfolio Reporting Summary linked to this article.

Data availability

All data generated in the current study are available from the corresponding author upon reasonable request. Outlines for brain regions were acquired from Paxinos and Franklin's the Mouse Brain in Stereotaxic Coordinates[63]. All mouse and neuron illustrations included in the main and extended data figures were created with BioRender.com during the subscription period. Source data are provided with this paper.

Code availability

No custom code was generated for this study.

References

58. Fenno, L. E. et al. Targeting cells with single vectors using multiple-feature Boolean logic. *Nat. Methods* **11**, 763–772 (2014).
59. Liu, P., Jenkins, N. A. & Copeland, N. G. A highly efficient recombineering-based method for generating conditional knockout mutations. *Genome Res.* **13**, 476–484 (2003).
60. Wang, F. et al. RNAscope: a novel in situ RNA analysis platform for formalin-fixed, paraffin-embedded tissues. *J. Mol. Diagn.* **14**, 22–29 (2012).
61. McQuin, C. et al. CellProfiler 3.0: next-generation image processing for biology. *PLoS Biol.* **16**, e2005970 (2018).
62. Erben, L. & Buonanno, A. Detection and quantification of multiple RNA sequences using emerging ultrasensitive fluorescent in situ hybridization techniques. *Curr. Protoc. Neurosci.* **87**, e63 (2019).
63. Franklin, K. B. J. & Paxinos, G. *Paxinos and Franklin's the Mouse Brain in Stereotaxic Coordinates* (Academic, 2013).
64. Schmittgen, T. D. & Livak, K. J. Analyzing real-time PCR data by the comparative CT method. *Nat. Protoc.* **3**, 1101–1108 (2008).
65. Jackman, S. L., Beneduce, B. M., Drew, I. R. & Regehr, W. G. Achieving high-frequency optical control of synaptic transmission. *J. Neurosci.* **34**, 7704–7714 (2014).
66. Bevins, R. A. & Besheer, J. Object recognition in rats and mice: a one-trial non-matching-to-sample learning task to study 'recognition memory'. *Nat. Protoc.* **1**, 1306–1311 (2006).

Acknowledgements

This work was supported by the NIMH Intramural Research Program (ZIA MH002970-04; to H.A.T.), a Brain and Behavior Research Foundation NARSAD Young Investigator Award (to H.A.T.), National Institutes of Health (NIH) Center for Compulsive Behavior Fellowships (to R.F.G. and H.E.Y.-C.), Department of Defense PRMRP Investigator-Initiated Award (PR141292; to Z.F.), Department of Defense PRMRP Expansion Award (PR210207; to Z.F.), John F. and Nancy A. Emmerling Fund of The Pittsburgh Foundation (to Z.F.), R01DA061243 (to Z.F.), R01ES034037 (to Z.F.), R01DK124219 (to Z.F.) and an NIH Post-Doctoral Research Associate Training Fellowship (to R.F.G). The funders had no role in study design, data collection and analysis, decision to publish or preparation of the manuscript. We thank S. Williams and J. Kuo of the NIMH Systems Neuroscience Imaging Resource and S. Hattar for their microscopy support. We also acknowledge Y. Chudasama, A. Graham and members of the NIMH Rodent Behavior Core for behavioral equipment support and S. Hattar for sharing running wheels. We also thank C. Schmauss, J. Javitch and M. Rubinstein for the design of the *Drd3*$^{fl/fl}$ mouse strain as well as S.-P. Yee and the Center for Mouse Genome Modification at UConn Health for the construction of the *Drd3*$^{fl/fl}$ mice. We additionally acknowledge V. Alvarez and members of the Alvarez laboratory including L. Dobbs and M. Bocarsly for all their invaluable help in making the *Drd3*$^{fl/fl}$ mice congenic with the C57BL/6J genetic background. Finally, we thank members of the Unit on Neuromodulation and Synaptic Integration and M. Penzo, M. Pignatelli, F. Lucantonio, E. Lewis, D. Vullhorst and A. Buonanno for discussions and critical reading of the manuscript.

Author contributions

Conceptualization: J.E.-T. and H.A.T. Software: J.E.-T., R.J.F. and S.R. Behavioral studies and analyses: J.E.-T., H.A.T., T.W., C.T.L., M.A., V.S.T. and R.J.F. Anatomy: J.E.-T., C.N., T.B.U., H.W. and S.R. Surgeries: J.E.-T., H.E.Y.-C., H.W., M.A. and C.N. Slice electrophysiology: J.E.-T., H.E.Y.-C. and H.A.T. Slice imaging: D.K. and A.L. Generation of *Drd3* loxP mice: Z.F. PCR: J.E.-T. and R.M. Novel selective D3R agonist: A.F.M and D.R.S. Data curation: J.E.-T. Writing: J.E.-T. and H.A.T. Editing: J.E.-T., Z.F. and H.A.T. Visualization: J.E.-T. Supervision: R.M. and H.A.T. Project administration: J.E.-T. and H.A.T. Funding acquisition: H.A.T.

Competing interests
The authors declare no competing interests.

Additional information
Extended data is available for this paper at https://doi.org/10.1038/s41593-024-01819-9.

Supplementary information The online version contains supplementary material available at https://doi.org/10.1038/s41593-024-01819-9.

Correspondence and requests for materials should be addressed to Zachary Freyberg or Hugo A. Tejeda.

Peer review information *Nature Neuroscience* thanks Nicolas Tritsch and the other, anonymous, reviewer(s) for their contribution to the peer review of this work.

Reprints and permissions information is available at www.nature.com/reprints.

https://doi.org/10.1038/s41593-024-01819-9

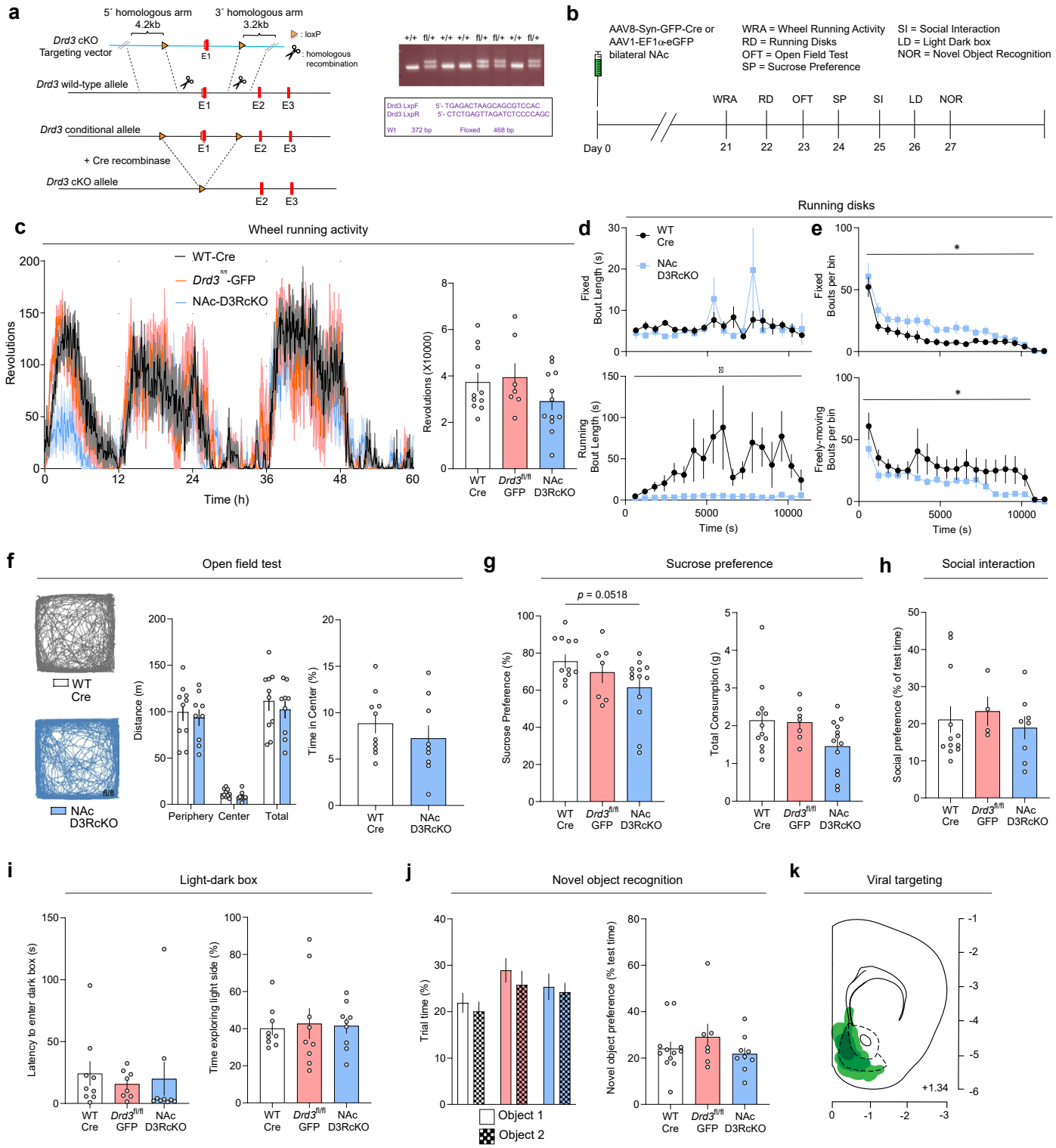

Extended Data Fig. 1 | See next page for caption.

https://doi.org/10.1038/s41593-024-01819-9

Extended Data Fig. 1 | Genetic ablation of mNAcSh D3Rs does not affect locomotion, anhedonia, social reward, anxiety or novel object-recognition. **a**. (Left) Schematic depicting the strategy used to generate the *Drd3*$^{fl/fl}$ conditional-knockout (cKO) mouse strain. loxP cassettes flanking the exon 1 were inserted in the coding region of the *Drd3* gene that encodes the D3R protein using homologous recombination approaches. (Right) Confirmation of the inserted loxP sites within the chimeric animals by using PCR strategies (see primers in purple). The successful insertion of the loxP elements was confirmed by the presence of two PCR bands (fl/+ lanes) versus a single band in the wildtype littermates (+/+ lanes). **b**. Experimental timeline of behavioral experiments. **c**. (Left) Timecourse of wheel-running activity for the entire duration of the experiment (60 hrs) in WT-Cre (black, n = 11), *Drd3*$^{fl/fl}$-GFP (red, n = 7) and NAc-D3RcKO (blue, n = 12) mice (two-way repeated measures ANOVA: Time effect, $F_{(12.86, 347.3)} = 18.12$, $P < 0.0001$; treatment effect, $F_{(2, 27)} = 1.552$, $P = 0.2301$; time × treatment, $F_{(1438, 19413)} = 1.633$, $P < 0.0001$). L = Light; D= Dark. (Right) Quantification of total revolutions per group during the entire 60 hr period (one-way ANOVA followed by two-sided Dunnett's test: $F_{(2, 27)} = 1.578$. Group comparisons, NAc-D3RcKO versus, WT-Cre, $P = 0.285$, NAc-D3RcKO versus *Drd3*$^{fl/fl}$-GFP, P = 0.0.2282). **d**. Length of visit (bout) to the fixed disk (top) or freely-moving disk (bottom, putative running bout) across the running disks session in WT-Cre (black, n = 11) and NAc-D3RcKO (blue, n = 12) mice (fixed disk: two-way repeated measures ANOVA: Time effect, $F_{(1.649, 26.68)} = 1.906$, $P = 0.1736$; genotype effect, $F_{(1, 20)} = 0.00014$, $P = 0.9907$; time × genotype, $F_{(17, 275)} = 1.138$, $P = 0.3172$; moving disk: two-way repeated measures ANOVA: Time effect, $F_{(2.803, 49.63)} = 1.391$, $P = 0.2574$; genotype effect, $F_{(1, 20)} = 7.456$, $P = 0.9907$; time × genotype $F_{(17, 301)} = 1.199$, $P = 0.2636$). **e**. Number of entries into the fixed (top) or freely-moving disk (bottom) across the running disks session in WT-Cre (black, n = 11) and NAc-D3RcKO (blue, n = 12) mice (fixed disk: two-way repeated measures ANOVA: Time effect, $F_{(3.329, 66.59)} = 23.39$, $P < 0.0001$; $F_{(1, 20)} = 7.270$, $P = 0.0139$; time × genotype, $F_{(18, 360)} = 0.9697$, $P = 0.4944$; moving disk: two-way repeated measures ANOVA: Time effect, $F_{(1.933, 38.67)} = 9.639$, $P = 0.0005$; genotype effect, $F_{(1, 20)} = 2.356$, $P = 0.0404$; time × genotype $F_{(18, 360)} = 0.9787$, $P = 0.4838$). **f**. (Left) Representative cumulative locomotion traces of open field activity in WT-Cre (n = 10 mice) and NAc-D3RcKO (n = 12 mice) groups. (Middle) Quantification of cumulative distance traveled (two-way repeated measures ANOVA: Zone effect, $F_{(1.033, 17.57)} = 209.1$, $P < 0.0001$; genotype effect, $F_{(1, 17)} = 0.4217$, $P = 0.5247$; zone × genotype, $F_{(2, 34)} = 0.1721$, $P = 0.8426$). (Right) Percentage of time spent in the center during the open field test (unpaired t-test (two-tailed), $t(17) = 0.9305$; $P = 0.3651$). **g**. (Left) Percentage of sucrose preference in WT-Cre (black, n = 12), *Drd3*$^{fl/fl}$-GFP (red, n = 7) and NAc-D3RcKO (blue, n = 13) mice (one-way ANOVA followed by two-sided Dunnett's test: $F_{(2, 29)} = 2.713$. Group comparisons, NAc-D3RcKO versus, WT-Cre, $P = 0.0518$, NAc-D3RcKO versus, *Drd3*$^{fl/fl}$-GFP, $P = 0.428$ (Right) Overall intake in the sucrose preference test (one-way ANOVA followed by two-sided Dunnett's test: $F_{(2, 29)} = 2.904$. Group comparisons, NAc-D3RcKO versus, WT-Cre, $P = 0.0635$, NAc-D3RcKO versus, *Drd3*$^{fl/fl}$-GFP, $P = 0.1606$). **h**. Social preference as reflected by the % time (test-habituation) spent interacting with a novel, juvenile mouse in WT-Cre (black, n = 12), *Drd3*$^{fl/fl}$-GFP (red, n = 4) and NAc-D3RcKO (blue, n = 8) groups (one-way ANOVA followed by two-sided Dunnett's test: $F_{(2, 21)} = 0.2411$. Group comparisons, NAc-D3RcKO versus, WT-Cre, $P = 0.8698$, NAc-D3RcKO versus, *Drd3*$^{fl/fl}$-GFP, $P = 0.7329$). **i**. Anxiety-like behavior as represented by the latency to enter dark chamber in the light–dark box (left; one-way ANOVA followed by two-sided Dunnett's test: $F(2, 23) = 0.1608$. Group comparisons, NAc-D3RcKO versus, WT-Cre, $P = 0.9391$, NAc-D3RcKO versus, *Drd3*$^{fl/fl}$-GFP, $P = 0.9449$) or time spent in the light side of the light-dark box (right; one-way ANOVA followed by two-sided Dunnett's test: $F_{(2, 23)} = 0.04904$. Group comparisons, NAc-D3RcKO versus, WT-Cre, $P = 0.9791$, NAc-D3RcKO versus, *Drd3*$^{fl/fl}$-GFP, $P = 0.9852$) in WT-Cre (black, n = 9), *Drd3*$^{fl/fl}$-GFP (red, n = 8) and NAc-D3RcKO (blue, n = 9) mice. **j**. (Left) Time spent interacting with each of the objects during the baseline period in WT-Cre (black, n = 12), *Drd3*$^{fl/fl}$-GFP (red, n = 7) and NAc-D3RcKO (blue, n = 9) mice (two-way repeated measures ANOVA: Object effect, $F_{(1, 25)} = 1.418$, $P = 0.245$; treatment effect, $F_{(2, 25)} = 2.734$, $P = 0.0844$; object × treatment, $F_{(2, 25)} = 0.1025$, $P = 0.903$). (Right) Preference for the novel object over a familiar one during the discrimination test (one-way ANOVA followed by two-sided Dunnett's test: $F_{(2, 25)} = 0.8822$. Group comparisons, NAc-D3RcKO versus, WT-Cre, $P = 0.8593$, NAc-D3RcKO versus, *Drd3*$^{fl/fl}$-GFP, $P = 0.3346$). **k**. Schematic of combined viral spread map of local *Drd3* cKO. Dark green indicates animals with most restricted expression and lighter green indicates animals with broader pattern of viral spread. All data in this figure are presented as mean ± SEM Error bars indicate SEM.

https://doi.org/10.1038/s41593-024-01819-9

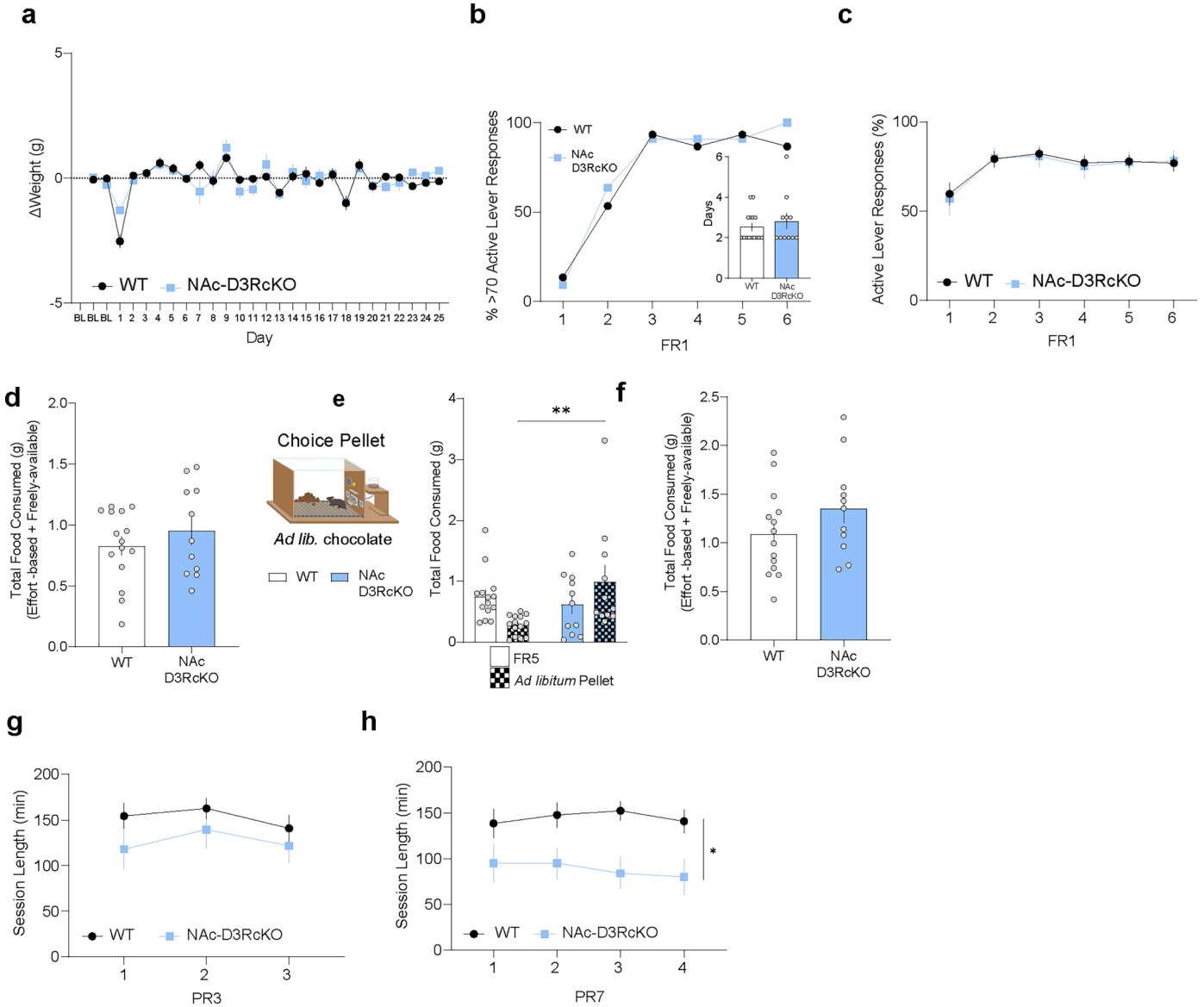

Extended Data Fig. 2 | mNAcSh D3R cKO decreases motivation towards working for rewards, but does not affect weight, or FR acquisition schedules of reinforcement. a Body weight changes at baseline before food deprivation and across the overall duration of operant conditioning procedures in Fig. 1 and Extended Data Fig. 1 in WT-Cre (black, n = 15) and NAc-D3RcKO (blue, n = 11) mice (two-way repeated measures ANOVA: Session effect, $F_{(8.178, 204.4)} = 11.95$, $P < 0.0001$; genotype effect, $F_{(1, 25)} = 0.4982$, $P = 0.4868$; object × treatment, $F_{(26, 650)} = 1.950$, $P = 0.0034$). **b** FR1 acquisition, as measured by the percentage of animals reaching the criteria of 70 active lever responses per session. (Inset) Days required to acquire FR1 (criteria for acquisition was 70 responses in a 45 min session) (unpaired t-test (two-tailed), $t_{(24)} = 0.7272$; $P = 0.4741$). **c** Percentage of active lever responses during FR1 schedules in WT-Cre (black, n = 15) and NAc-D3RcKO (blue, n = 11) mice (two-way repeated measures ANOVA: Session effect, $F_{(2.060, 51.62)} = 11.19$, $P < 0.0001$; genotype effect, $F_{(1, 24)} = 0.1973$, $P = 0.6609$; session x genotype, $F_{(5, 117)} = 0.3905$, $P = 0.8545$). **d** Total food consumed in choice chow session in WT-Cre (black, n = 15) and NAc-D3RcKO (blue, n = 11) mice (unpaired t-test (two-tailed), $t_{(24)} = 0.9353$; $P = 0.3589$). **e** (Left) Diagram of the FR5 choice pellet session. (Right) Amount of food consumed, which is represented as FR5 effort-based or freely-available chocolate pellets in WT-Cre (black, n = 15) and NAc-D3RcKO (blue, n = 11) mice (two-way repeated measures ANOVA: Type of food effect, $F_{(1, 23)} = 0.07947$, $P = 0.7805$; genotype effect, $F(1, 23) = 4.808$, $P = 0.0387$; type of food x genotype, $F(1, 23) = 6.314$, $P = 0.0194$). **f** Total food consumed in FR5 choice pellet session in WT-Cre (black, n = 15) and NAc-D3RcKO (blue, n = 11) mice (unpaired t-test (two-tailed), $t_{(24)} = 1.382$; $P = 0.0.1802$). **g** PR3 session length in WT-Cre (black, n = 15) and NAc-D3RcKO (blue, n = 11) mice (two-way repeated measures ANOVA: Session effect, $F_{(1.709, 38.46)} = 1.264$, $P = 0.2899$; genotype effect, $F_{(1, 24)} = 2.267$, $P = 0.1452$; session x genotype, $F_{(2, 45)} = 0.2682$, $P = 0.766$). **h** PR7 session length in WT-Cre (black, n = 15) and NAc-D3RcKO (blue, n = 11) mice (two-way repeated measures ANOVA: Session effect, $F_{(2.013, 48.31)} = 0.3719$, $P = 0.6927$; genotype effect, $F_{(1, 24)} = 9.612$, $P = 0.0049$; session x genotype, $F_{(3, 72)} = 0.5050$, $P = 0.68$). All data in this figure are presented as mean ± SEM Error bars indicate SEM. Schematics were generated using BioRender.com.

https://doi.org/10.1038/s41593-024-01819-9

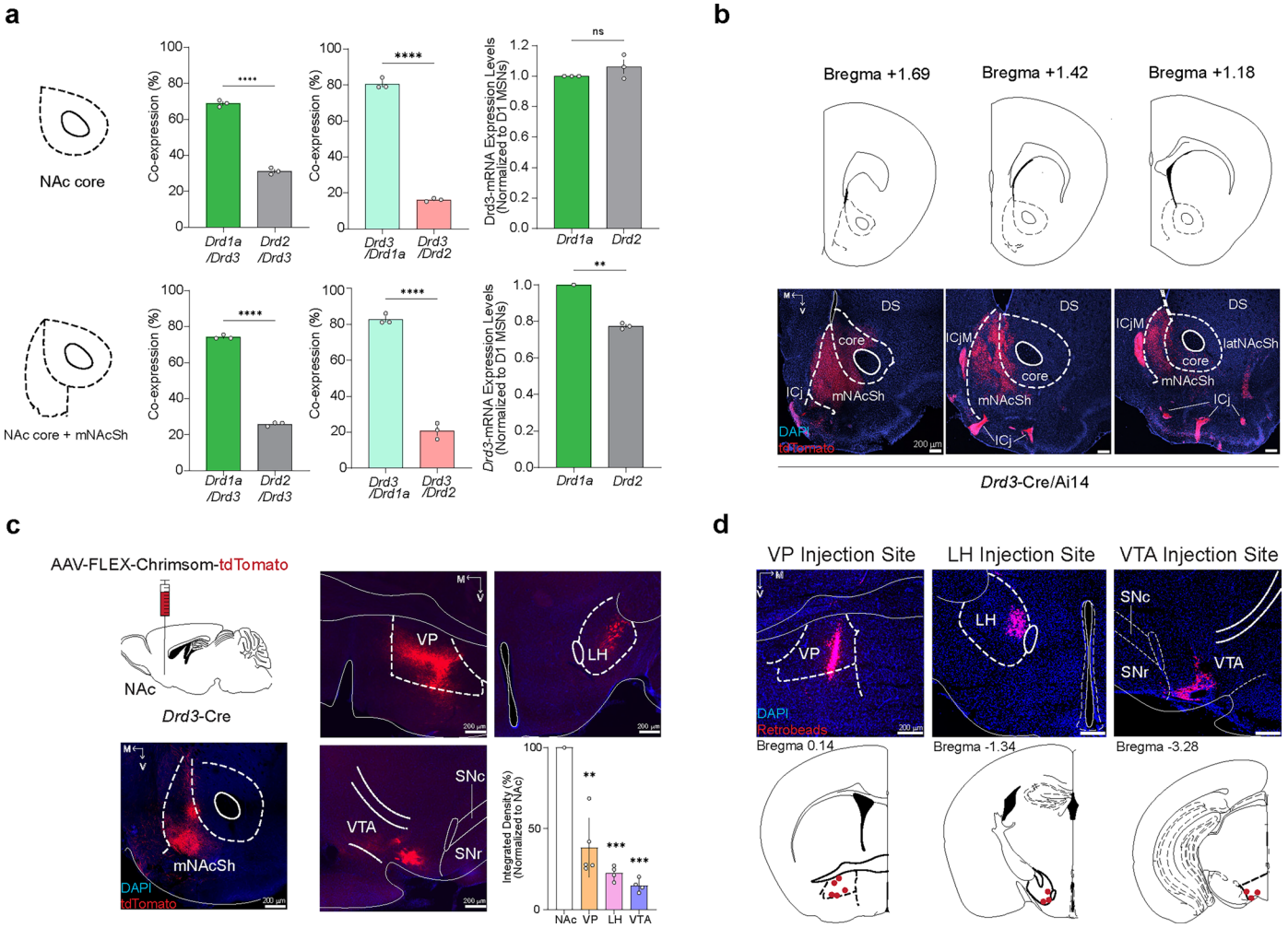

Extended Data Fig. 3 | *Drd3*-Cre lines provide genetic access to Drd3 expression in the mNAcSh and outputs of D3-MSNs. a RNA *in-situ* hybridization results for NAc core (top) or overall NAc (bottom) cells of WT (n = 3) mice. **b** *Drd3* expression in the mNAcSh of *Drd3*-Cre/Ai14 mice. Coronal diagrams depicting the region analyzed (top) and confocal images showing the *Drd3* expression pattern in the mNAcSh along the dorsal-ventral and rostral-caudal axis (bottom). DS = dorsal striatum; ICj = islands of Calleja; ICjM = major island of Calleja; latNAcSh = lateral NAc shell. **c** (Left) A virus encoding the anterograde tracer (AAV1-Syn-FLEX-Chrimsom-tdTomato) was targeted to the mNAcSh in *Drd3*-Cre mice that express tdTomato in a Cre-dependent manner. (Right) Representative images and quantification of tdTomato$^+$ fibers in mNAcSh (n = 4 mice), VP (n = 4 mice), LH (n = 4 mice) and VTA (n = 3 mice) regions (one-way ANOVA followed by two-sided Tukey's test: $F_{(3,10)} = 14.66$. Group comparisons, NAc versus, VP, **P = 0.0039, NAc versus LH, ***P = 0.0009, NAc versus VTA, ***P = 0.0004, VP versus LH, P = 0.2659, VP versus VTA, P = 0.0651, LH versus VTA, P = 0.8112). **d** Representative images (top) and reconstructions (bottom) of VP, LH, and VTA retrobead injection sites for experiments shown in Fig. 2l. All data in this figure are presented as mean ± SEM Error bars indicate SEM.

https://doi.org/10.1038/s41593-024-01819-9

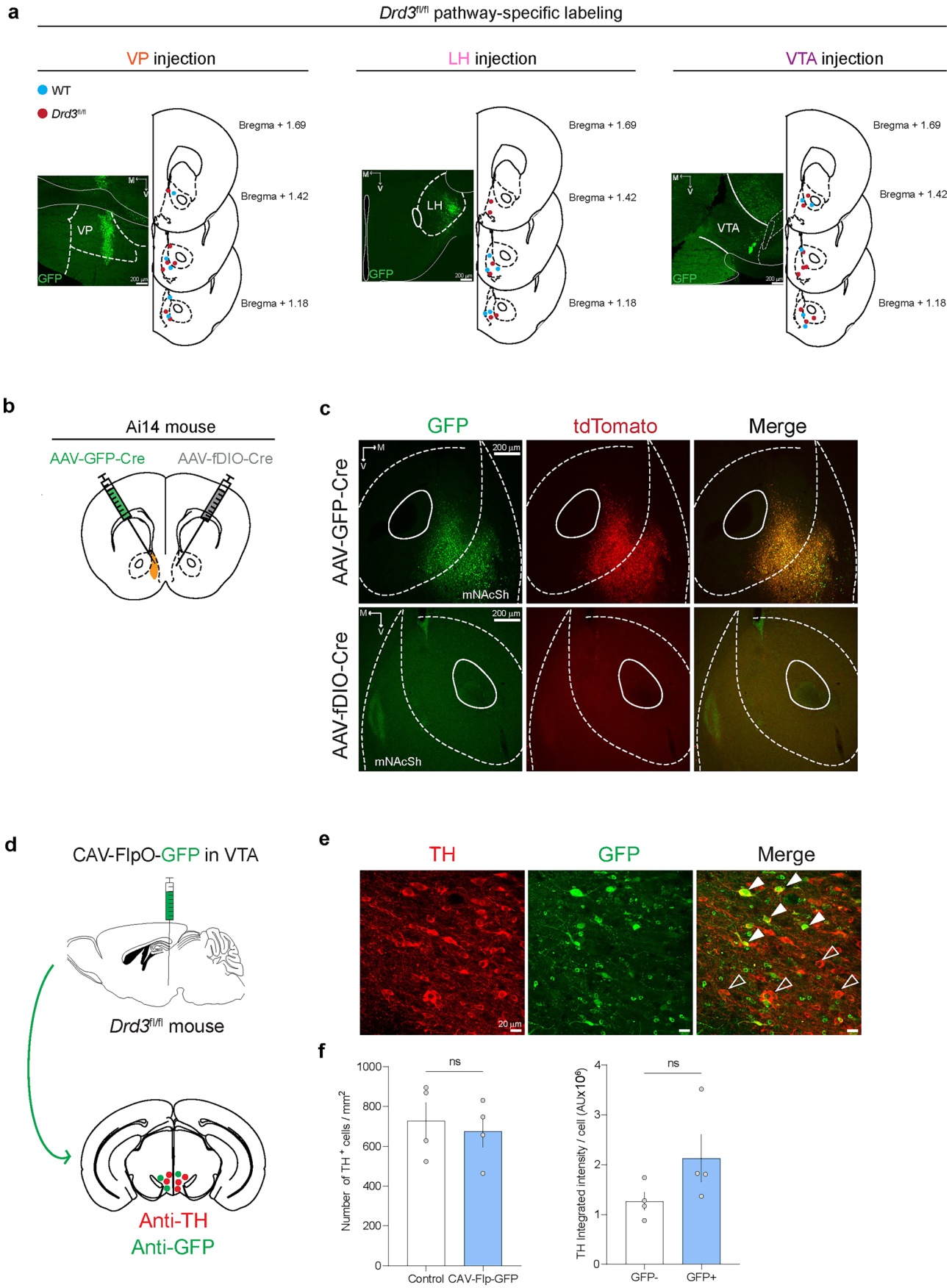

Extended Data Fig. 4 | See next page for caption.

https://doi.org/10.1038/s41593-024-01819-9

Extended Data Fig. 4 | Histological validation of our intersectional approach for pathway-specific NAc Drd3 cKO. a. Viral injection placements for pathway-specific deletion of NAc D3Rs experiment. For each manipulation representative images of injection sites of CAV-Flp-GFP (left) and serial reconstructions of tdTomato expression in the NAc (right) are shown. Each circle depicts the position of the strongest tdTomato expression for each subject. **b** Scheme of the experimental design to validate the lack of Cre leakage in our pathway-specific strategy for the cKO of NAc *Drd3*. AAV8-Syn-GFP-Cre and AAV9-EF1a-fDIO-Cre were injected in contralateral hemispheres of Ai14-tdTomato reporter mouse. **c** Representative images showing colabeling of GFP and tdTomato in the hemisphere injected with AAV-GFP-Cre (top) and lack of tdTomato expression in the hemisphere injected with AAV-fDIO-Cre (bottom). **d** Scheme of the experimental design to address the potential toxicity of CAV injection in DA cell degeneration of the VTA. CAV-FlpO-GFP was injected in the VTA and slices containing the VTA were immunostained for TH and GFP. **e** Representative images of TH expression and GFP labeling in the VTA. Filled arrows indicate double positive GFP and TH neurons; empty arrows indicate single-positive TH neurons (that is GFP-negative). **f** (Left) Quantification of number of TH-positive cells in control (n = 4) and injected (n = 4) mice (unpaired t-test (two-tailed), $t_{(6)}$= 0.4512; P = 0.6677). (Right) TH integrated density in GFP-negative or GFP-positive cells (unpaired t-test (two-tailed), $t_{(6)}$= 1.698; P = 0.1404). All data in this figure are presented as mean ± SEM Error bars indicate SEM.

https://doi.org/10.1038/s41593-024-01819-9

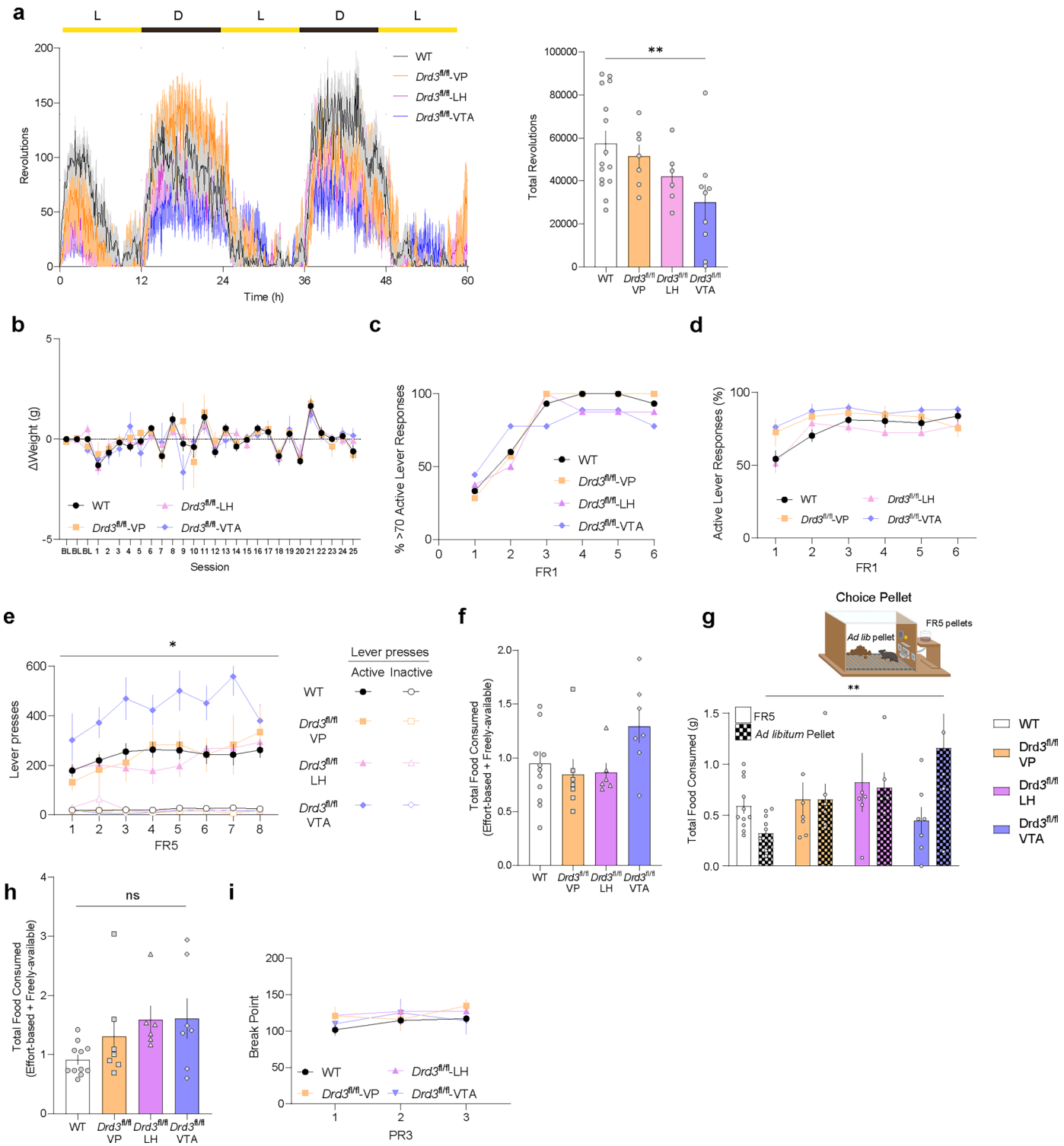

Extended Data Fig. 5 | See next page for caption.

https://doi.org/10.1038/s41593-024-01819-9

Extended Data Fig. 5 | NAc D3R function supports running and working for reward, but does not regulate acquisition of reinforcement. a. Wheel running activity for pathway-specific deletion of NAc D3Rs (WT, n = 15 mice; *Drd3*$^{fl/fl}$-VP, n = 7 mice; *Drd3*$^{fl/fl}$-LH, n = 6 mice; *Drd3*$^{fl/fl}$-VTA, n = 9 mice). (Left) Timecourse of running activity during the complete 60-hr experiment (two-way repeated measures ANOVA: Time effect, $F_{(2.013, 48.31)}$= 0.3719, P < 0.0001; treatment effect, $F_{(3, 34)}$= 2.361, P = 0.0887; time x treatment, $F_{(2157, 24446)}$= 1.538, P < 0.0001). (Right) Quantification of total revolutions during the 60-hr period (one-way ANOVA followed by two-sided Dunnett's test: $F_{(3, 33)}$= 3.556. Group comparisons, WT versus *Drd3*$^{fl/fl}$-VP, P = 0.4806, WT versus *Drd3*$^{fl/fl}$-LH, P = 0.1265, WT versus *Drd3*$^{fl/fl}$-VTA, P = 0.0903). **b** Body weight changes at baseline before food deprivation and across the overall duration of operant conditioning procedures in Fig. 3 (WT, n = 11 mice; *Drd3*$^{fl/fl}$-VP, n = 7 mice; *Drd3*$^{fl/fl}$-LH, n = 6 mice; *Drd3*$^{fl/fl}$-VTA, n = 7 mice) (two-way repeated measures ANOVA: Session effect, $F_{(5.885, 185.7)}$ = 8.340, P < 0.0001; treatment effect, $F_{(3, 852)}$= 0.7685, P = 0.5118; session x treatment, $F_{(81, 852)}$= 0.8500, P = 0.8212). **c** FR1 acquisition, as measured by the percentage of animals reaching the criteria of 70 active lever responses per session. **d** Percentage of active lever responses during FR1 schedules (WT, n = 11 mice; *Drd3*$^{fl/fl}$-VP, n = 7 mice; *Drd3*$^{fl/fl}$-LH, n = 6 mice; *Drd3*$^{fl/fl}$-VTA, n = 7 mice) (two-way repeated measures ANOVA: Session effect, $F_{(3.485, 85.73)}$= 16.46, P < 0.0001; treatment effect, $F_{(3, 26)}$= 2.953, P = 0.0511; session x treatment, F(15, 123)= 1.975, P = 0.0221). **e** Lever presses during FR5 acquisition sessions (WT, n = 11 mice; *Drd3*$^{fl/fl}$-VP, n = 7 mice; *Drd3*$^{fl/fl}$-LH, n = 6 mice; *Drd3*$^{fl/fl}$-VTA, n = 7 mice) (two-way repeated measures ANOVA: Session effect, $F_{(4.782, 120)}$= 10.98, P < 0.0001; treatment effect, $F_{(3, 28)}$= 2.718, P = 0.0635; session x treatment, $F_{(30, 251)}$= 2.247, P = 0.0004). **f** Total food consumed in choice chow session (WT, n = 11 mice; *Drd3*$^{fl/fl}$-VP, n = 7 mice; *Drd3*$^{fl/fl}$-LH, n = 6 mice; *Drd3*$^{fl/fl}$-VTA, n = 7 mice) (one-way ANOVA followed by two-sided Dunnett's test: F (3, 28) = 2.347. Group comparisons, WT versus *Drd3*$^{fl/fl}$-VP, P = 0.8858, WT versus *Drd3*$^{fl/fl}$-LH, P = 0.9406, WT versus *Drd3*$^{fl/fl}$-VTA, P = 0.1408). **g** (Top) Diagram of the FR5 choice pellet session. (Bottom) Amount of food consumed which is represented as either FR5 effort-based (solid) or freely-available chocolate pellets (checkered) (WT, n = 11 mice; *Drd3*$^{fl/fl}$-VP, n = 7 mice; *Drd3*$^{fl/fl}$-LH, n = 6 mice; *Drd3*$^{fl/fl}$-VTA, n = 7 mice) (two-way repeated measures ANOVA: Type of food effect, $F_{(1, 27)}$= 0.6669, P = 0.4213; treatment effect, $F_{(3, 27)}$= 2.258, P = 0.1044; type of food x treatment, $F_{(3, 27)}$= 3.256, P = 0.037). **h** Effects of region-specific D3R cKO on total consumption of chocolate pellets in a FR5 choice pellet session (WT, n = 11 mice; *Drd3*$^{fl/fl}$-VP, n = 7 mice; *Drd3*$^{fl/fl}$-LH, n = 6 mice; *Drd3*$^{fl/fl}$-VTA, n = 7 mice; one-way ANOVA: followed by two-sided Dunnett's test $F_{(3, 27)}$= 2.258, Group comparisons, WT versus *Drd3*$^{fl/fl}$-VP, P = 0.4806, WT versus *Drd3*$^{fl/fl}$-LH, P = 0.1265, WT versus *Drd3*$^{fl/fl}$-VTA, P = 0.0903). **i** Break points during the PR3 reinforcement schedule for VP-, LH-, and VTA-specific D3R cKO versus WT controls (two-way repeated measures ANOVA: Session effect, $F_{(1.491, 41.00)}$= 3.086, P = 0.0702; treatment effect, $F_{(3, 31)}$= 0.6072, P = 0.6153; session x treatment, $F_{(6, 55)}$= 0.8598, P = 0.5302). All data in this figure are presented as mean ± SEM Error bars indicate SEM. Schematics were generated using BioRender.com.

https://doi.org/10.1038/s41593-024-01819-9

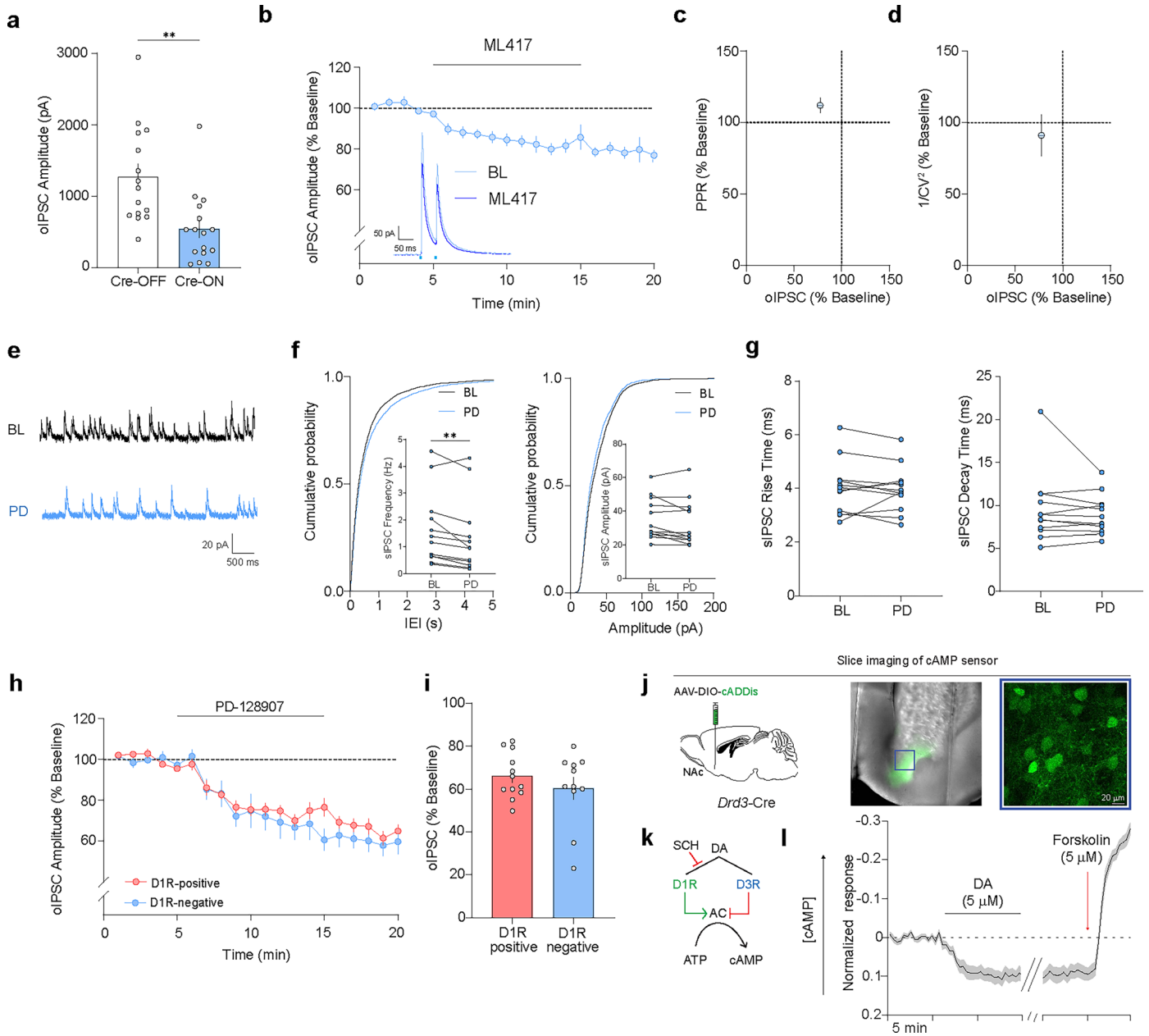

Extended Data Fig. 6 | Activation of mNAcSh D3R decreases GABA release probability presynaptically onto both D1- and D2-MSNs. a Mean baseline oIPSC amplitude (pA) for Cre-OFF (white bar, n = 15 cells from 7 mice) and Cre-ON (blue bar, n = 16 cells from 9 mice) evoked in mNAcSh MSNs (unpaired t-test (two-tailed), $t_{(29)}$= 3.420; **P = 0.0019). **b** Timecourse of oIPSCs in mNAcSh MSNs before, during and after bath application of the D3R-selective agonist ML417 (1 μM) in *Drd3*-Cre mice expressing Cre-dependent ChR2 (blue, n = 11 cells from 8 mice). (Inset) Representative oIPSC traces recorded in mNAcSh MSNs before and after bath application of ML417. **c** Paired-pulse ratio (PPR, % baseline) versus oIPSC (% baseline) after ML417 application (n = 11 cells from 8 mice). **d** Coefficient of variation (1/CV^2, % baseline) versus oIPSC (% baseline) after ML417 application (n = 11 cells from 8 mice). **e** Representative traces of sIPSCs during baseline (BL, black) and after bath-application of the D3R-selective agonist PD-128907 (PD, blue). **f** Cumulative probability of sIPSC inter-event interval (left; Kolmogorov-Smirnov test, ks = 36.740988, P < 0.0001) and amplitude (right; Kolmogorov-Smirnov test, ks = 2.401130, P < 0.0001) recorded from mNAcSh MSNs (n = 12 cells from 7 mice). (Inset) Quantification of frequency (paired t-test (two-tailed), $t_{(11)}$= 3.131; **P = 0.0096) and amplitude (paired t-test (two-tailed), $t_{(11)}$= 1.851; P = 0.0912) of sIPSCs events during baseline and after PD-128907 application. **g** Rise (left; paired t-test (two-tailed), $t_{(11)}$= 0.3225; P = 0.7531) and decay time (right, paired t-test (two-tailed), $t_{(11)}$= 1.029; P = 0.3256) of sIPSC events during baseline and after PD-128907 application (n = 12 cells from 7 mice). **h** Time-course of oIPSCs before, during and after bath application of PD-128907 in mNAcSh D1R-positive (red, n = 12 cells from 5 mice) and D1R-negative neurons (putative D2-MSNs) (blue, n = 11 cells from 5 mice) in the Cre-ON condition (two-way repeated measures ANOVA: Time effect, $F_{(3.888, 81.65)}$= 42.52, P < 0.0001; cell identity effect, $F_{(1, 21)}$= 0.7339, P = 0.4013; time x cell identity, $F_{(19, 399)}$= 0.9070, P = 0.5744). (Inset) Representative oIPSCs traces recorded in mNAcSh D1- and D2-MSNs before and after bath application of PD-128907. **i** Bar-graph quantification of oIPSC inhibition after PD-128907 application in D1R-positive (n = 12 cells from 5 mice) and D1R-negative (n = 11 cells from 5 mice) mNAcSh MSNs (unpaired t-test (two-tailed), $t_{(21)}$= 0.9825; P = 0.337). **j** Schematics of experiment to determine regulation of *ex-vivo* cAMP signaling by D3Rs. (Left) *Drd3*-Cre mice (n = 5) we injected with AAV1-hSyn-DIO-cADDs in the mNAcSh and slices containing the mNAcSh were imaged on a two-photon microscope. (Right) Representative images of cADDis expression in the mNAcSh (left) and 40X magnification (right). **k** Diagram showing the experiment setup. Bath-application of DA in the presence of SCH-39166, a D1R antagonist, inhibited cAMP levels through D3R signaling. **l** Timecourse of cADDis fluorescence changes before and after DA application. Forskolin was added after the experiment to confirm the specificity of changes in fluorescence. All data in this figure are presented as mean ± SEM Error bars indicate SEM.

https://doi.org/10.1038/s41593-024-01819-9

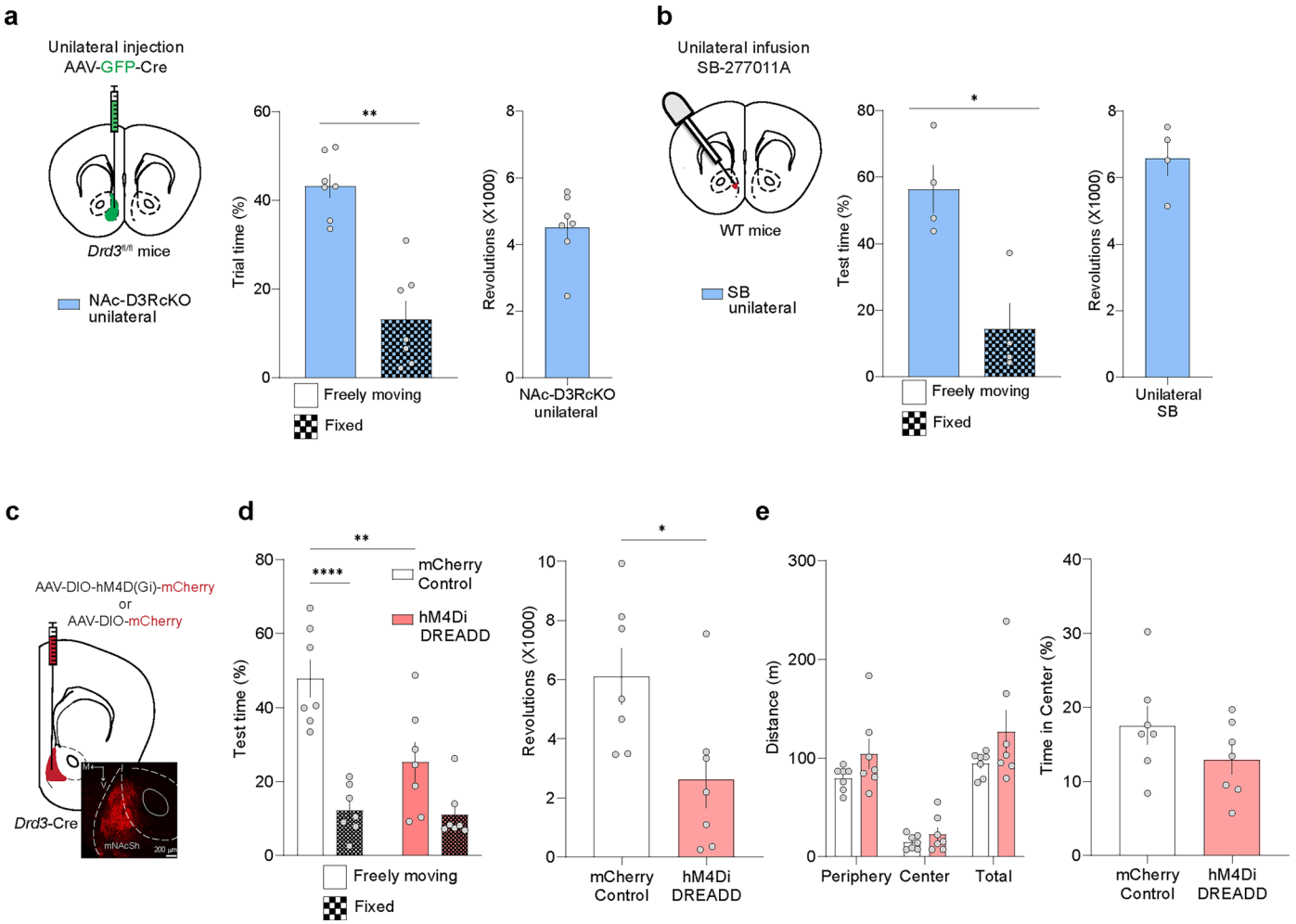

Extended Data Fig. 7 | Unilateral suppression of D3R signaling does not disrupt motivated running behavior. a Quantification of time spent in the freely-moving and fixed disk and revolutions for *Drd3*$^{fl/fl}$ mice expressing unilateral Cre recombinase (n = 7 mice) (paired t-test (two-tailed), $t_{(6)}$= 5.129; **P = 0.0022). **b** Same as in (a) but for WT control mice unilaterally infused with SB-277011A into the mNAcSh (n = 4 mice) (paired t-test (two-tailed), $t_{(3)}$= 3.570; *P = 0.0376). **c** Schematic (top) and representative image (bottom) of viral expression of AAV5-hSyn-DIO-mCherry in the mNAcSh of *Drd3*-Cre mice. **d** (Left) Percentage of time spent on fixed or freely-moving disk during the running disk task for mCherry (n = 7 mice) and hM4Di (n = 7 mice) groups. (two-way repeated measures ANOVA: Disk effect, $F_{(1, 24)}$= 36.29, P < 0.0001; treatment effect, $F_{(1, 24)}$= 8.250, P = 0.0084; disk x treatment, $F_{(1, 24)}$= 6.752, P = 0.0158). (Right) Running behavior as represented by the number of revolutions registered in the freely moving disk (unpaired t-test (two-tailed), $t_{(12)}$= 2.581; *P = 0.024) (mCherry Control, n = 7 mice; hM4Di, n = 7 mice). **e** (Left) Quantification of cumulative distance traveled in each zone during the open-field test (two-way repeated measures ANOVA: Zone effect, $F_{(1.230, 14.75)}$= 131.1, P < 0.0001; treatment effect, $F_{(1, 12)}$= 2.206, P = 0.1632; zone x treatment, $F_{(2, 24)}$= 2.177, P = 0.1353) (mCherry Control, n = 7 mice; hM4Di, n = 7 mice). (Right) Percentage of time spent in center (unpaired t-test (two-tailed), $t_{(12)}$= 1.428; P = 0.1788) (mCherry Control, n = 7 mice; hM4Di, n = 7 mice). All data in this figure are presented as mean ± SEM Error bars indicate SEM.

https://doi.org/10.1038/s41593-024-01819-9

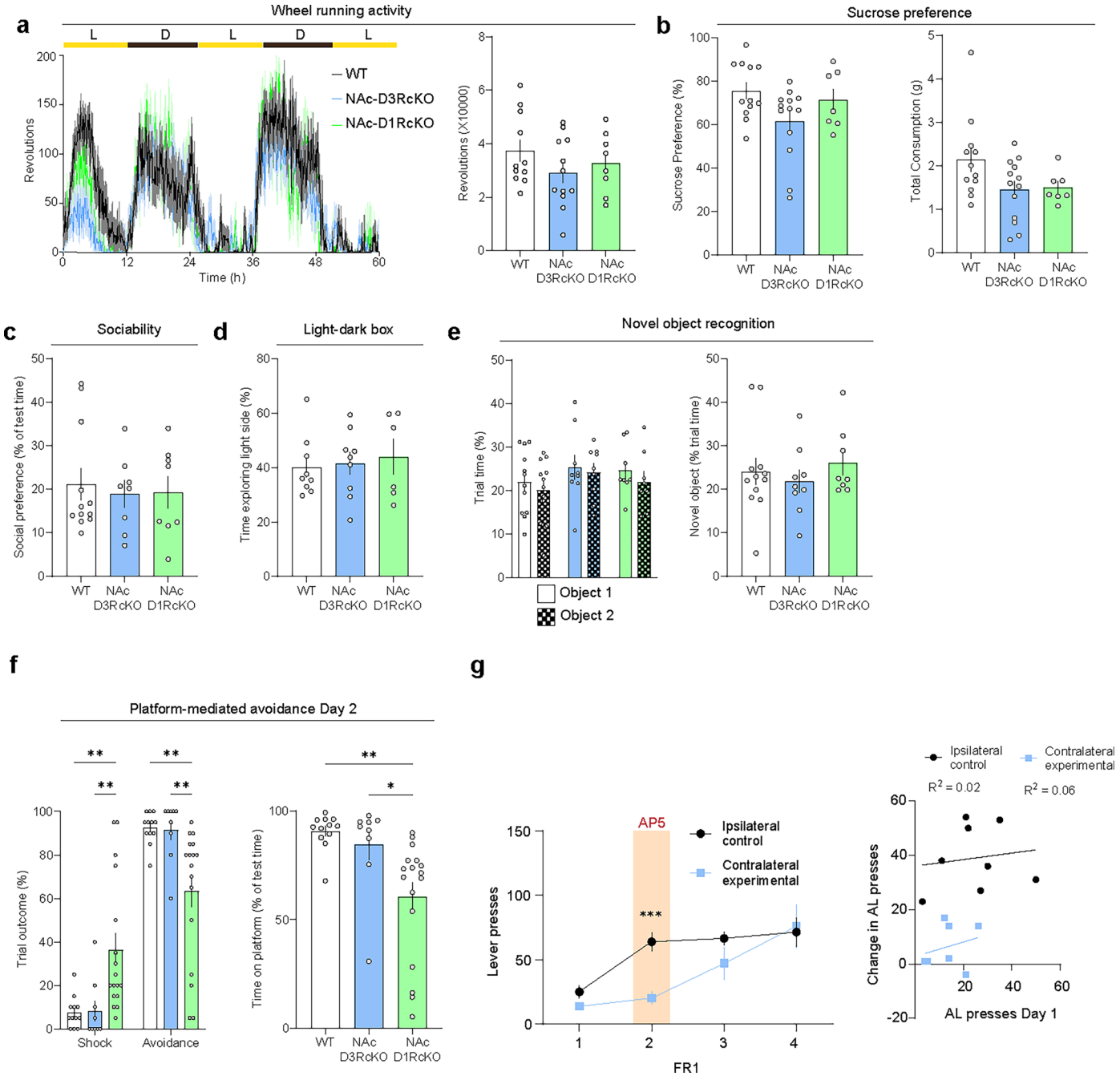

Extended Data Fig. 8 | See next page for caption.

https://doi.org/10.1038/s41593-024-01819-9

Extended Data Fig. 8 | cKO of mNAcSh D1Rs do not disrupt motivated, anxiety-like or social reward or sucrose preference. a (Left) Time course of wheel-running activity across the entire duration of the experiment (60-hrs) for WT (n = 11 mice), NAc-D3RcKO (n = 12 mice) and NAc-D1RcKO (n = 8 mice) groups in 5 min bins (two-way repeated measures ANOVA: Time effect, $F_{(15.51, 434.3)} = 20.27$, $P < 0.0001$; genotype effect, $F_{(2, 28)} = 1.738$, $P = 0.1943$; time x genotype, $F(1438, 20132) = 1.513$, $P < 0.0001$). (Right) Quantification of total revolutions across the 60 hr period (one-way ANOVA: followed by two-sided Dunnett's test, $F_{(2, 28)} = 1.197$, Group comparisons, NAc-D1RcKO vs WT, $P = 0.6507$, NAc-D1RcKO vs NAc-D3RcKO, $P = 0.7421$). **b** (Left) Percentage of sucrose preference for WT (n = 12 mice), NAc-D3RcKO (n = 13 mice) and NAc-D1RcKO (n = 7 mice) groups (one-way ANOVA: followed by two-sided Dunnett's test, $F_{(2, 29)} = 2.937$, Group comparisons, NAc-D1RcKO vs WT, $P = 0.752$, NAc-D1RcKO vs NAc-D3RcKO, $P = 0.2671$). (Right) Overall water and sucrose intake (one-way ANOVA: followed by two-sided Dunnett's test, $F_{(2, 29)} = 2.941$, Group comparisons, NAc-D1RcKO vs WT, $P = 0.1447$, NAc-D1RcKO vs NAc-D3RcKO, $P = 0.9841$). **c** Social preference as reflected by the % time (test-habituation) spent interacting with a novel, juvenile mouse (WT, n = 12 mice; NAc-D3RcKO, n = 8 mice and NAc-D1RcKO, n = 8 mice) (one-way ANOVA: followed by two-sided Dunnett's test, $F_{(2, 25)} = 0.1187$, Group comparisons, NAc-D1RcKO vs WT, $P = 0.9026$, NAc-D1RcKO vs NAc-D3RcKO, $P = 0.9971$). **d** Anxiety-like behavior as represented by the time spent in the light side of the box (WT, n = 9 mice; NAc-D3RcKO, n = 9 mice and NAc-D1RcKO, n = 6 mice) (one-way ANOVA: followed by two-sided Dunnett's test, $F_{(2, 21)} = 0.1626$, Group comparisons, NAc-D1RcKO vs WT, $P = 0.7825$, NAc-D1RcKO vs NAc-D3RcKO, $P = 0.902$). **e** (Left) Time spent interacting with each of the objects during the baseline period of the novel object recognition test (two-way repeated measures ANOVA: Object effect, $F_{(1, 26)} = 1.381$, $P = 0.2506$; genotype effect, $F_{(2, 26)} = 1.187$, $P = 0.3212$; object x genotype, $F_{(2, 26)} = 0.06934$, $P = 0.9332$). (Right) Preference for the novel object over a familiar one during the discrimination session (one-way ANOVA: followed by two-sided Dunnett's test, $F_{(2, 26)} = 0.4785$, Group comparisons, NAc-D1RcKO vs WT, $P = 0.8305$, NAc-D1RcKO vs NAc-D3RcKO, $P = 0.5168$) (WT, n = 12 mice; NAc-D3RcKO, n = 9 mice and NAc-D1RcKO, n = 8 mice). **f** (Left) Quantification of trial outcome (avoidance or shock responses) upon re-exposure to the platform-mediated avoidance task on day 2 (two-way repeated measures ANOVA: Outcome effect, $F(1, 35) = 77.30$, $P < 0.0001$; genotype effect, $F_{(2, 35)} = 0.000$, $P > 0.9999$; outcome x genotype, $F_{(2, 35)} = 7.892$, $P = 0.0015$) (WT, n = 12 mice; NAc-D3RcKO, n = 9 mice and NAc-D1RcKO, n = 17 mice). (Right) Overall time spent on platform (Day 2) as percentage of test time (one-way ANOVA: followed by two-sided Dunnett's test, $F_{(2, 35)} = 7.912$, Group comparisons, NAc-D1RcKO vs WT, $^{**}P = 0.0014$, NAc-D1RcKO vs NAc-D3RcKO, $^{*}P = 0.0201$). **g** (Left) Absolute number of active lever responses in FR1 sessions for D1R-NMDAR disconnection experiments. AP5 infusion was performed on Day 2 of FR1 (unpaired t-test (two-tailed), $t_{(13)} = 4.933$; $^{***}P = 0.0003$) (Ipsilateral, n = 8 mice; contralateral, n = 7 mice). (Right) Correlation between number of AL presses on Day 1 and change in active lever presses on Day 2 (AP5 challenge) (simple linear regression, $F_{(1, 11)} = 0.05037$, $P = 0.8265$). All data in this figure are presented as mean ± SEM Error bars indicate SEM.

nature portfolio

Corresponding author(s): Hugo A. Tejeda
Zachary Freyberg

Last updated by author(s): Sep 16, 2024

Reporting Summary

Nature Portfolio wishes to improve the reproducibility of the work that we publish. This form provides structure for consistency and transparency in reporting. For further information on Nature Portfolio policies, see our Editorial Policies and the Editorial Policy Checklist.

Statistics

For all statistical analyses, confirm that the following items are present in the figure legend, table legend, main text, or Methods section.

n/a	Confirmed
☐	☒ The exact sample size (*n*) for each experimental group/condition, given as a discrete number and unit of measurement
☐	☒ A statement on whether measurements were taken from distinct samples or whether the same sample was measured repeatedly
☐	☒ The statistical test(s) used AND whether they are one- or two-sided *Only common tests should be described solely by name; describe more complex techniques in the Methods section.*
☒	☐ A description of all covariates tested
☐	☒ A description of any assumptions or corrections, such as tests of normality and adjustment for multiple comparisons
☐	☒ A full description of the statistical parameters including central tendency (e.g. means) or other basic estimates (e.g. regression coefficient) AND variation (e.g. standard deviation) or associated estimates of uncertainty (e.g. confidence intervals)
☐	☒ For null hypothesis testing, the test statistic (e.g. *F*, *t*, *r*) with confidence intervals, effect sizes, degrees of freedom and *P* value noted *Give P values as exact values whenever suitable.*
☒	☐ For Bayesian analysis, information on the choice of priors and Markov chain Monte Carlo settings
☒	☐ For hierarchical and complex designs, identification of the appropriate level for tests and full reporting of outcomes
☐	☒ Estimates of effect sizes (e.g. Cohen's *d*, Pearson's *r*), indicating how they were calculated

Our web collection on statistics for biologists contains articles on many of the points above.

Software and code

Policy information about availability of computer code

Data collection	Wheel running data were obtained using Clocklab version 1 (Actimetrics, IL). Running disks data were collected through Anymaze version 6.36 (Stoelting, Ireland) and TopScan Suite (CleverSys, VA). Social interaction data were collected with Anymaze software 6.36 (Stoelting, Ireland). Operant conditioning and Pavlovian reward discrimination data were collected with MED-PC V software (MedAssociates, VT). Platform-mediated avoidance behavior was controlled and acquired using Anymaze version 6.36 (Stoelting, Ireland). Patch-clamp electrophysiology data were collected using Clampex 10.3 (Molecular Devices, CA). Further details can be found in the Methods section.
Data analysis	All data were analyzed using GraphPad Prism version 9.3.0 (GraphPad Software). TopScan software (CleverSys) was used for video tracking of running disks, open field, and novel object tests. Immunohistochemistry and RNAscope images were analyzed with ImageJ (Fiji, version 2017 May 30) and CellProfiler version 3.1.9. (Broad Institute Inc). Electrophysiology data was analyzed using Clampfit 10.6 (Molecular Devices), MiniAnalysis 6.0.3 (Synaptosoft, Inc) and Excel 16.16.26 (Microsoft). Specific pipelines for each of these programs are available from the corresponding author upon reasonable request.

For manuscripts utilizing custom algorithms or software that are central to the research but not yet described in published literature, software must be made available to editors and reviewers. We strongly encourage code deposition in a community repository (e.g. GitHub). See the Nature Portfolio guidelines for submitting code & software for further information.

Data

Policy information about availability of data

All manuscripts must include a data availability statement. This statement should provide the following information, where applicable:

- Accession codes, unique identifiers, or web links for publicly available datasets
- A description of any restrictions on data availability
- For clinical datasets or third party data, please ensure that the statement adheres to our policy

All data supporting the findings presented in this study are available from the corresponding author (Hugo A Tejeda) upon reasonable request. Source data are provided with this paper. Outlines for brain regions were acquired from the Paxinos and Franklin's Mouse Brain in Stereotaxic Coordinates (Fifth Edition). A complete data availability statement is also provided in the manuscript.

Research involving human participants, their data, or biological material

Policy information about studies with human participants or human data. See also policy information about sex, gender (identity/presentation), and sexual orientation and race, ethnicity and racism.

Reporting on sex and gender	N/A
Reporting on race, ethnicity, or other socially relevant groupings	N/A
Population characteristics	N/A
Recruitment	N/A
Ethics oversight	N/A

Note that full information on the approval of the study protocol must also be provided in the manuscript.

Field-specific reporting

Please select the one below that is the best fit for your research. If you are not sure, read the appropriate sections before making your selection.

☒ Life sciences ☐ Behavioural & social sciences ☐ Ecological, evolutionary & environmental sciences

For a reference copy of the document with all sections, see nature.com/documents/nr-reporting-summary-flat.pdf

Life sciences study design

All studies must disclose on these points even when the disclosure is negative.

Sample size	Sample sizes were based on pilot and previously (similar types of) experiments and were not statistically predetermined. Experiments were powered to match sample sizes typical of the technique reported in the field (ref 11,12 and 30), though no formal power analysis was performed a priori.
Data exclusions	Mice without correct targeting of viral expression, cannula placements and/or tracers were excluded from this study. For ex-vivo electrophysiology experiments, recordings were rejected when the access resistance increased by >20% during the experiment.
Replication	To ensure replication, multiple cohorts of mice were used. All animal, sample and biological replicate numbers in this study are in line with well accepted standards from the literature for each method. All experiments were successfully replicated at least once.
Randomization	Mice were randomly allocated to the different experimental conditions (genotype, pharmacological treatments or viral injections) reported in this study. Counterbalancing of sex and testing was employed.
Blinding	Experimenters were not blinded during data acquisition since they are aware of the mouse genotype from the information on the cage; analyses were performed blinded to the scorer or did not require manual scoring.

Reporting for specific materials, systems and methods

We require information from authors about some types of materials, experimental systems and methods used in many studies. Here, indicate whether each material, system or method listed is relevant to your study. If you are not sure if a list item applies to your research, read the appropriate section before selecting a response.

Materials & experimental systems

n/a	Involved in the study
☐	☒ Antibodies
☒	☐ Eukaryotic cell lines
☒	☐ Palaeontology and archaeology
☐	☒ Animals and other organisms
☒	☐ Clinical data
☒	☐ Dual use research of concern
☒	☐ Plants

Methods

n/a	Involved in the study
☒	☐ ChIP-seq
☒	☐ Flow cytometry
☒	☐ MRI-based neuroimaging

Antibodies

Antibodies used

Primary antibodies used in this study include rabbit anti-TH monoclonal (1:1000; PelFreez Biologicals; P40101-150) and chicken anti-GFP antibody (1:1000; Abcam, ab13970). Fluorophore-conjugated secondary antibodies and include Goat-anti-chicken Alexa Fluor 488 (1:500, Abcam, ab150173) and donkey anti-rabbit Alexa Fluor 594 (1:500, Jackson Immuno, 711-585-152)

Validation

All primary antibodies were suitable for IHC according to the vendor. Anti-TH antibody selectively stained VTA and SNc along the midbrain in our hands. Anti-GFP antibody stained selectively in virus infected area in our hands, and was validated according to the manufacturer's website by obtaining positive staining in GFP transfected in HEK-293E cells while no signal in non-transfected cells

Animals and other research organisms

Policy information about studies involving animals; ARRIVE guidelines recommended for reporting animal research, and Sex and Gender in Research

Laboratory animals

Drd3fl/fl mice were kindly provided by Z. Freyberg and and maintained in the C57BL/6J genetic background at NIMH facilities. Drd1afl/fl mice were acquired from The Jackson Laboratory (JAX, 025700). Drd1a-tdTomato were acquired from Jackson Laboratories (JAX, 016204) and Drd1a-tdTomato/Drd3-Cre mice were bred in NIMH facilities. Drd3-Cre mice were obtained from GENSAT (founder line KI196). In addition, we used Ai14 (JAX, 007914), ROSA26-FlpER (JAX, 018906) and wild-type (WT; C57BL/6J, JAX, 000664) mice. Mice used in this study were group housed under a reverse 12-h light-dark cycle (8 p.m. to 8 a.m. light), at temperature of 70–74°F and 40–65% humidity, with food and water ad libitum. Wheel running experiments required single housing prior the start of experiments and operant conditioning experiments required single housing and food restriction. For all strains, mice (females and males) were aged 8-20 weeks at the start of the experiments.

Wild animals

No wild animals were used in this study.

Reporting on sex

Both female and male mice were used for all experiments.

Field-collected samples

No field-collected samples were used in this study.

Ethics oversight

All procedures were performed in accordance with the Guide for the Care and Use of Laboratory Animals and were approved by the National Institute of Mental Health (NIMH) Animal Care and Use Committee

Note that full information on the approval of the study protocol must also be provided in the manuscript.

Plants

Seed stocks

Report on the source of all seed stocks or other plant material used. If applicable, state the seed stock centre and catalogue number. If plant specimens were collected from the field, describe the collection location, date and sampling procedures.

Novel plant genotypes

Describe the methods by which all novel plant genotypes were produced. This includes those generated by transgenic approaches, gene editing, chemical/radiation-based mutagenesis and hybridization. For transgenic lines, describe the transformation method, the number of independent lines analyzed and the generation upon which experiments were performed. For gene-edited lines, describe the editor used, the endogenous sequence targeted for editing, the targeting guide RNA sequence (if applicable) and how the editor was applied.

Authentication

Describe any authentication procedures for each seed stock used or novel genotype generated. Describe any experiments used to assess the effect of a mutation and, where applicable, how potential secondary effects (e.g. second site T-DNA insertions, mosiacism, off-target gene editing) were examined.